

PL-TR-92-2127

2

**AD-A256 677**

PL-TR-92-2127



**REGIONAL SEISMIC STUDIES IN CENTRAL ASIA**

**Keith Priestley**

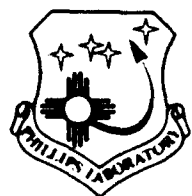
**University of Nevada, Reno  
Seismological Laboratory  
Reno, Nevada 89557**

**5 May 1992**

**DTIC  
ELECTE  
SEP 02 1992  
S D**

**Scientific Report No. 1**

**APPROVED FOR PUBLIC RELEASE; DISTRIBUTION UNLIMITED**



**PHILLIPS LABORATORY  
AIR FORCE SYSTEMS COMMAND  
HANSCOM AIR FORCE BASE, MASSACHUSETTS 01731-5000**

92 8 31 081

**92-24171**

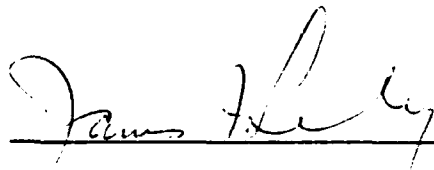


The views and conclusions contained in this document are those of the authors and should not be interpreted as representing the official policies, either expressed or implied, of the Air Force or the U.S. Government.

This technical report has been reviewed and is approved for publication.



JAMES F. LEWKOWICZ  
Contract Manager  
Solid Earth Geophysics Branch  
Earth Sciences Division



JAMES F. LEWKOWICZ  
Branch Chief  
Solid Earth Geophysics Branch  
Earth Sciences Division

  
DONALD H. ECKHARDT, Director  
Earth Sciences Division

This document has been reviewed by the ESD Public Affairs Office (PA) and is releasable to the National Technical Information Service (NTIS).

Qualified requestors may obtain additional copies from the Defense Technical Information Center. All others should apply to the National Technical Information Service.

If your address has changed, or if you wish to be removed from the mailing list, or if the addressee is no longer employed by your organization, please notify PL/IMA, Hanscom AFB MA 01731-5000. This will assist us in maintaining a current mailing list.

Do not return copies of this report unless contractual obligations or notices on a specific document requires that it be returned.

# REPORT DOCUMENTATION PAGE

*Form Approved*  
OMB No. 0704-0188

Public reporting burden for this collection of information is estimated to average 1 hour per response, including the time for reviewing instructions, searching existing data sources, gathering and maintaining the data needed, and completing and reviewing the collection of information. Send comments regarding this burden estimate or any other aspect of this collection of information, including suggestions for reducing this burden, to Washington Headquarters Services, Directorate for Information Operations and Reports, 1215 Jefferson Davis Highway, Suite 1204, Arlington, VA 22202-4302, and to the Office of Management and Budget, Paperwork Reduction Project (0704-0188), Washington, DC 20503.

<b>1. AGENCY USE ONLY (Leave blank)</b>		<b>2. REPORT DATE</b> May 5, 1992	<b>3. REPORT TYPE AND DATES COVERED</b> Scientific #1 (1 Aug 1990-31 Aug 1991)	
<b>4. TITLE AND SUBTITLE</b>  Regional Seismic Studies in Central Asia			<b>5. FUNDING NUMBERS</b>  Contract F19628-90-K-0046	
<b>6. AUTHOR(S)</b>  Keith Priestley			PE 62101F PR 7600 TA 09 WU AX	
<b>7. PERFORMING ORGANIZATION NAME(S) AND ADDRESS(ES)</b>  Seismological Laboratory University of Nevada, Reno Reno, Nevada 89557			<b>8. PERFORMING ORGANIZATION REPORT NUMBER</b>	
<b>9. SPONSORING/MONITORING AGENCY NAME(S) AND ADDRESS(ES)</b>  Phillips Laboratory Hanscom AFB, Ma 01731-5000  Contract Manager: James Lewkowicz/GPEH			<b>10. SPONSORING/MONITORING AGENCY REPORT NUMBER</b>  PL-TR-92-2127	
<b>11. SUPPLEMENTARY NOTES</b>				
<b>12a. DISTRIBUTION/AVAILABILITY STATEMENT</b>  Approved for public release Distribution unlimited			<b>12b. DISTRIBUTION CODE</b>	
<b>13. ABSTRACT (Maximum 200 words)</b>  This report describes research efforts performed during the first year of contract F19628-90-K-0046. Section A describes our preliminary analysis of the 2400 km long western Norilsk-Lake Baikal deep seismic sounding profile. Seismograms for the three nuclear explosions have been digitized, corrected for gain changes, and record sections constructed. We have compared these data with travel times predicted from several existing velocity models for Eurasia and begun modelling the data. Section B describes a study of the tectonics of the South Caspian region. Earthquake mechanisms show overthrusting of the south Caspian basin from the North, west, and south. The combined effect will lead to the eventual destruction of the South Caspian basin and the possible formation of an intermediate depth seismic zone within the continental interior similar to the Hindu Kush.				
<b>14. SUBJECT TERMS</b>  Deep Seismic Sounding(DSS), Sieberia, Caspian			<b>15. NUMBER OF PAGES</b> 88	
			<b>16. PRICE CODE</b>	
<b>17. SECURITY CLASSIFICATION OF REPORT</b> unclassified	<b>18. SECURITY CLASSIFICATION OF THIS PAGE</b> unclassified	<b>19. SECURITY CLASSIFICATION OF ABSTRACT</b> unclassified	<b>20. LIMITATION OF ABSTRACT</b> SAR	

## CONTENTS

<b>Section A:</b>	<b>Preliminary Analysis of the Western Norilsk - Lake Baikal Deep Seismic Sounding Profile</b>	<b>1</b>
	Introduction	1
	The Data	2
	Discussion of the Observed Record Stations	3
	Comparison With Published Eurasian Mantle Models	4
	Discussion	5
	References	5
<b>Section B:</b>	<b>Implications of Earthquake Focal Mechanism Data for the Active Tectonics of the South Caspian Basin and Surrounding Regions</b>	<b>15</b>
	Summary	15
	Introduction	16
	Geological and Geophysical Setting	17
	Determination of Earthquake Focal Parameters	18
	An Example of Waveform Analysis: The Earthquake of 4 November 1978	19
	The Earthquake of 6 March 1986	21
	Tectonics of the South Caspian Basin	24
	Discussion	28
	References	29
<b>Appendix</b>		<b>58</b>

**DTIC QUALITY INSPECTED 3**

<b>Accession For</b>	
NTIS GRA&I	<input checked="" type="checkbox"/>
DTIC TAB	<input type="checkbox"/>
Unannounced	<input type="checkbox"/>
Justification _____	
By _____	
Distribution/	
Availability Codes	
Dist	Avail and/or Special
A-1	

## SECTION A

### PRELIMINARY ANALYSIS OF THE WESTERN NORILSK - LAKE BAIKAL DEEP SEISMIC SOUNDING PROFILE

Keith F. Priestley, Department of Earth Sciences, Cambridge University  
John Cipar, Phillips Laboratory, Hanscom AFB, Ma 01731  
N.I. Pavlenkova, and A.V. Egorkin, Russian Academy of Sciences  
Moscow, U.S.S.R.

#### ABSTRACT

Seismograms from a 2400 km long deep seismic sounding profile extending from Norilsk to Lake Baikal have been analyzed to determine the upper mantle structure beneath the Siberian platform. As a initial interpretation of these data we have constructed one dimensional models for each shot point. The motivation for this is to provide a reference model for further investigations of lateral variations in mantle structure and comparison with previously derived models of upper mantle structure of the Eurasian landmass.

#### INTRODUCTION

The reliable determination of upper mantle velocity structure is an area of considerable geophysical interest since it bears upon problems of mantle composition and mantle convection. Variations in upper mantle velocity structure also have important implications in a nuclear discrimination/verification context as regional seismic phases will play a major role in monitoring any future test ban treaties. Most upper mantle velocity models published in the western literature are based on analysis of body waves or surface waves from earthquakes, or analysis of teleseismic body waves of nuclear explosions (Given and Helmberger, 1980). These provide average upper mantle velocity structure, but do not allow for the elucidation of detailed velocity structure required to address current questions.

During the past 30 years the Soviet Ministry of Geology has conducted an extensive seismic exploration program of the Eurasian crust and upper mantle. Many of these lines use nuclear explosions as seismic sources for recording at large offsets (up to 3000 km) and conventional explosives for shorter offsets. This has permitted interpretation of velocity structure (from refraction) to upper mantle depths (150-200 km) and of velocity contrasts (from reflections) at much deeper depths. The Soviet analysis of the data has been performed using a method analogous to forward raytracing methods. Yegorkin *et al*, (1977) describe a forward modeling procedure by which travel times

are computed for successively deeper penetrating rays and the theoretical travel times for a proposed structure are compared with the observed travel time until they fit to within prescribed error limits (about 0.3-0.5 sec). Soviet seismologists consider wave amplitudes by comparing observed seismic amplitudes with the density of computed rays. Results for only a few of these profiles are discussed in the western literature (Yegorkin and Pavlenkova, 1981; Pavlenkova and Yergorkin, 1983; Egorkin *et al*, 1984) and until recently none of the data have been available to western seismologists.

In this paper we discuss analysis of one of these profiles recorded across the Siberian platform.

## THE DATA

The 2400-km long "RIFT" profile recorded in 1982, extends across the Siberian platform from Norilsk to Lake Baikal (Fig. 1). Seismograms from three nuclear shot points were recorded. The northernmost shot point (SP 245) is in western Norilsk within the West Siberian rift, on the northwest edge of the Siberian Platform. This failed rift developed in the Triassic (235-215 mya) during the initial breakup of Pangea. Following the extinction of extension, the rift was buried beneath approximately 15 km of sediment. Geochemical analysis of basalts within the rift show a chemical composition similar to ocean tholeiites. The profile extends southeast across the Tunguss Basin, a region of Late Paleozoic extension and widespread intraplate flood basalts ( $1.2 \times 10^6 \text{ km}^3$  in 10 Ma), to the presently active Baikal rift. The central shot point (SP 173) is in western Tura within the Tunguss Basin, approximately 700 km southeast of the first shot point. Data from this shot extends 560 km northwest reversing a section of the profile from the first shot point and 1700 km southeast across the Baikal rift. The southernmost shot point (SP 35) is located 250 km north of Lake Baikal. Data from this shot extends 325 km to the south across the Baikal rift and nearly 2200 km to the north reversing both the northern and central shots. Unfortunately, instrumental problems led to a 640 km gap in the profile from 80 to 720 km. This gap is filled in by a large chemical shot (SP 36) just north of SP 35. Body wave magnitudes of the three nuclear shots range from 5.0 to 5.2 and as such are observable on low-noise, high gain teleseismic stations. Table 1 list relevant source parameters obtained from the International Seismological Centre bulletin.

The nuclear shots were recorded at 260 sites each equipped with the "Taiga" seismic system (Chichinin *et al.*, 1969). These stations record six data channels in analogue form as well as radio time signals. Three components are recorded: vertical, radial, and transverse. The six channels are used to record each component at high and low gain, thus greatly increasing the dynamic range. The sensors had a natural frequency of 1.5 Hz and the recording system as a whole had a usable bandwidth between 0.5-20 Hz.

Data for these profiles were obtained in the form of large paper record sections (25 mm/sec x 2.5 mm/km) with station locations accurate to 0.1 km. The traces were commercially digitized and corrected for amplitude scaling to produce trace-normalized

record sections (Fig. 2a-c). The paper record sections were plotted using the high-gain channel for the first arrival and, if necessary, the low-gain channel for the remainder of the seismogram. An overlap of 1-3 seconds allowed most traces to be rescaled with proper relative amplitude. In addition to the nuclear shots a detailed system of crustal observations has also been made. Chemical explosions (3000-5000 Kg each) were detonated at approximately 70 km intervals along the profile and recorded on reversed profiles 250-300 km long. One of these, SP 36, is shown in Fig. 2d.

## DISCUSSION OF THE OBSERVED RECORD SECTIONS

The clear differences between the seismograms from the three explosions imply that the velocity structure of the lithosphere is variable along the profile. Here we discuss the general features of the record sections - more detailed comments on the record sections for each shot point are given in the figure captions.

Near each shot point, crustal arrivals are prominent, especially the  $P_g$  phase. Mantle refractions are recorded as first arrivals at offsets of 150-200 km. Due to the scale,  $P_n$  appears to be comparatively weak on these figures, but can be clearly seen in the digital data. Apparent upper mantle velocities range between 8.3 and 8.45 km/sec based on fitting a straight line to first arrivals in the 200-600 km range. Estimated crustal thickness ranges from 50 km in the West Siberian Rift to 42 km beneath the Siberian craton. At longer ranges, the first arrivals appear to have variable amplitudes and arrival times, and reflect real variations in the lithosphere as they are correlated over several hundred kilometers. Likewise, the amplitude variations are complex. For example, in the distance range 1300-1500 km for SP 245 (Fig. 2a), high amplitude arrivals that begin after the first arrival at 1300 km, progressively move forward, becoming the first arrival at 1500 km. This pattern is consistent with a reflected phase from a high velocity layer. Several repetitions of this structure indicate complex layering within the upper several hundred kilometers of the mantle. At least some, if not all, of these observations may be due to lateral variations in structure (Pavlenkova and Egorkin, 1983).

At longer ranges, arrivals from the mantle zone can be observed. The reflection/refraction from the 410-km discontinuity is a clear secondary arrival beginning about 1700 km, becoming the first arrival by 2200 km. At 2100-2300 km range, a bright reflection from the 660-km discontinuity can be observed at about 12 sec reduced time. There is no clear evidence of the 550-km discontinuity described by Shearer (1990), although the seismograms in this distance range are complex. Also there is a considerable difference between SP 245 (Fig. 2a) and SP 35 (Fig. 2c) data at comparable transition zone ranges. Whereas SP 245 indicates strong arrivals from transition zone discontinuities, the SP 35 data do not contain similar arrivals. At this stage, it is unclear whether this observation is the result of lateral variation in the mantle or the result of near surface feature which may mask the arrivals.

From 1000-2200 km this section is characterized by low-amplitude first arrivals followed by a more energetic arrival 1-3 seconds later. The stronger second arrival in the

range 1000-1800 km is interpreted as a reflection from a discontinuity at approximately 200 km depth. The low amplitude of the first arrivals from 1600-2200 km implies a low velocity gradient below this discontinuity.

From 1540-2140 km a strong phase follows the first arrivals by 10 seconds at shorter ranges diminishing to 2 seconds at longer ranges. This phase is associated with high gradients or a discontinuity near 400 km depth. The 400 km phases cross over to become the first arrival beyond 2230 km. The apparent velocity of the first arrival increases from 8.7 km/sec at distances of 1600-2100 km to 10.6 km/sec beyond 2200 km.

From 2230-2570 km distance there is another prominent phase following the first arrival by 3-1 seconds that is interpreted as energy returned from a discontinuity near 650 km depth.

Figure 2 clearly shows the presence of significant structure within the upper mantle. We have constructed a radially stratified velocity model to fit the travel times and amplitudes of the various phases using a combination of travel time and synthetic seismogram modeling. Our objective has been to construct a representative velocity structure for the region and so have concentrated on the major features of the data and model.

#### COMPARISON WITH PUBLISHED EURASIAN MANTLE MODELS

First arrival times and prominent secondary arrival times for SP 245 were read from the original record section and are shown in Figure 5. The data are compared to two published models for the Eurasian upper mantle: model K8 (Given and Helmberger, 1980) was derived using long-period seismograms of Soviet nuclear blasts recorded in Europe, and model KCA (King and Calcagnile, 1976) was derived from P wave phase velocity measurements at NORSAR. A comparison of the velocity-depth function for these models is shown in the inset to Fig. 3. The first arrivals define a travel time branch of variable amplitude. Note especially the long-wavelength, 1-1.5 second travel time variation from about 750 to 1450 km range. This consistency suggests the presence of a large-scale velocity anomaly in the upper mantle, probably in the depth range 70-150 km. Neither upper mantle model accounts for these travel time anomalies. The chief difference between the two models is the presence of a low-velocity zone between 150-200 km depth in K8 as well as a higher gradient in K8 between the LVZ and the 420-km discontinuity. The K8 LVZ produces a pronounced shadow zone in the travel time curve that is not supported by the observations. KCA, on the other hand, with a smooth upper mantle, generally predicts the overall shape of the observed travel times. Neither model accounts for the relatively slow arrivals in the 250-270 km range. Both models generally predict the arrival times of waves from the transition zone discontinuities. In general, KCA accounts for the overall shape and amplitude behavior of the SP245 travel time observations.

Figure 4 compares part of the SP 245 record section in the range 1600-2400 km with the travel time curve for the KCA (King and Calcagnile, 1976). As noted above, the



branch from above the 400 km discontinuity is about 1 second slow compared to the observations. Reflections (dashed line) and refraction (solid line) from the 420-km are in general agreement although, again, slightly late. The critical point should be shifted from about 1760 km to 1800 km where the data show a prominent bright spot. By far the worst fit is for the reflection branch (D) from the 690-km discontinuity. The KCA curve both misses the prominent bright spot by 1-1.5 seconds and has an apparent velocity much greater than observed.

## DISCUSSION

The purpose of this investigation is to improve our understanding of the Eurasian crust and upper mantle velocity structure. Improvement of our understanding in these areas will help in evaluating the significant factors controlling the propagation of regional seismic phases; in "calibrating" the IRIS seismographs and the Scandinavian array in terms of the seismic wavefield resulting from Kazakh Test Site (KTS) explosions; and in assessing the efficiency of high frequency propagation, and its use in elucidating source characteristics of Central Asian seismic events. An improved understanding of the propagation characteristics of regional seismic phases will facilitate interpretation of source characteristics from the seismograms.

One of the motivations for constructing the velocity model shown in Figure 4 has been to provide a reference model for future investigations of lateral variations of the mantle velocity structure. As such we have avoided interpreting features in the data that may be produced by localized velocity gradients in the region sampled by this data set. Observations of lateral heterogeneity across Siberia will be discussed in a future paper.

## REFERENCES

- Egorkin (Yegrokin), A. V., S. K. Ziuganov, and N. M. Chernyshev (1984), The upper mantle of Siberia, *Proceeding of the 27th International Geological Congress*, 8, 29-56.
- Given, J. W. and D. V. Helmberger (1980), Upper mantle structure of Northwestern Eurasia, *J. Geophys. Res.*, 85, 7183-7194.
- Hill, D. P. (1971), Velocity gradients and anelasticity from crustal body wave amplitudes, *J. Geophys. Res.*, 76, 3309-3325.
- Hill, D. P. (1973), Critically refracted waves in a spherically symmetric radially heterogeneous earth model, *Geophys. J. R. astr. Soc.*, 34, 149-177.
- Kennett, B.L.N. (1991). IASPEI 1991 Seismological Tables, published by The Research School of Earth Sciences, Australian National University.

King, D.W. and G. Calcagnil (1976). P-wave velocities in the upper mantle beneath Fennoscandia and western Russia, *Geophys. J. R. astr. Soc.*, *46*, 407-.

LeFevre, L.V., and D.V. Helmberger (1989). Upper mantle P velocity structure of the Canadian Shield, *J. Geophys. Res.*, *94*, 17749-.

Mellman, G.R., and D.V. Helmberger (1974), High-frequency attenuation by a thin high-velocity layer, *Bull. Seis. Soc. Am.*, *64*, 1383-1388.

Pavlenkova, N.I. and A.V. Yegorkin (1983), Upper mantle heterogeneity in the northern part of Eurasia, *Phys. Earth Planet. Int.*, *33*, 180-193.

Priestley, K.F., G. Zandt, and G.E. Randall (1988), Crustal structure in eastern Kazakh, U.S.S.R. from teleseismic receiver functions, *Geophys. Res. Lett.*, *15*, 613-616.

Scheimer, J.F. and I.Y. Borg (1984), Deep seismic sounding with nuclear explosives in the Soviet Union, *Science*, *226*, 787-792.

Stark, P.B., R.L. Parker, G. Masters, and J.A. Orcutt (1988), Strict bounds on seismic velocity in the spherical Earth, *J. Geophys. Res.*, *91*, 13892-13902.

Yegorkin, A.V., V.Z. Ryaboy, L.P. Starobinets, and V.S. Druzhinin (1977), Velocity cross sections of the upper mantle from DSS data on land, *Izvestiya, Earth Physics*, *13*, 467-477.

Yegorkin, A.V. and N.I. Pavlenkova (1981), Studies of mantle structure of U.S.S.R. territory on long-range seismic profiles, *Phys. Earth Planet. Int.*, *25*, 12-26.

**TABLE 1**

Shot	Date	Origin Time	Coordinates		$m_b$	$M_S$	Location
SP035	7/30/82	21 00 02.2	53.810°N	104.130°E	5.1	3.8	Lake Baikal
SP173	9/25/82	17 59 57.1	64.313°N	97.834°E	5.1		Central Siberia
SP245	9/04/82	17 59 58.4	69.206°N	81.647°E	5.2	3.5	Western Siberia

**FIGURE CAPTIONS**

Figure 1. Simplified tectonic map of Central Asia. The "RIFT" profile is marked by the heavy solid line and the shot points by the solid circles.

Figure 2. Record sections for recordings of the three nuclear explosions. The seismograms have been reduced by a velocity of 8.2 k/s - (a) SP245; (b) SP173; (c) SP35; (d) SP36.

Figure 3. Comparison of the observed travel times from shot point SP245 (open circles) with travel times predicted from models K8 (solid line, Given and Helmberger, 1980) and KCA (dashed line, King and Calcagnile, 1976). The inset shows the P-wave velocity-depth functions for the models.

Figure 4. Comparison of the observed seismograms in the distance range 1600 - 2200 km for the SP245 shot point, and travel times computed for model KCA

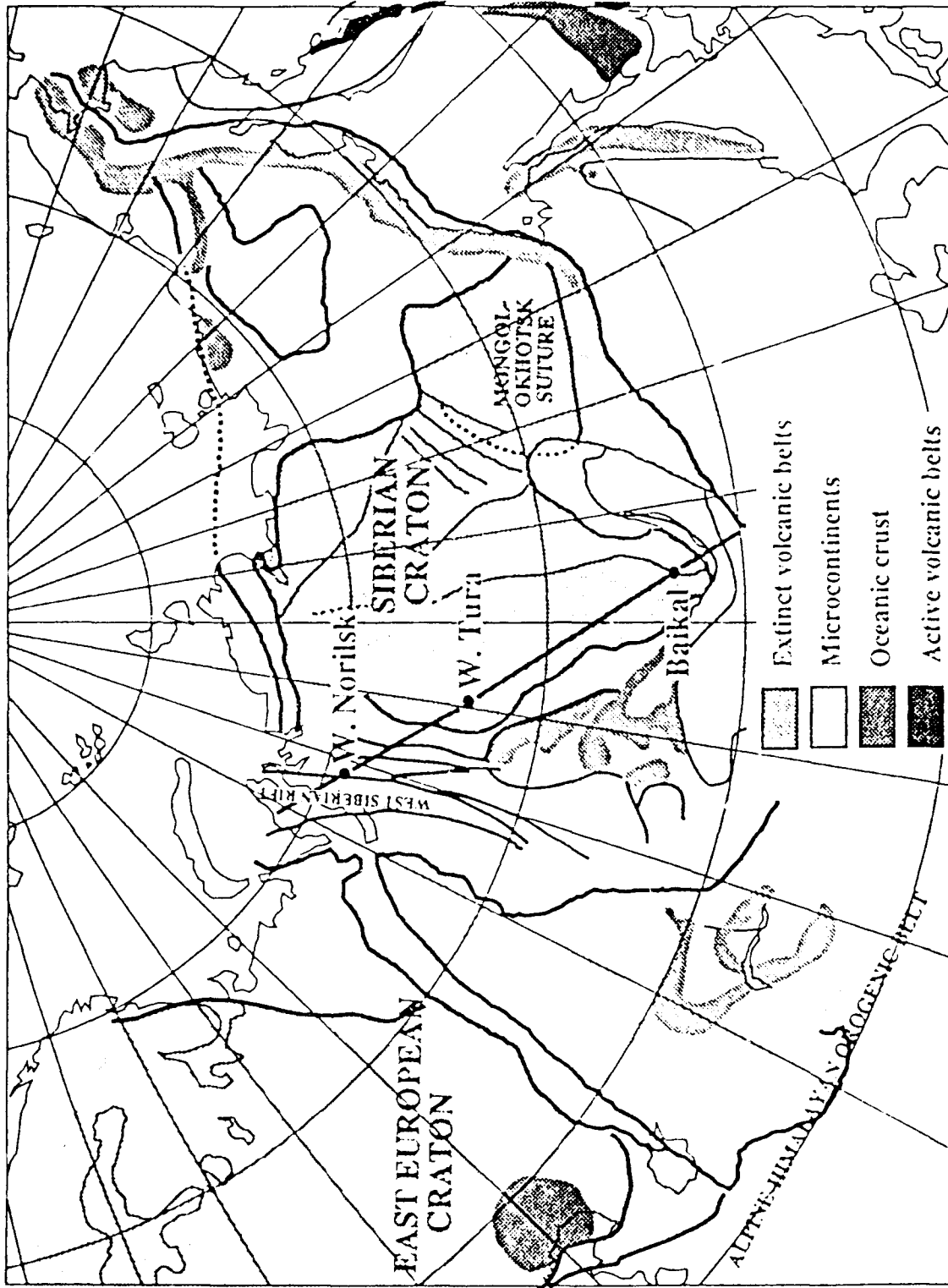


FIGURE 1

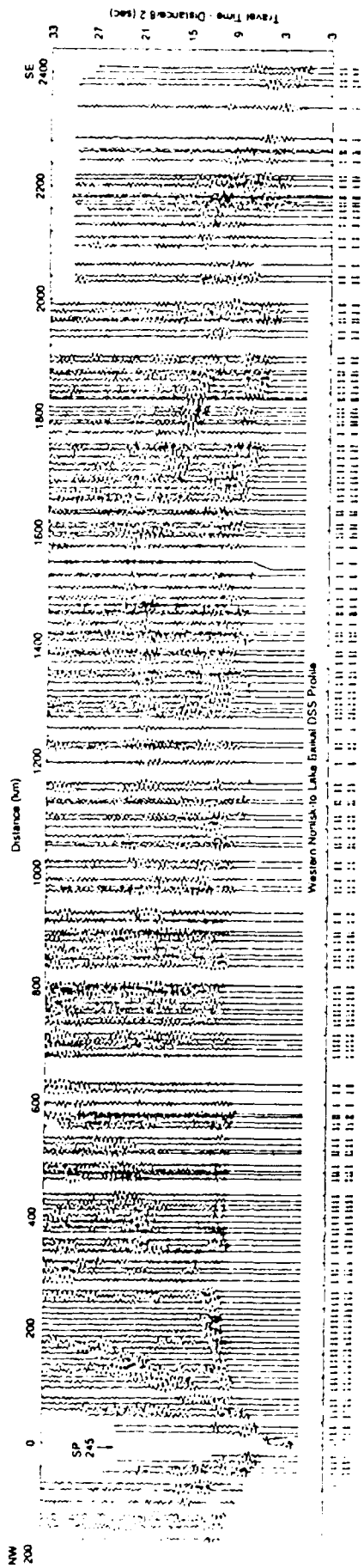


FIGURE 2a

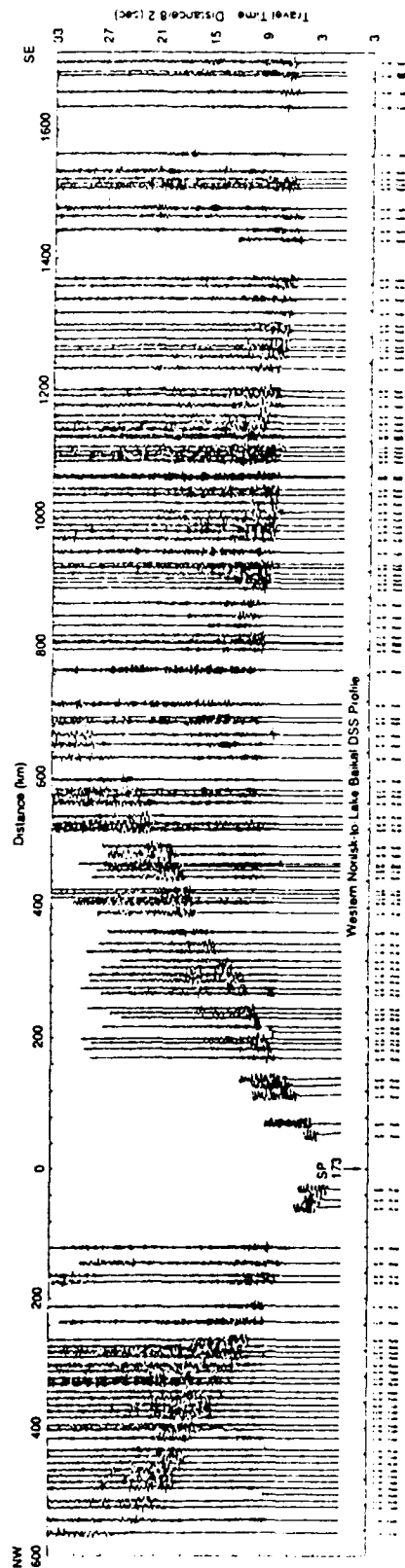


FIGURE 2b

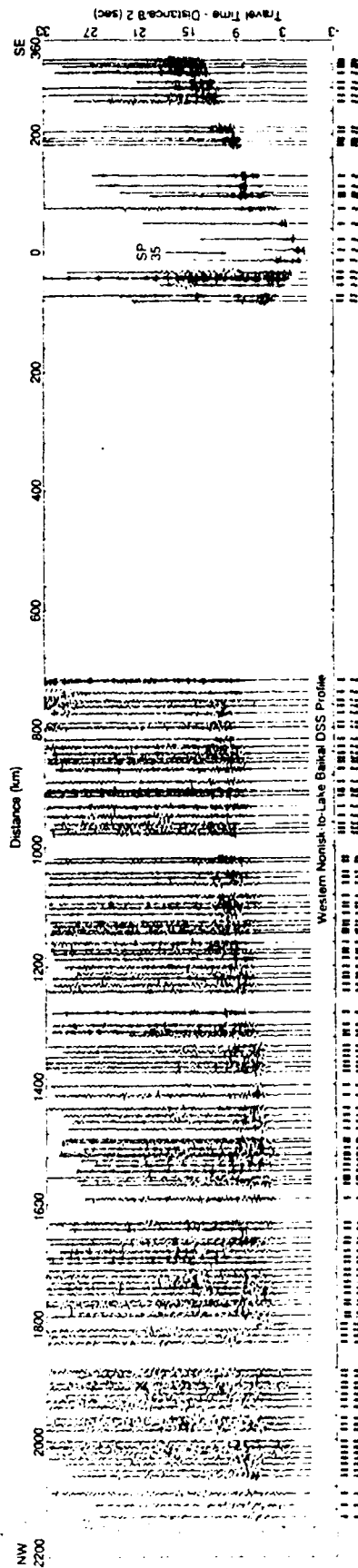


FIGURE 2c

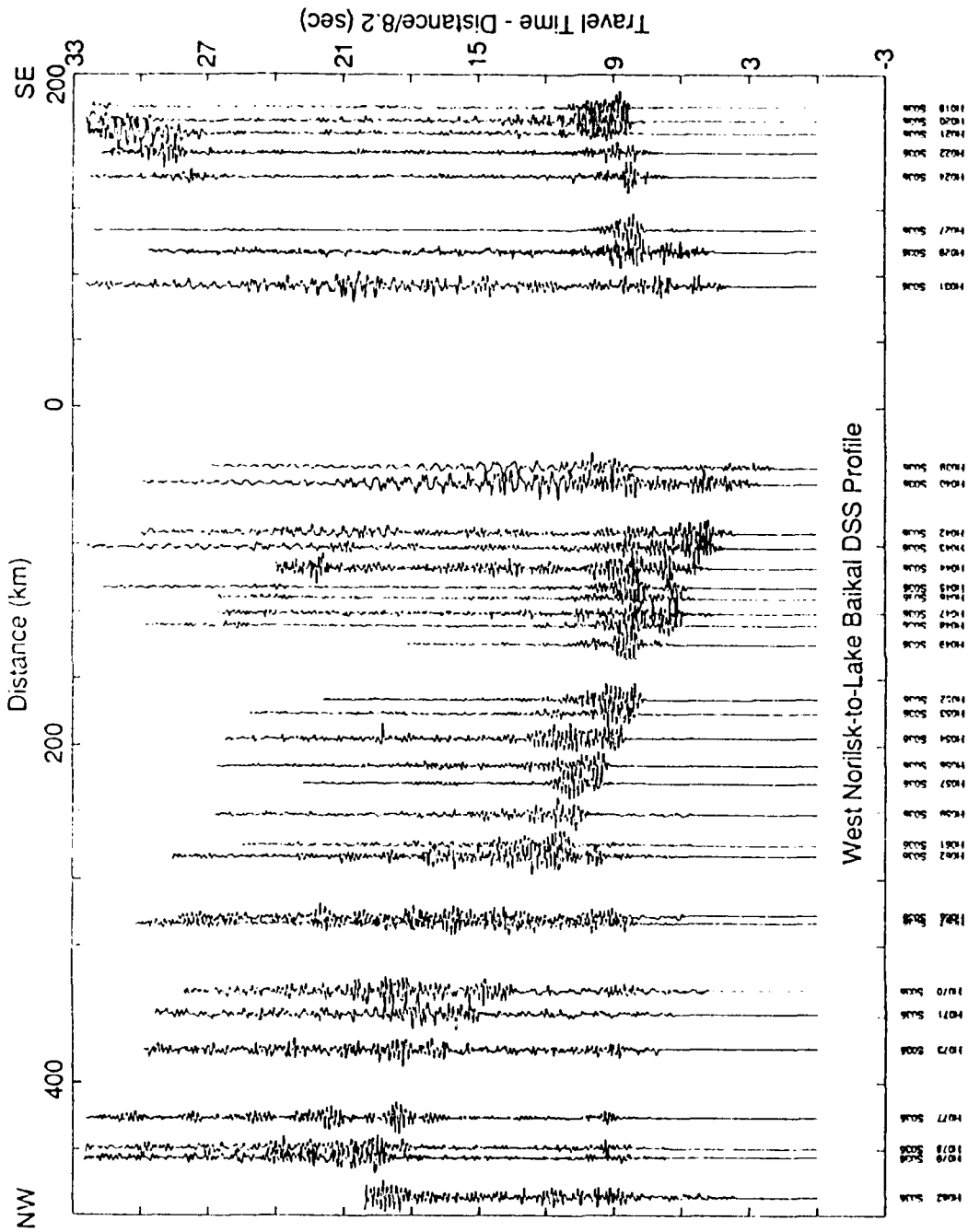


FIGURE 2d

COPY AVAILABLE TO DTIC DOES NOT PERMIT FULLY LEGIBLE REPRODUCTION

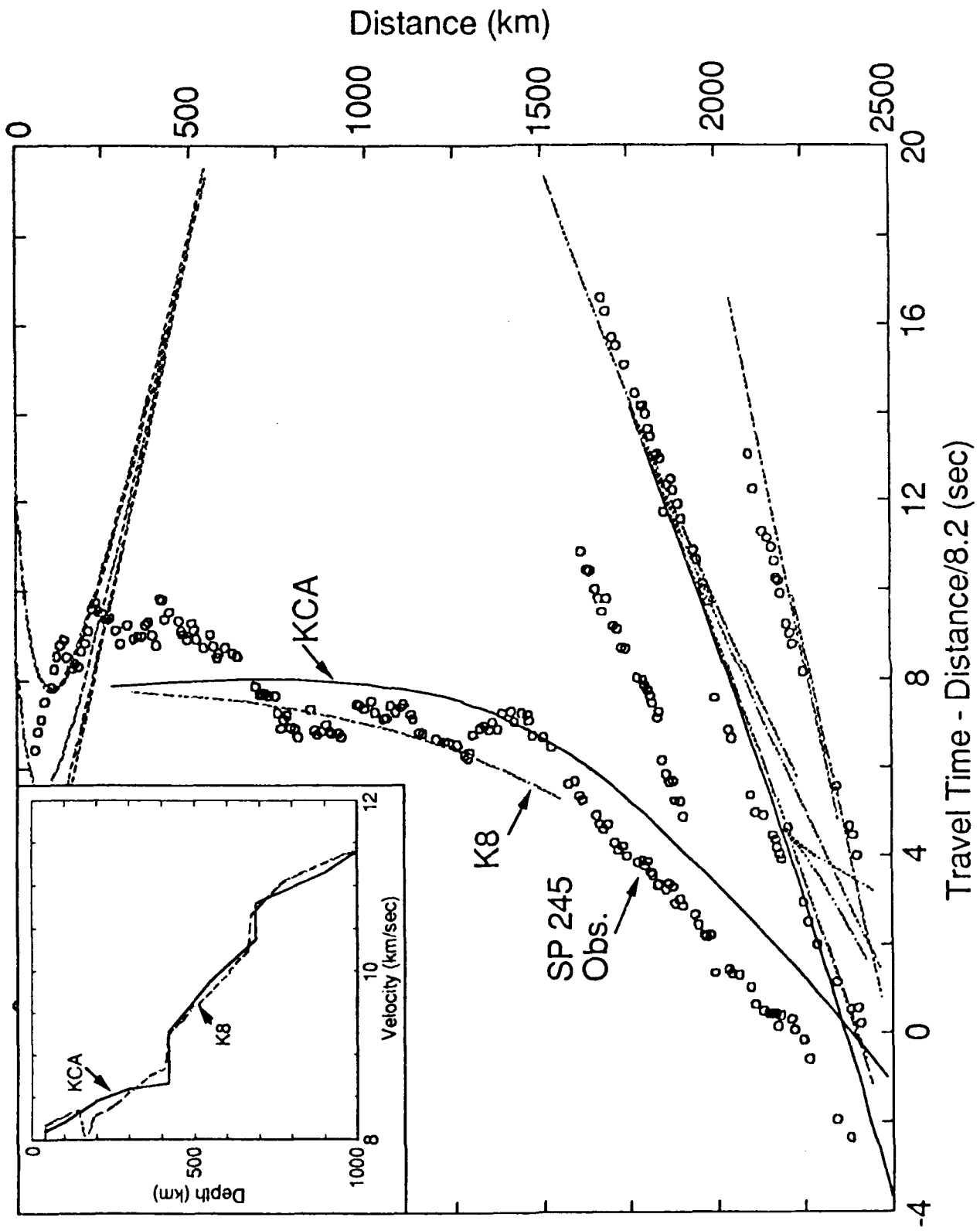


FIGURE 3



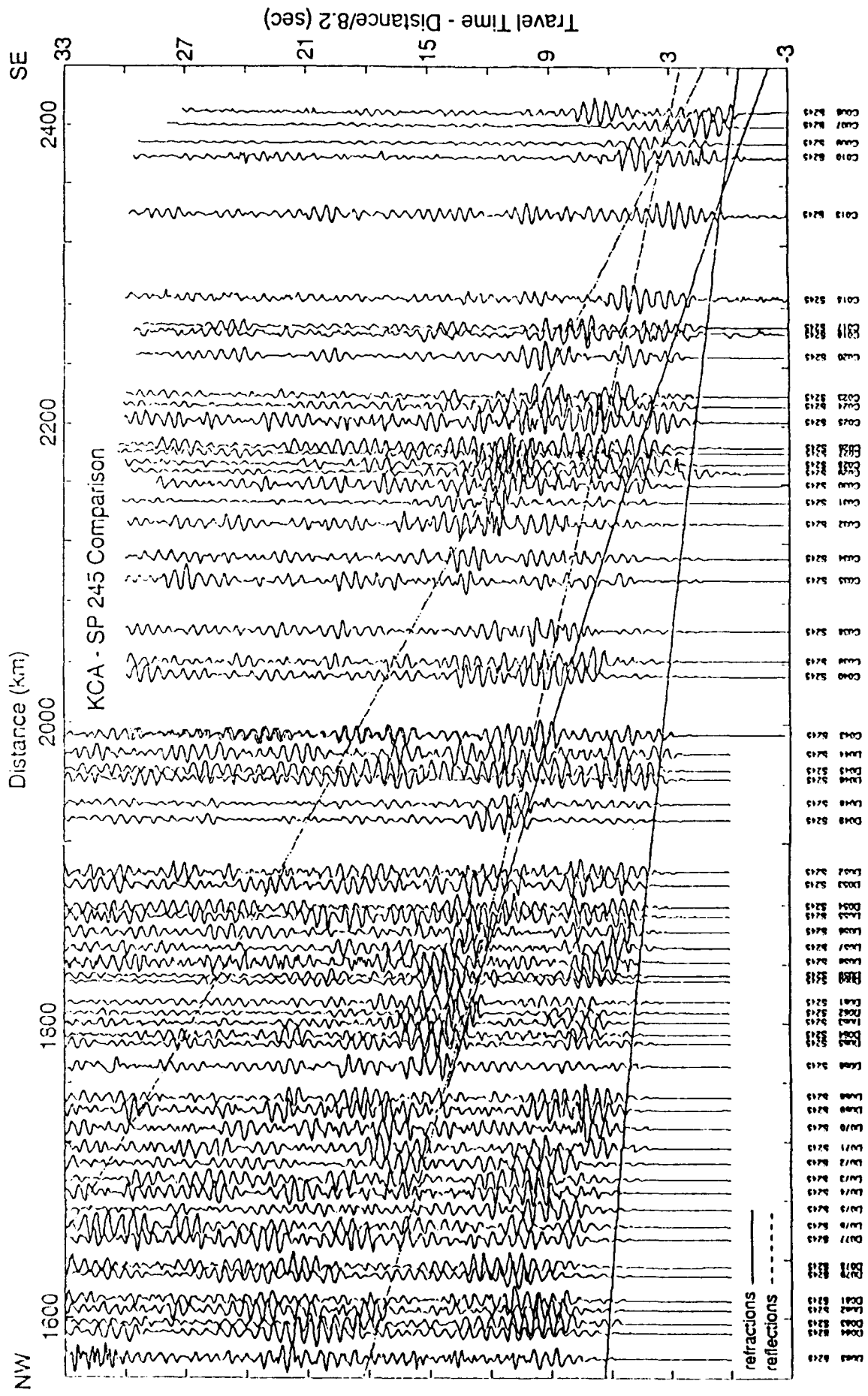


FIGURE 4

## SECTION B

# IMPLICATIONS OF EARTHQUAKE FOCAL MECHANISM DATA FOR THE ACTIVE TECTONICS OF THE SOUTH CASPIAN BASIN AND SURROUNDING REGIONS

Keith Priestley<sup>1</sup>

Department of Geological Sciences  
and Seismological Laboratory  
University of Nevada, Reno  
Reno, Nevada 89557

Calum Baker, James Jackson  
Department of Earth Sciences  
University of Cambridge  
Cambridge, CB3 0EZ, United Kingdom

## SUMMARY

The south Caspian Basin is a relatively aseismic block within the Alpine-Himalayan Belt, but is surrounded by zones of high seismicity. We used the focal mechanisms of 16 earthquakes whose source parameters we determined from inversion of body waves, and the mechanisms of 15 other earthquakes to determine the style of faulting in the seismic belts that surround the south Caspian Basin. Earthquakes beneath the Talesh Mountains of NW Iran and immediately off-shore in the SW Caspian Sea have shallow thrust mechanisms, showing that the continental crust of NW Iran is overthrusting the "oceanic-like" crust of the south Caspian Basin. Earthquakes south of the Caspian Sea in northern Iran show a mixture of focal mechanisms. Both high angle reverse faulting and left-lateral strike slip faulting are observed in the high Alborz Mountains. Farthers south, on the edge of the central Iran plateau, oblique left-lateral reverse mechanisms are observed. It seems that the NE direction of shortening between central Iran and the south Caspian Basin is partitioned into pure left-lateral strike-slip and thrusting in the WNW trending high Alborz, but is accommodated by oblique faulting in lower elevations. Earthquakes in the Kopet Dag Mountains east of the Caspian Sea also show a mixture of high angle reverse and strike-slip faulting mechanisms and thus may be another example of the partitioning of oblique slip into strike-slip and thrust motion. Normal faulting mechanisms at centroid depths of 35 to 50 km dominate in the belt of seismicity which extends across the central Caspian Sea. The significance of the normal faulting earthquakes is enigmatic. It is improbable that these events represent the motion between the southern Caspian Basin and Eurasia for they imply a sense of motion which is incompatible with the observed topography and

---

<sup>1</sup>now at: Department of Earth Sciences, University of Cambridge, Cambridge, CB30EZ, United Kingdom

folding in the sediments. Two shallow earthquakes at about 12 km depth in this belt, one a small event and the other a large second sub-event of a multiple earthquake, have thrusting mechanisms suggesting that shortening occurs as the continental crust of the northern Caspian is thrust over the "oceanic-like" crust of the southern Caspian Basin. Shortening is also suggested by the orientations of folds in the sedimentary cover south of the central Caspian Sea seismic belt. We suggest that this shortening does indeed represent a NNE motion of the Caspian Sea relative to Eurasia, but that the motion is slow and has not produced many earthquakes. The deep, normal faulting may be related to bending or down-dip extension of the incipient subducted slab. If the motion of the Caspian Sea relative to Eurasia is indeed slow, then the motion in the Alborz between central Iran and the south Caspian Basin will be almost the same as that between Iran and Eurasia, as has previously been assumed.

The combined effect of the overthrusting of the south Caspian Basin by the Talesh-Alborz mountains in the south, and by the continental crust of the northern Caspian Sea in the north will lead to the eventual destruction of the south Caspian Basin and the possible formation of an intermediate depth, dipping seismic zone within the continental interior, similar to that presently observed in the Hindu Kush.

## INTRODUCTION

This paper is concerned with the active faulting in and around the south Caspian Basin, which is a relatively aseismic block within the Alpine-Himalayan Belt but is surrounded by highly active seismic zones.

There were two motivations for this study. The first was to discover the nature of the deformation in the belt of seismicity extending across the central Caspian Sea from the Caucasus in the west to the Kopet Dag in the east. Before 1986, no earthquakes of  $m_b \leq 5.5$  had occurred in this belt since the installation of the World Wide Standard Seismic Network (WWSSN) in the early 1960's and thus no reliable fault plane solutions were available. As a result, discussions of the motion of the south Caspian Basin with respect to Eurasia have largely been speculative. Nowroozi (1972) believed that the south Caspian is moving northwestward relative to Eurasia. Jackson & McKenzie (1984) pointed out that the thrust faulting earthquakes that occur throughout the Caucasus, Alborz, and Kopet Dag Mountains all have similar slip vectors directed NE, suggesting that the south Caspian is moving northeastward relative to Eurasia, although less rapidly than Iran. We have studied the mechanisms of several earthquakes in the Trans-Caspian seismic belt to better define the motion of the south Caspian Basin.

A second motivation for the study was to better understand the tectonic setting of the 6 June 1990 earthquake in the Talesh Mountains of the southwest Caspian. This was by far the largest earthquake ( $M_w$  7.2) to occur in the region this century, and it had a focal mechanism quite unlike that of neighboring events. A detailed field and seismological report on this earthquake is published elsewhere (Berberian et al, 1991).

The principale new data we present new observations of earthquake focal mechanisms and depths determined from P-wave first motion and P- and SH-waveform data. These are much better constrained than the anisms and in earlier studies (eg. Jackson and

McKenzie, 1984), which were based on P wave first motions alone, and extend the period of observation to 1990.

## GEOLOGICAL AND GEOPHYSICAL SETTING

The seismicity of the Middle East is dispersed over bands 100 - 300 km wide, which surround regions such as the south Caspian Basin and central Iran within which the seismicity is relatively low (Fig. 5 and Jackson & McKenzie 1984). The western and southern margins of the south Caspian Basin are bounded by an active arcuate fold and thrust belt in the Talesh and Alborz Mountains (Fig. 6a). To the east of the south Caspian Sea lies the west Turkmenian lowlands, which are structurally part of the south Caspian Basin. Farther to the east lie the seismically active Kopet Dag Mountains. The deeper water ( $\approx 1000\text{m}$ ) of the south Caspian Basin is separated from the shallower water ( $\approx 200\text{m}$ ) of the central and north Caspian Sea by the Apscheron - Balkhan sill, a shallow, seismically active zone extending from the Caucasus Mountains in the west to the Kopet Dag Mountains in the east (Fig. 5, 6b).

Deep seismic sounding (DSS) data from the south Caspian Basin reveal a crust consisting of a thick (15-20 km) low velocity ( $V_p$  3.5 to 4.0  $\text{kms}^{-1}$ ) sedimentary section resting on a high velocity ( $V_p \geq 6.7 \text{kms}^{-1}$ ) layer (Galperin et al, 1962; Malovitsky, 1968; Neprochnov, 1968; Rezanov & Chamo, 1969; Malovitsky et al, 1970; Fedynsky et al, 1972) (Fig. 6a). DSS data to the east of the south Caspian Basin indicate the existence of a  $V_p$  6.0  $\text{kms}^{-1}$  layer, thought to represent continental basement, which pinches out towards the southwest and disappears beneath the Turkmenian lowlands. The existence of a 6.0  $\text{kms}^{-1}$  layer is also apparent in DSS data from north of the Apscheron-Balkhan sill and in the Talesh and Alborz Mountains in northern Iran (Berberian, 1983), to the south of the Caspian Sea. The high velocity crustal layer of the south Caspian Basin has been assumed by many to be "oceanic-like crust" and this view is supported by observations of  $L_g$  blockage and efficient  $S_n$  propagation for paths crossing the south Caspian Basin (Kadinsky - Cade, et al, 1981). Seismic profiling shows that the sedimentary cover of the south Caspian Basin has undergone considerable deformation (Zonenshain & Le Pichon, 1986).

In the western part of the basin the fold axes trend NNW-SSE to N-S (Fig. 6a). Fold axes in the north and south parts of the basin trend NW-SE roughly parallel with the Apscheron-Balkhan Sill and the north Iranian coast, respectively (Fig. 6a).

The tectonic history of the south Caspian Basin has been reviewed by Berberian & King (1981), Berberian (1983), and Zonenshain & Le Pichon (1986). The age of the "oceanic" basement is uncertain. Paleoreconstruction of the Iranian region (Berberian and King, 1981) indicates that if the high velocity layer is oceanic it could be a relic of an ocean that closed in either the Triassic or the Cretaceous, or else a marginal sea that developed behind an island arc. The region has been dominated by compression during the Pliocene-Pleistocene. Some Soviet earth scientists (e.g. Muratov, 1972; Yanshin et al, 1980; Shlezinger, 1981) propose that the south Caspian Basin is young and was formed by the eclogitization and subsidence of granitic continental crust during the mid- to late Cenozoic. Others, (e.g. Amurski et al, 1968; Sorokhtin, 1979; Vardapetyan, 1981) consider the south Caspian Basin to be pre-Hercynian in age and a remnant of the Early Mesozoic Tethys

sea floor. Evidence cited in support of the latter hypothesis includes the great thickness of sediment and low observed heat flow. Shikalibeily & Grigoriants (1980) suggest that the south Caspian Basin is Jurassic and is overlain by Cretaceous volcanic rocks. Adamia et al (1977) and Letouzey et al (1977) consider the south Caspian Basin as a remnant back-arc basin resulting from spreading behind a Late Cretaceous - Paleogene volcanic arc. Despite the uncertainty in the age, most authors agree that the high velocity "oceanic-like" basement extends eastward beneath the western Turkmenian lowlands and to the western coastal region of the Azerbaijan-Caspian coast (Amursski et al, 1968). A more detailed discussion of the tectonic history of the region surrounding the south Caspian Basin can be found in Berberian (1983) and Zonenshain and Le Pichon (1986).

#### DETERMINATION OF EARTHQUAKE FOCAL PARAMETERS

We have used P-wave first motion polarities and P- and SH-waveforms to constrain the source parameters of moderate size earthquakes occurring in the region surrounding the south Caspian Basin. The earthquakes whose mechanisms we have studied plus those whose mechanisms we have taken from Jackson & McKenzie (1984), the Harvard centroid moment tensor (CMT) catalogue, or Gao & Wallace (1991), are listed in Table 2.

The P-wave first motions shown in Figure 7 are from WWSSN seismograms read by the authors. In almost all cases these were read from the long-period vertical component. In a few cases where the long-period vertical onset was too small or obscured by noise, we read the first motion from the short-period vertical component providing the onset was clear, impulsive, and recognizable as the instrument impulse response. In all cases, we used a P-wave velocity at the source of  $6.8 \text{ km s}^{-1}$  to plot the station positions on the focal sphere.

The P- and SH-waveform data are from the WWSSN and Global Digital Seismic Network (GDSN) stations in the distance range  $30^\circ - 95^\circ$ . Our analysis followed the approach described by McCaffrey & Nabelek (1987) and subsequently used in a number of other studies (e.g., Molnar & Lyon-Caen 1989; Taymaz et al., 1990). Source parameters were determined using McCaffrey & Abers' (1988) version of Nabelek's (1984) waveform inversion procedure. This routine minimizes in a least squares sense, the misfit between the observed shape and amplitude of the long-period P- and SH-waveforms and synthetic waveforms. The synthetic seismograms are computed for a point source embedded in a simplified Earth structure by combining the direct arrival (either P or S) with the near source reflections (pP and sP, or sS) and near source multiples. The earthquakes were assumed to be either embedded in a velocity structure which was a simplified version of a published crustal velocity model for the same region, or embedded in a crustal velocity structure of a tectonically analogous region if no published velocity model exist in the region of the earthquake. Seismographs are assumed to be located on a homogeneous half space. When available, we have taken the Harvard CMT solution reported in the Preliminary Determination of Epicenters (PDE) as the starting point in the inversion; where unavailable, we have used the first motion fault plane solution of Jackson & McKenzie (1984). The time durations of the seismogram inversion windows were chosen to be long enough to include the near source reflected phases pP, sP, or sS. We examined the wave-

forms where we thought the PcP or ScS arrival might be within the inversion window. If we thought these phases might be of significant amplitude, we truncated our inversion window.

Synthetic waveform amplitudes are corrected for geometrical spreading, and anelastic attenuation is accounted for by applying a Futterman (1962) Q operator with  $t_p^* = 1$  sec and  $t_s^* = 4$  sec. Uncertainties in  $t^*$  mainly affect estimates of source duration and seismic moment, but have smaller effects on source orientation or centroid depth (Fredrich et al, 1988). To avoid complications introduced by the upper mantle triplication or core phase interference we restricted the body waveform inversion (with one exception discussed in the Appendix) to P-waves in the 30° to 90° distance range and S-waves in the 35° to 84° distance range. In the inversion process, SH seismograms were given only 50% of the weight of the P-wave seismograms, and all seismograms were azimuthally weighted; that is, seismograms from stations clustered together in azimuth were given lower weight than seismograms from isolated stations. We assumed that all slip occurs at the same point in space, the centroid location, but is distributed in time, the source time function. This is usually a good approximation for events less than about  $M_s$  6.5. However, in one case complexities observed in the seismograms suggest the existence of a second source. The source time function is described by a series of overlapping isosceles triangles (Nabelek, 1984). We initially selected the number and duration of the isosceles triangles using the event magnitude as a guide. We then eliminated late occurring, small amplitude elements of the source time function if we felt these were the result of noise. The inversion routine minimizes the misfit between the observed and synthetic waveforms by varying the strike, dip, slip, centroid depth, seismic moment, and source time function.

The "best-fitting" set of source parameters is found by the inversion routine. However, the statistical description of the inversion misfit underestimates the true uncertainties. Similar to McCaffrey & Nabelek (1987), once we had obtained the minimum misfit solution, we performed a series of tests to assess realistic uncertainties and examine tradeoffs between the various factors. Our test procedure was to fix the source parameter being examined at a series of values that bracket the "best-fitting" value, then reinvert the waveform data to examine what effect variations in the fixed parameters had on the free parameters. In summary, we found that reasonable variations in crustal velocity structure do not result in significant changes in strike, dip and rake, but can affect centroid depth, moment, and the source time function. Our tests showed that the strike, dip, rake, and centroid depth are relatively independent of each other: that is, when one parameter was held fixed at a value within a few degrees or kilometers of its minimum misfit value and the waveforms reinverted, the resulting values of the free parameters were close to their minimum misfit values.

#### AN EXAMPLE OF WAVEFORM ANALYSIS: THE EARTHQUAKE OF 4 NOVEMBER 1978

The 4 November 1978 (1978.11.04) Siahbil earthquake belongs to a group of events occurring in northwest Iran which we have studied, and whose mechanisms are consistent with overthrusting of the south Caspian Basin by the Azerbaijan-Talesh block of northwest

Iran. This event has been examined in several previous studies and provides a good example of the waveform analysis conducted in this study. P-wave first motion polarities (Fig. 7) constrain a  $347^\circ$  striking, high angle ( $79^\circ$  ENE) plane. This does not conform to any mapped faults in the area (Berberian, 1983) and is taken as the auxiliary plane. The shallow dipping fault plane is poorly constrained by the first motion data. Berberian (1983) studied P- waveforms of this event by forward modelling and concluded that the earthquake occurred on a  $168^\circ$  striking fault dipping  $9^\circ$  WSW at a depth of  $20 \pm 4$  km. One plane of the best fitting double couple to the Harvard CMT solution strikes  $177^\circ$ , dips  $9^\circ$  WSW, has a rake of  $87^\circ$ , and has a centroid depth of 15 km. Figure 8 shows the match between the observed seismograms and synthetic P and SH seismograms computed for the minimum misfit solution. We used the Harvard CMT solution as the starting point in the inversion procedure. The velocity structure used in obtaining these results consisted of a 12 km thick layer ( $V_p$   $5.60 \text{ kms}^{-1}$ ,  $V_s$   $3.24 \text{ kms}^{-1}$ ,  $\rho$   $2600 \text{ kgm}^{-3}$ ) overlying a half-space ( $V_p$   $6.80 \text{ kms}^{-1}$ ,  $V_s$   $3.93 \text{ kms}^{-1}$ ,  $\rho$   $2900 \text{ kgm}^{-3}$ ). The inversion routine requires that the source be located in the half-space. The source parameters from our inversion (given in the title of Figure 8 and in Table 3) are not significantly different from previously determined solutions for this event. The inversion procedure is nonlinear and the result may be dependent on the starting parameters. To verify that we had not found a local minimum, we significantly displaced the starting solution from the Harvard solution and reinverted the waveform data to verify that we still obtained a similar solution.

Having determined a minimum misfit solution, we performed a series of tests to estimate the effect on the source parameters produced by variations in the source velocity structure and to place bounds on the source parameters.

Source Region Velocity Structure: Since the crustal velocity structure in the south Caspian region is poorly known, our approach was to use a simplified version of a published crustal velocity models in the area of the earthquake if they exist, or the crustal velocity models of an analogous tectonic region if no crustal velocity model in the vicinity of the earthquake has previously been determined. We performed a number of tests for the 1978.11.04 earthquake to see how reasonable variations in source velocity structure affect estimates of the source parameters and just how different the source velocity structure could be before it significantly affected the inversion results. Figure 9 shows the results of our tests. The velocity models tested are given in the figure caption.

The McCaffrey-Abers inversion routine allows for only a simplified source structure. The first row in Figure 9 shows the minimum misfit solution from Figure 8. In our first test (Row B), we altered the velocity structure in such a way so as to give the same delay time between the direct phase and the surface reflection (the controlling factor in determining the depth), as the delay determined for the crustal velocity structure we thought most realistic (used in computing Row A). We then reinverted the whole data set. The synthetic waveforms for the minimum misfit solution for this velocity structure are indistinguishable from those in Row A. The focal parameters strike, dip, rake, and centroid depth are not significantly different from the results in Row A and only the seismic moment is different. We next made changes in the velocity structure which still would represent reasonable crustal velocity structures (Row C - D) without attempting to preserve the delay time

above the source. This again produced negligible changes in the synthetic waveforms from those shown in Row A. Row E and F show minimum misfit synthetics for more radical (and probably unrealistic) changes in the crustal velocity structures. These do show more significant changes but even in these cases, the source orientations have hardly changed from those in Row A. We conclude from these tests that reasonable variations in crustal velocity structure affect strike, dip, and rake less than other factors. Varying the source velocity structure did have a significant effect on centroid depth and seismic moment. These arise from variations in delay times between the direct and surface - reflected phases, and from variations in the reflection coefficients.

**Assessment of Source Parameter Uncertainties:** Thorough discussions of the assignment of uncertainties are given in McCaffrey & Nabelek (1987) and Molnar & Lyon-Caen (1989). For each event we studied, we have made extensive tests to determine uncertainty bounds on the centroid depth, and the strike, dip, and rake of the fault plane. These uncertainties are listed in Table 3.

Figure 10 summarizes only the tests we have made to place bounds on the strike, dip, rake and centroid depth of the 1978.11.04 event. The first row compares the observed seismograms and those computed for the minimum misfit solution. The following four rows compare the observed seismograms with those computed when one source parameter is held fixed at the smallest displacement from the minimum misfit value which resulted in a significant degradation of the synthetic fit. In making the full range of tests, we held one parameter (e.g. centroid depth) fixed at a value different from the minimum misfit value, and inverted for the remaining source parameters. We then successively increased the difference between the fixed parameter we were testing and its minimum misfit value until a significant difference was apparent between the observed seismograms and the synthetics computed for the particular combination of source parameters. Based on a range of tests of these parameters which are summarized in Figure 10, we estimate that for the 1978.11.04 earthquake the bounds on the centroid depth are  $\pm 5$  km, strike  $\pm 15^\circ$ , dip  $\pm 4^\circ$ , and rake  $\pm 20^\circ$ . For low-angle faulting events such as the 1978.11.04 earthquake the rake is not tightly constrained. The bounds on focal parameters shown in Table 3 are of similar magnitude to those noted in comparable studies in other regions (e.g. Molnar & Lyon-Caen, 1989; Taymaz et al., 1990).

## THE EARTHQUAKE OF 6 MARCH 1986

We now discuss the earthquake of 1986.03.06 in some detail for two reasons: it was the first moderately large earthquake to have occurred in the central Caspian seismic zone since the installation of the WWSSN, and it was the only event we studied whose seismograms suggested to us the possibility of a complex multiple rupture involving sub-events of different mechanisms. The S-wave spectrum from seismograms recorded at Askhabad (Golensky et al., 1989) and the coda spectrum (Rautian - personal communication) are complex, showing a constant low frequency level, a low frequency corner at 0.08 Hz above which there is a high frequency decay of  $\omega^{-1}$  to a second high frequency corner at 1.0 Hz above which the spectrum decays as  $\omega^{-2}$ . Smith et al (1991) attribute such a spectral shape to source complexity with the low frequency corner corresponding to the overall



source dimension and the high frequency corner related in some fashion to the size of the subevents. The P-wave first motion polarities (Fig. 7) tightly constrain a near vertical nodal plane, striking  $300^\circ$ . Our single source minimum misfit inversion solution is shown in Figure 11a. This solution is very similar to the best fitting double couple solution from the Harvard CMT catalogue. The agreement between the observed and synthetic seismograms is good at most stations. However, waveforms of stations lying on the focal sphere near the P-wave nodal plane (e.g. SHL, KOD, PTO, STU) show a weak initial P-wave arrival in keeping with the nodal position, but also show a large second pulse, shaped like an inverted "W", that follows the first motion by about 20 seconds. The single source shown in Figure 11a cannot reproduce the late pulse observed at these stations since the direct P and pP are both nodal, and hence of small amplitude, and sP leaves the focal sphere close to the node in the S radiation pattern.

With our poor knowledge of the undoubtedly complex crustal velocity structure in the vicinity of the Apshecon-Balkhan sill, it is impossible to adequately assess the contribution to seismogram complexity resulting from three-dimensional velocity structure. However, what appears to be missing from the P-waveforms of the near nodal seismograms is an inverted "W" P-wave arrival reminiscent of shallow depth, reverse faulting earthquakes (e.g., Jackson & Fitch, 1981). This suggests to us that the 6 March 1986 earthquake may have been a multiple event. Source complexity is also suggested by the shape of the source spectrum at regional stations in the U.S.S.R. (Golensky et al., 1989; Ratuian - personal communication). We therefore reinverted the P- and SH-waveforms, allowing for the existence of a second, delayed, reverse-faulting event. The starting source model for the second waveform inversion consisted of an initial event with the source mechanism shown in Figure 11a, followed 10 seconds later by a second reverse faulting event. The starting source orientation for the second reverse faulting event was guided by our interpretation of the observed waveforms. The reversed mechanism must be constrained to produce the observed P-waveforms at nodal stations such as SHL, KOD, PTO and STU, but not disturb the observed P-waveforms at African stations such as SLR and WIN, nor disturb the nodal character of the SH-waveforms at these stations. A  $45^\circ$  reverse faulting event with a strike near  $300^\circ$ , similar to the strike of the initial event, conforms to these requirements. We reinverted the waveform data, first constraining the mechanisms of the first event and solving for the fault plane parameters, centroid depth, source time function, and origin time offset of the second event. To produce the final solution shown in Figure 11b, we inverted the waveform data with all parameters of both events free. Synthetic waveforms for this double event solution fit observed waveforms at all azimuths equally well. The nodal character of SH-waves observed at African stations is preserved and provides the main constraints on the strike of the second event.

To assure ourselves that the initial conditions we assumed in constructing the second source were not overly restrictive and biasing our result, we reinverted the waveform data with both events having a starting solution similar to the normal faulting mechanism shown in Figure 11a, but the second source delayed by 10 seconds. The mechanism for the first event changed little, and the solution of the second event changed from having a normal to reverse mechanism. We reinverted the data with other starting depths for the second

event and again the final result was very near the solution shown in Figure 11b.

Figure 12 compares results for the single and double source solution and individual waveforms for the elements of the double source. The upper row compares the observed seismograms with those computed for the single source, minimum misfit solution. Stations SHL, KOD, PTO, and STU lie on the focal sphere near the P-wave node for the single source; station WIN lies near an SH node. The single source synthetics poorly match the observed seismograms at the four P-wave nodal stations, as discussed above. The P-wave seismogram recorded at SLR is reasonably well fit by the synthetic, with the exception of the large back swing. The SH nodal character observed in the WIN seismogram is preserved and the SH waveform observed at KOD is reasonably well fit with the exception of the large back swing which is larger in the synthetic than in the observed seismogram.

The second row of seismograms compares observed waveforms at the same stations with synthetic seismograms computed for the double source solution. The fit at WIN is similar to that for the single source, and fits for all other stations are significantly improved. Rows 3 and 4 show the contributions to the seismograms of the individual components of the double source. Both events have similar seismic moments. We performed a series of tests as described above, to estimate bounds on the centroid depth, strike, dip, and rake of the second event on the synthetic and compare these with the observed seismogram. From this comparison we estimate that the centroid depth, strike, dip, and rake of the second event are resolved to  $\pm 4$  km,  $\pm 15^\circ$ ,  $\pm 5^\circ$ , and  $\pm 8^\circ$ , respectively. Note that the seismic moment of this second source is almost as great as that of the first source. The combined seismic moment of the two subevents is  $5.1 \times 10^{17}$  Nm compared to  $6.4 \times 10^{17}$  Nm for the Harvard CMT solution.

It is difficult to assess whether the three dimensional velocity structure in the source region of the 1986.03.06 earthquake could produce the seismogram complexity that we attribute to a later sub-event. Two other moderate-sized earthquakes occurred in the central Caspian Sea on 16 and 17 September 1989 (1989.09.16, 1989.09.17) and our waveform inversion results for these two events are shown in Figures A13 and A14. P-waveforms of 1986.03.06, 1989.09.16, and 1989.09.17 at common stations are compared in Figure 13. As a result of the decline in performance of the WWSSN, data for the 1989 events are less complete than for 1986.03.06. The minimum misfit solution for both of the 1989 events have a normal faulting mechanism similar to the single source minimum misfit solution for 1986.03.06. However, WWSSN seismograms recorded to the northwest (e.g., PTO, VAL, NUR, WES), while not showing the same initial nodal character as seismograms recorded at similar azimuths for the 6 March 1986 event, do show some evidence for a similar later pulse in the P-wave train (Figs. A13, A14). Although the GDSN instrument response tends to blur details of the source time function and WWSSN data are scarce for the 1989 events, we inverted seismograms for the 1989.09.16 earthquake allowing the possibility of a second source. This resulted in a mechanism where the first source was similar to that in Figure A13, and a second source whose seismic moment was less than 10% that of the initial source. Three double earthquakes with similar time delays and mechanisms for the second events are somewhat suspect, and this may imply that the secondary arrivals result from crustal velocity structure complexities in the source region.

However in a plane layered structure there is no direct P or SH arrival for the European and Indian stations showing the second pulse. It would therefore be necessary for the late pulse to be the result of bent raypaths, that is rays refracted after leaving the focal sphere at different take off angles. On the other hand, there is another, smaller earthquake in this central Caspian belt (1987.12.19) with a Harvard CMT solution having almost the same reverse faulting mechanism as we postulate for the second sub-event of 1986.03.06. The earthquake of 1987.12.19 was too small for us to be able to confirm the Harvard CMT solution using long period P and SH waveforms. Although we prefer the double source explanation for the P-wave complexities discussed above for 1986.03.06, we are not able to rule out the possibility that complexities in the observed waveforms are the result of source region velocity structure.

### TECTONICS OF THE SOUTH CASPIAN BASIN

The minimum misfit solutions for the other fourteen events we studied are presented in Appendix A. Their orientations are consistent to within a few degrees with the first motion polarity data. The few inconsistent first motion polarities are discussed in Appendix A. Figure 14a shows the fault plane solutions for these events (Table 3). Figure 14b shows fault plane solutions for other events which we have not analyzed: either first motion solutions of Jackson & McKenzie (1984) which occurred prior to establishment of the WWSSN (1957.07.02) or which produced insufficient long-period waveforms for us to analyze using the procedure outlined above, Harvard CMT solutions that were too small for us to study their P and SH waveforms, or the 20 June 1990 event (Gao & Wallace, 1991). With some exceptions, the patterns of focal mechanisms shown in Figures 14a and 14b are generally similar, giving us some confidence in the solutions we were unable to confirm by waveform inversion. In our discussion of the tectonics, we will rely primarily on the sixteen events we have studied (Fig. 14a) and the mechanism of the 20 June 1990 event (Gao & Wallace, 1991) (large symbol, Fig. 14b), but we will make cautious use of the first motion and CMT solutions of the smaller events.

**Slip Vectors:** Figure 15 shows the horizontal projection of the slip vectors for the events in Figure 14. Choosing the slip vector required us to identify one of the two nodal planes in each fault plane solution as the fault plane. Both the Buyin Zara earthquake (1962.09.01) (Appendix A) and the Rudbar-Tarom earthquake (1990.06.20) (Berberian et al, 1991) were accompanied by surface faulting, and the choice of the fault plane is straightforward (Ambraseys, 1963; Berberian et al, 1991). No surface faulting was recognized for the Karnaveh earthquake (1970.07.30). However, relative relocations of the aftershocks of this event defined an elongated pattern trending north-northeast (Jackson & Fitch, 1979), approximately parallel to the strike of one of the nodal planes (Figure A2) and also parallel to a nodal plane of a large aftershock with a similar mechanism to that of the main shock. The aftershock pattern suggests that the Karnaveh earthquake occurred on a northeast-trending fault with predominantly left-lateral strike-slip motion.

Other earthquakes such as the 1957.07.02, 1969.01.03, and 1983.07.22 events are almost pure thrust and hence the choice of the slip vector orientation is not very sensitive to the

choice of the fault plane. For the 1969.01.03 and 1983.07.22 events we chose the planes dipping northeast to be consistent with the local topography; however, in both cases choosing the other plane would change the orientation of the slip vector by less than  $10^\circ$ . The other events studied all have one nodal plane that, if chosen as the fault plane, implies a slip vector similar to that of an adjacent earthquake whose slip vector ambiguity is resolved. This determined our choice of slip vectors for those events.

In the case of strike-slip events, this reasoning is dangerous. The 1990.06.20 event, which produced surface faulting, had a slip vector almost perpendicular to that of a nearby reverse faulting earthquake (1983.07.22) (See Berberian et al, 1991; Gao & Wallace, 1991). Three other strike-slip events occurred near thrust faulting earthquakes (1983.03.26, 1984.02.22, and 1990.01.20). For all of these we mark both possible slip vectors on Figure 15. The convention we have used in Figure 15 is to show the motion of the S or E side relative to the N or W side.

The inset in Figure 15 shows the orientation of the tension axes of the five normal faulting events in the central Caspian. All of these events have a shallow dipping, NNE striking tension axis.

**Talesh Mountains:** It is clear from the earthquake mechanisms we have studied that the Talesh and NW Alborz mountains overthrust the south Caspian Basin as suggested by Berberian (1983) and Jackson & McKenzie (1984). The slip vectors on the shore of the Talesh Mountains show the motion of the Caspian Sea westward beneath the Azerbaijan-Talesh block, which moves east relative to both Iran and the Arabian-Eurasia collision zone in eastern Turkey. This motion of the Azerbaijan-Talesh block may be accommodated inland by conjugate strike-slip faulting. The focal mechanism of the 1976.02.03 earthquake (Fig. 14b) is consistent with left lateral faulting on a NNE plane, parallel to a prominent NNE lineament followed by the Araxes River. Berberian & Arshadi (1976), Tchalenko (1977), and Ambraseys & Melville (1982) have studied faulting associated with two large northwest Iranian earthquakes which occurred in 1721 and 1786 (Fig. 6b). All agree that the southwest side of the fault was down-dropped, but disagree as to whether there was a significant right-lateral strike-slip component. Stream diversions are visible on aerial photographs (Tchalenko, 1977) suggesting right lateral offset but these have not been verified on the ground. The combination of left lateral faulting following the Araxes lineament along the Iran-USSR border, probable right lateral faulting extending southeast from the North Anatolian fault system, and low angle thrusting along the Talesh Mountains support Jackson & McKenzie's (1984) suggestion of the easterly expulsion of northwest Iran away from the collision zone in the Caucasus and the overthrusting of the south Caspian Basin. This motion is probably responsible for the N-S trending folds seen in the sedimentary cover offshore, east of the Talesh Mountains (Fig. 6a), and is presumably favored by the "oceanic-like" crust of the south Caspian Basin.

**Alborz Mountains:** The Rudbar-Tarom earthquake (1990.06.20) was by far the largest earthquake to occur in northern Iran this century. Berberian et al (1991) report at least 80 km of surface faulting along three discontinuous fault segments. These are arranged

in a right-stepping en-echelon pattern, and are separated by gaps in the observed surface rupture. The three segments range in strike from  $95^\circ$  to  $120^\circ$  and have oblique, left-lateral and reverse motion on faults that are sub-vertical or have steep dips to the S or SSW. The maximum surface displacements were 60 cm horizontal (left-lateral) and 95 cm vertical with the south side up. The moment tensor solution (Gao & Wallace, 1991) for the main shock suggests a complex rupture consisting of at least three sub-events, and had a significant non-double couple component. However, no change in fault geometry or slip direction during the main rupture could be resolved. The best fitting double couple (Table 4) has a strike  $292^\circ$ , dip  $88^\circ$ , and rake  $-9^\circ$  which are consistent with the mapped faults. Berberian et al (1991) also reported mechanisms for two aftershocks. The largest (1990.06.21) had a focal mechanism involving thrusting (strike  $26^\circ$ , dip  $69^\circ$ , rake  $87^\circ$ ) with a centroid depth of 17 km and a moment of  $5.7 \times 10^{17}$  Nm ( $M_w$  5.8) similar to those in the adjacent Talesh Mountains. A second large aftershock (1990.06.24) had a mechanism similar to that of the main shock (strike  $235^\circ$ , dip  $70^\circ$ , rake  $-164^\circ$ ), a significantly shallower centroid depth (8 km), and a moment of  $2.2 \times 10^{17}$  Nm ( $M_w$  5.5).

The 1990.06.20 earthquake occurred close to an earthquake that involved high-angle reverse faulting (1983.07.22). The slip vector of the 1990.06.20 main shock is in the wrong sense (left-lateral) to represent the relative motion between the Talesh-Azerbaijan block and Iran. We think it probable that the deformation in this part of the NW Alborz Mountains involves oblique, left-lateral shortening that is partitioned into pure left-lateral strike-slip (i.e. 1990.06.20) and pure thrusting (i.e. 1983.07.22) in almost the same region. Such an interpretation is consistent with the almost perpendicular slip vectors for the 1990.06.20 and 1983.07.22 earthquakes, and with those slip vectors being approximately parallel and perpendicular, respectively, to the regional topography and fold axes (see also Berberian et al, 1991). Jackson & McKenzie (1984) suggested that the more easterly oriented slip vectors observed further south (e.g. the slip vector of  $42^\circ$  in 1962.09.01) represent the direction of regional convergence between Iran and South Caspian. As a consequence, there should be a component of left-lateral slip in the Alborz Mountains. In the high Alborz Mountains, it appears that this oblique regional convergence is partitioned into strike-slip (1990.06.20) and reverse faulting (1983.07.22) whereas it remains as oblique slip in the lower elevations to the south in north-central Iran. The component of left-lateral slip in the Alborz Mountains is small, which may account for the apparent infrequency of strike-slip faulting earthquakes in the range.

The confirmed existence of adjacent strike-slip and thrust mechanisms with nearly perpendicular slip vectors in the NW Alborz Mountains makes us unsure of the actual slip vector for the strike slip events near thrust events elsewhere in the Alborz Mountains, which is why we include both possible slip vectors for 1983.03.26 and 1990.01.20. If the EW nodal planes were the fault planes in these earthquakes, their slip vectors are similar and in the same sense as for the 1990 Rudbar-Tarom earthquake. In this case, these events too are evidence for partitioning of strike-slip and thrust motion in the Alborz. South of the high Alborz Mountains, in the Central Iranian Plateau, the motion is apparently not partitioned and occurs as faults with oblique slip (e.g. 1962.09.01, 1980.12.19, 1980.12.22).

Most slip vectors in the Alborz are directed NE (Fig. 15) consistent with convergence

between central Iran and the south Caspian Basin. Apart from the strike slip events, which we have discussed above, the only exception is a small ( $M_w$ 5.1) normal faulting event (1988.08.23) for which only a Harvard CMT solution is available (Fig. 14b). We are uncertain how to assess this event and cannot evaluate the reliability of the solution. There are no other normal fault solutions like it in the Alborz (The 1970.07.30 Karnaveh earthquake, although it had a normal component, had a slip vector consistent with the NE motion between Iran and the south Caspian Basin). Below a certain threshold in magnitude it is quite common for small events to have a greater variety of mechanisms than the larger events (e.g. Lyon - Caen et al, 1988). Taymaz et al (1991) report a well-constrained reverse-faulting event of  $M_w$ 5.5 in a region of NW Turkey that is dominated by normal faulting. With only one anomalous event (that is probably not well constrained) in the Alborz, we cannot assess its significance further. The component of normal faulting seen in 1970.7.30 suggests that the low elevations and thick sediments in the Turkmenian Lowlands, (Fig. 6a) may be partly related to extension-induced subsidence.

**The Kopet Dag Mountains:** The Kopet Dag has an abrupt northeast topographic front (Fig. 6a) that was associated with a large earthquake in 1948 near the city of Askhabad. Field and teleseismic data for this earthquake are ambiguous (Rustanovich & Shirakova, 1964; Tchalenko, 1975; and Jackson & McKenzie, 1984), but several authors associate the linearity of the abrupt topographic scarp with right-lateral strike-slip motion, whereas elsewhere in the Kopet Dag there is certainly thrust faulting with northeast directed slip vectors. One other event (1984.02.22, Figure 14a) further NW is consistent with right lateral strike-slip on this trend. The Kopet Dag may thus be another example of partitioning of strike-slip and thrust motion that are postulated to occur in the Alborz Mountains.

**Central Caspian Seismic Belt:** In the belt of seismicity which extends across the central Caspian Sea following the Apscheron - Balkan sill, normal faulting mechanisms with an ESE strike and focal depths of 30-50 km dominate. It is improbable that the normal faulting events represent the motion between the southern Caspian and Eurasia. If the steep nodal planes were the fault planes, then the sense of motion, north side down, is the reverse of that seen in the bathymetry, i.e., deep water and thick sediments to the south; if the nodal planes dipping gently south were the fault planes, some expression of extension might be expected at the surface. Yet seismic reflection surveys report folding of the surface sediments (Zonenshain & Le Pichon, 1986), suggesting shortening. This is compatible with the high angle reverse faulting mechanism that we postulate for a possible second sub-event of the 1986.03.06 earthquake at a shallower depth than the normal faulting earthquakes. The CMT solution for the 1987.12.19 earthquake (Fig. 14b) shows reverse faulting with a NW-SE strike, and supports this interpretation. However, it was a small ( $M_w$ 4.9) event, and in the light of the anomalous small event (1988.08.23) in the Alborz Mountains (Fig. 14b), we do not place much confidence in it.

We suspect that shortening occurs as the continental crust of the northern Caspian is thrust over the "oceanic" crust of the southern Caspian Basin, and that the normal faulting events occur in the deep (possible mantle) basement of the material being overthrust. It

is possible that a subducting mantle slab with very low seismicity dips north beneath the Apsheron-Balkhan sill, accounting for the north-dipping T axes of the normal faulting solutions. Another possibility is that the normal faulting is the result of plate bending exceeding the elastic strain limit as the north side of the Caspian Sea is thrust over the south Caspian Basin. This would be analogous to the normal faulting seaward of the oceanic trench and is a possible cause of the normal faulting beneath the Ganges Basin south of the Himalayas thrust front (Lyon-Caen & Molnar, 1985). The low level of seismic shortening across the central Caspian suggests that most of the Iran-Eurasia shortening is accommodated in the much more active Alborz thrust belt. The seismicity of the trans-Caspian belt continues northwest into the Caucasus and southeast into the Kopet Dag. Reverse faulting and thrusting on ESE striking planes are dominant in both of these areas.

## DISCUSSION

The two most important new results that our study demonstrates are the partitioning of thrust and strike slip motion in the Alborz, and the existence of a belt of normal faulting earthquakes across the central Caspian Sea. Both have important implications for the tectonics of the region.

The partitioning of oblique shortening into pure thrust and pure strike-slip motion is not particularly rare, though there is some debate as to why it occurs (e.g. McKenzie & Jackson 1983, Zoback et al., 1987, Mount & Suppe 1987, Molnar 1991). McKenzie & Jackson (1983) point out that, if fault-bounded blocks move in response to forces imposed on their bases by continuous flow in the mantle lithosphere beneath the seismogenic upper crust, then oblique slip on faults oriented obliquely to the strike of the deforming zone cannot accommodate large finite deformation because they rotate about a vertical axis as they move. One way in which the faults can take up large finite strains is if the motion on them is partitioned into pure shortening and pure strike slip. A clue to this process may lie in the observation that the motion is partitioned in the high Alborz, where strains are obviously large, but not in the lower elevations of north-central Iran, where strains are presumably smaller. The faults may have become organized into a stable geometry as the strain increased. This may explain why partitioning is common in other places where strains are large, such as in California (e.g. Mount & Suppe, 1987), the NW Zagros and NE Kopet Dag Mountains of Iran (Tchalenko & Braud, 1974; Tchalenko, 1975; Jackson & McKenzie, 1984) and in island arcs (e.g. Fitch, 1972), but oblique slip is by no means rare in places where total strain is probably relatively small, such as in the lower elevations of central Iran (Jackson & McKenzie, 1984). If partitioning really does occur because it is the favored way for crustal rocks to accommodate large-scale and large magnitude oblique motion, then knowledge of the orientations of stress in the upper crust adjacent to such faults will provide little insight into the dynamics of the deformation, as pointed out by Molnar (1991).

The significance of the normal faulting earthquakes in the belt across the central Caspian Sea is enigmatic. For reasons expressed above we do not believe that they represent a southward motion of the Caspian Sea relative to Eurasia. Shortening at depths shallower than the normal faulting is implied by the orientation of folds in the sediment,

a possible (but ambiguous) second sub-event of the 1983.03.06 earthquake that involved reverse faulting, and a CMT solution for a small (and probably not well-constrained) earthquake that involved thrusting on 1987.12.19 (Fig 14b). We suspect that this shortening does indeed represent a NNE motion of the south Caspian basin relative to Eurasia, but that the motion is slow and has not produced many earthquakes. In this respect the convergence may be similar to that in the Makran of SE Iran (Jackson & McKenzie, 1984) and along the Washington - Oregon coast of the NW United States (Heaton & Kanamori, 1984), both of which have rather low levels of seismicity, but may be capable of generating infrequent large earthquakes. Our preferred interpretation of the normal faulting events is that they are related to either bending or shallow down-dip extension of a slab of mantle lithosphere attached to and beneath the Caspian Sea, as it is overthrust by Eurasia, but this interpretation cannot be regarded as conclusive. If the motion of the Caspian Sea relative to Eurasia is indeed slow, then the motion in the Alborz between central Iran and the south Caspian Basin will be almost the same as that between Iran and Eurasia, as was assumed by Jackson & McKenzie (1984) in their analysis of the tectonics of Iran.

We conclude that the active tectonics implied by the observed faulting in the Talesh, Alborz and central Caspian Sea will lead to the eventual destruction of the south Caspian Basin and perhaps the formation of an intermediate depth, dipping seismic zone in the continental interior, similar to that presently observed in the Hindu Kush.

#### ACKNOWLEDGEMENT

We thank M. Zirbes for supplying digital GDSN data for recent events, B. Dost for use of computing facilities at the ORFEUS Data Center, R. McCaffrey for giving us the most recent copy of his waveform inversion routine, V. Martynov for helping us with the Soviet literature and T. Taymaz for supplying copies of the WWSSN records of the March 6, 1986 Caspian earthquake. D. McKenzie and M. Berberian provided helpful comments and reviewed the manuscript. We would like to thank Heather Lynskey for patient typing of the manuscript over an over an .. This work was partially supported by the Lawrence Livermore National Laboratory contract number -740-ENG-48, the Defense Advanced Research Projects Agency contract number F19628-89-K-0022 and Air Force Geophysical Laboratory contract number F19628-90-K-0046. This work was largely done while Keith Priestley was at the University of Cambridge while on sabbatical leave from the University of Nevada, Reno. James Jackson thanks the Dean of the School of Earth Sciences, Stanford University, for support during completion of this work.

#### REFERENCES

- Adamia, S.A., Lordkipanidze, M.B., & Zakariadze, G.S., 1977. Evolution of an active continental margin as exemplified by the Alpine history of the Caucasus, *Tectonophysics*, 40, 183-199.
- Ambraseys, N.N., 1963. The Buyin-Zara (Iran) earthquake of September, 1962: a field report, *Bull. Seism. Soc. Am.*, 53, 705-740.
- Ambraseys, N.N., & Melville, C.P., 1982. *A History of Persian Earthquakes*, Cambridge University Press, 219p.



- Amursski, G.I., Tiunov, K.V., Khrikov, B.A., & Shlezinger, A.E., 1968. Structure and tectonic position of the Great Balkhan, *Akademii Nauk SSSR*, 53p.
- Berberian M., & Arshadi, S., 1976. On the evidence of the youngest activity of the North Tabriz fault and the seismicity of Tabriz city, Rep. Geol. Surv. Iran, No. 39, 397-418.
- Berberian, M., & King, G.C.P., 1981. Towards a paleogeography and tectonic evolution of Iran, *Can. J. of Earth Sci.*, 18, 210-265.
- Berberian, M., 1983. The Southern Caspian: A compressional depression floored by a trapped, modified oceanic crust, *Can. J. Earth Sci.*, 20, 163-183.
- Berberian, M., Qorashi, M., Jackson, J.A., Priestley, K.F., Wallace, T., The Rudbar-Tarom earthquake of 20 June 1990 in NW Persia: preliminary field and seismological observations, and its tectonic significance, *Bull. Seism. Soc. of Am.*, in press
- Fedynsky, V.V., Fomenko, K.E., Garkalenkov, J.A., Goncharov, V.P., Khrychev, B.A., Malovitsky, Y.P., Milashin, A.P., Neprochnov, Y.P., & Ushakov, S.A., 1972. The Earth's crust of the inland seas and continental depressions of the west Tethys region, 24th International Geological Congress, Montreal, P.Q. Section 3, 51-57.
- Fitch, T.J., 1972. Plate convergence, transcurrent faults, and internal deformation adjacent to southeast Asia and the western Pacific, *J. Geophys. Res.*, 77, 4432-4460.
- Fredrich, J., McCaffrey, R., & Denham, D., 1988. Source parameters of seven large Australian earthquakes determined by body waveform inversion, *Geophys. J.*, 95, 1-13.
- Futterman, W.I., 1962. Dispersive body waves, *J. Geophys. Res.*, 67, 5279-5291.
- Galperin, E.I., Kosminskaya I.P., & Krakshina, P.M., 1962. Main characteristics of deep waves registered by deep seismic sounding in the central part of the Caspian Sea, Deep Sounding of the Earth's Crust in the USSR. Moscow. Gosloptekhizdat, 227-250, (in Russian).
- Gao, L., & Wallace, T.C., 1991. Aftershocks of the 1990 western Iran ( $M_w$  7.3) earthquake, *Bull. Seism. Soc. Am.*, to be submitted.
- Golensky, G.L, Kondorskya, N.V., Zakarova, A.E., Vandeshiva, N.V., Agalapova, E.B., Agamepzor, S.R., Bruk, M.G., Garagozov, D., Kuleiv, F.T., Logova, N.A., Muragov, C.M., Rautian, T.G., Panake, B.M., Rakemov, A.R., Rogozhen, E.A., Shafadeyaiv, R.H., & Chepkunac, L.C., 1989. The Caspian earthquake of March 6, Earthquakes in the U.S.S.R. in 1986, *Akademii Nauk SSSR*, 58.
- Heaton, T.H., & Kanamori, H., 1984. Seismic potential associated with subduction in the northwestern United States, *Bull. Seism. Soc. Am.*, 74, 933-947.
- Jackson, J.A., & Fitch, T.J., 1979. Seismotectonic implications of relocated aftershock sequences in Iran and Turkey, *Geophys. J. R. astr. Soc.*, 57, 209-229.
- Jackson, J.A., & Fitch, T.J., 1981. Basement faulting and the focal depths of the larger earthquakes in the Zagros mountains (Iran), *Geophys. J. R. astr. Soc.*, 64, 561-586.
- Jackson, J., & McKenzie, D., 1984. Active tectonics of the Alpine-Himalayan Belt between western Turkey and Pakistan, *Geophys. J. R. astr. Soc.*, 77, 185-264.
- Kadinsky-Cade, K., Barazangi, M., Oliver, J., & Isacks, B., 1981. Lateral variations of high frequency seismic wave propagation at regional distances across the Turkish and Iranian plateaus, *J. Geophys. Res.*, 86, 9377-9396.
- Letouzey, J., Biju-Duval, B., Dorkel, A., Gonnard, R., Kristchev, K., Montadert, L., & Sungurlu, O., 1977. The Black Sea: A marginal basin, geophysical and geological data,

In: Biju-Duval, B., & Montadert, L., (editors), *International Symposium on the Structural History of the Mediterranean Basin*, Edition Technip, Paris, 363-379.

Lyon-Caen, H., & Molnar, P., 1985. Gravity anomalies, flexure of the Indian Plate, and the structure, support and evolution of the Himalaya and Ganga Basin, *Tectonics*, 4, 513-538.

Lyon-Caen, H., Armijo, R., Drakopoulos, J., Baskoutas, J., Delibassis, N., Gaulon, R., Kouskouna, V., Latoussakis, J., Makropoulos, K., Papadimitriou, P., Papanastassiou, D., & Pedotti, G., 1988. The 1986 Kalamata (S. Peloponnese) earthquake: Detailed study of a normal fault and tectonic implications, *J. Geophys. Res.*, 93, 14,967-15,000.

Malovitsky, Y.P., 1968. History of the geotectonic development of the depression of the Caspian Sea, *Izvestiya Akademii Nauk SSSR, Seriya Geologicheskaya*, 10, 103-120.

Malovitsky, Y.P., Levin, L.E., Milashin A.P., & Zorina, Y.G., 1970. Gruppya Youshnykh Morey. Tektonika I Neftegazonosnost Okrunnykh I Vnutrennykh Morey SSSR, Nedra, Moscow.

McCaffrey, R., & Nabelek, J., 1987. Earthquakes, gravity, and the origin of the Bali Basin: an example of a nascent continental fold-and-thrust belt, *J. Geophys. Res.*, 92, 441-460.

McCaffrey, R., & Abers, G., 1988. SYN3: A program for inversion of teleseismic body wave forms on microcomputers, Air Force Geophysics Laboratory Technical Report, AFGL-TR-88-0099, Hanscom Air Force Base, MA, 50p. ADA198940

McKenzie, D.P., & Jackson, J.A., 1983. The relationship between strain rates, crustal thickening, paleomagnetism, finite strain and fault movements within a deforming zone, *Earth Planet. Sci. Lett.*, 65, 182-202, and correction, *ibid.*, 1984. 70, 444.

Molnar, P., 1991. Brace-Goetze strength profiles, the partitioning of strike-slip and thrust faulting at zones of oblique convergence, and the stress-heat flow paradox of the Andreas Fault, In: *The Brace Volume*, Evans B., & Wong, T.F., (editors), in press.

Molnar, P., & Lyon-Caen, H., 1989. Fault plane solutions of earthquakes and active tectonics of the Tibetan Plateau and its margin, *Geophys J. Int.* 99, 123-153.

Mount, V.S., & Suppe, J., 1987. State of stress near the San Andreas Fault: implications for wrench tectonics, *Geology*, 15, 1143-1146.

Muratov, M.V., 1972. Formation history of the deep Black Sea basin as compared with deep basins of the Mediterranean, *Geotektonika*, 5, 22-41 (in Russian).

Nabelek, J., 1984. Determinations of earthquake source parameters from inversion of body waves, *Ph.D. thesis*, M.I.T., Cambridge, MA.

Neprochnov, Y.P., 1968. Structure of the Earth's crust of epicontinental seas: Caspian, Black and Mediterranean, *Can. J. of Earth Sci.*, 5, 1037-1043.

Nowroozi, N.N., 1972. Focal mechanism of earthquakes in Persia, Turkey, West Pakistan and Afghanistan and plate tectonics of the Middle East, *Bull. Seis. Soc. Am.*, 62, 823-850.

Rezanov, I.A., & Chamo, S.S., 1969. Reasons for absence of a granitic layer in basins of the South Caspian and Black Sea type, *Can. J. of Earth Sci.*, 6, 671-678.

Rustanovich, D.N., & Shinakova, E.I., 1964. Some results of a study of the Askhabad earthquake of 1948, *Izvestiya Akademii Nauk SSSR, Seriya Geofizika*, 1077-1080.

Shikalibeily, E.S., & Grigoriant, B.V., 1980. Principal feature of the crustal structure of the south Caspian basin and the conditions of its formation, *Tectonophysics*, 69, 113-121.

Shlezinger, A.Y., 1981. Structure of the Sedimentary Cover of the Black Sea Basin, In:

Peive A.V. & Pushcharovskii, Y.N., (editors), *Problemy Tektoniki Zemnoi Kory*, Nauk, Moscow, 237-262 (in Russian).

Smith, K.D., Brune, J.N., & Priestley, K.F., 1991. The seismic spectrum, radiated energy, and the Savage and Wood inequality for complex earthquakes, *Tectonophysics*, 188, 303-320.

Sorokhtin, O.G. (editor), 1979. Geodynamics, *In: Okeanologiya. Geofizika Okeanshogo Dna*. Nauk. Moscow, 2, 375 (in Russian).

Taymaz, T., Jackson, J.A., & Westaway, R., 1990. Earthquake mechanisms in the Hellenic Trench near Crete, *Geophys. J. Int.*, 102, 695-731.

Taymaz, T., Jackson, J., & McKenzie, D., 1991. Active tectonics of the north and central Aegean Sea, *Geophys. J. Int.*, 106, 433-490.

Tchalenko, J.S., 1975. Seismicity and structure of the Kopet Dagh (Iran, USSR), *Phil. Trans. R. Soc.*, 278, 1-25.

Tchalenko, J.S., 1977. A reconnaissance of the seismicity and tectonics at the northern border of the Arabian plate; Lake Van region, *Rev. Geogr. Phys. Geol. Dyn*, 19, 189-208.

Tchalenko, J.S., & Braud, J., 1974. Seismicity and structure of the Zagros (Iran): the Main Recent Fault between 33 and 35°N, *Phil. Trans. R. Soc. A*, 277, 1-25.

Vardapetyan, A.N., 1981. Late Cenozoic plate tectonics of the Black Sea-Caspian region, Ph.D. thesis, Inst. of the Oceanology, Moscow, 24 (in Russian).

Yanshin, A.L., Bassenyants, S.A., Pilipenko A.I., & Shlezinger, A.E., 1980. New Data on the time of formation of the Black Sea deep basin, *Dokl. Akad. Nauk SSSR*, 252, 223-227 (in Russian).

Zoback, M.D., Zoback, M.L., Mount, V.S., Suppe, J., Eaton, J.P., Healy, J.H., Oppenheimer, D., Reasenber, P., Jones, L.M., Raleigh, C.B., Wong, I.G., Scotti, O., & Wentworth, C., 1987. New evidence on the state of stress of the San Andreas fault system, *Science*, 238, 1105-1111.

Zonenshain, L.P., & Le Pichon, X., 1986. Deep basins of the Black Sea and Caspian Sea as remnants of Mesozoic back-arc basins, *In: Aubouin, J., Le Pichon, X., & Monin, A.S., (editors), Evolution of the Tethys, Tectonophysics*, 123, 181-211.

Table 2 : Earthquake Hypocentral Data

d	Date		Origin Time	Latitude ( °N )	Longitude ( °E )	Depth(km)		m <sub>b</sub>	M <sub>s</sub>	Source*	Number of Stations
	m	y				P	pP				
2	7	1957	00:42:23	36.14	52.7 <sup>^</sup>	10			6.8	ISS	
1	9	1962	19:20:40	35.63	49.87	27			7.2	ISS	
3	1	1969	03:16:37	37.10	57.83	4		5.4		ISC	163
30	7	1970	00:52:20	37.85	55.94	22		5.7		ISC	306
14	2	1971	16:27:32	36.62	55.74	4		5.3		ISC	236
3	2	1976	16:40:41	39.93	48.41	67		5.2		ISC	226
25	5	1977	11:01:47	34.91	52.06	39	41	5.3		ISC	258
4	11	1978	15:22:19	37.71	48.95	37	36	6.0	6.1	ISC	418
1	10	1979	07:37:01	40.07	51.87	42	47	5.0	4.4	ISC	150
9	12	1979	09:12:04	35.14	56.87	23		5.2	5.5	ISC	248
4	5	1980	18:35:19	38.09	49.07	36	36	5.3	6.1	ISC	323
22	7	1980	05:17:08	37.36	50.35	37	36	5.3	5.1	ISC	238
3	12	1980	04:26:15	37.17	50.47	44	22	5.1	4.7	ISC	233
19	12	1980	01:16:56	34.50	50.67	29	43	5.5	5.8	ISC	354
22	12	1980	12:51:21	34.49	50.67	39	18	5.4	5.2	ISC	299
4	8	1981	18:35:43	38.21	49.41	40	29	5.4	5.2	ISC	358
19	11	1981	14:10:37	40.78	49.26	42	42	5.1	4.2	ISC	236
26	3	1983	04:07:19	36.06	52.28	33	25	5.4	4.9	ISC	261
22	7	1983	02:41:01	36.98	49.23	43	33	5.6	5.0	ISC	299
22	2	1984	05:44:37	39.52	54.11	0		5.1	5.8	ISC	296
29	10	1985	13:13:40	36.75	54.81	13	8	6.0	6.0	ISC	518
6	3	1986	00:05:37	40.37	51.60	28	63	6.1	6.2	ISC	614
11	6	1986	20:15:41	40.28	51.71	41	49	5.2	4.6	ISC	305
10	4	1987	06:43:20	37.21	57.70	6	35	5.0		ISC	226
7	9	1987	11:32:27	39.37	54.76	39		5.5	5.5	ISC	442
19	12	1987	08:27:36	40.72	52.05	80	67	4.9		ISC	198
23	8	1988	05:30:51	35.42	52.28	35	25	5.0	4.8	ISC	249
16	9	1989	02:05:09	40.34	51.53	55		6.4	6.5	PDE	563
17	9	1989	00:53:40	40.20	51.75	51		6.1	6.1	PDE	533
20	1	1990	01:27:10	35.83	52.95	25		5.5	5.9	PDE	348
20	6	1990	21:00:10	36.96	49.41	19		6.4	7.7	PDE	352

ISS International Seismological Summaries ( - 1963)  
 SC International Seismological Center (1964 - 1988)  
 EDR Earthquake Data Reports (1989 - 1990)  
 PDE Preliminary Determination of Epicenters (1990 - )

Table 3 : Source Mechanism Data

d	Date		Depth (km)	Mo $\times 10^{17}$ Nm	$M_w$	Strike	Dip	Rake	Slip* Vector	Phases	
	m	y								P	SH
1	9	1962	10±4	367.8	7.0	101° ± 10°	52° ± 3°	70° ± 15°	42°	10	4
3	1	1969	7±4	1.9	5.5	132° ± 15°	50° ± 5°	95° ± 8°	33°	6	4
30	7	1970	11±4	42.9	6.3	293° ± 20°	56° ± 5°	210° ± 10°	23°	23	16
14	2	1971	11±5	4.0	5.7	336°	39°	93°	62°	9	
4	11	1978	21±5	19.0	6.1	346° ± 15°	79° ± 4°	95° ± 20°	77°	22	16
4	5	1980	15±5	40.2	6.3	181° ± 10°	84° ± 10°	267° ± 15°	91°	21	17
19	12	1980	14±8	14.0	6.0	115° ± 20°	41° ± 8°	120° ± 15°	25°	10	11
22	12	1980	15±5	2.8	5.6	113° ± 20°	56° ± 8°	125° ± 15°	23°	4	8
4	8	1981	20±8	2.4	5.6	154° ± 15°	35° ± 15°	32° ± 20°	64°	15	10
22	7	1983	10±8	1.9	5.6	120° ± 20°	35° ± 8°	83° ± 15°	30°	10	7
22	2	1984	27±4	5.1	5.7	106° ± 20°	60° ± 10°	174° ± 20°	16°	7	21
29	10	1985	13±5	21.8	6.2	246° ± 15°	66° ± 10°	71° ± 10°	16°	31	14
6	3	1986a	31	25.2	6.2	299° ± 15°	88° ± 5°	275° ± 8°	29°	35	15
6	3	1986b	13±4	21.8	6.2	114° ± 15°	63° ± 5°	87° ± 8°	23°	35	15
7	9	1987	30±8	2.3	5.5	305° ± 10°	10° ± 10°	103° ± 20°	22°	14	12
16	9	1989	31±10	68.4	6.5	80° ± 15°	26° ± 5°	225° ± 15°	38°	22	14
17	9	1989	35±10	21.7	6.2	277° ± 15°	50° ± 5°	249° ± 15°	38°	21	20

\*Slip vector direction is for S or E side of fault relative to N or W side

Table 4 : Source Mechanisms From Other Studies.

Date			Depth (km) <sup>†</sup>	M <sub>0</sub> x10 <sup>17</sup> Nm	M <sub>w</sub>	Fault Plane			Slip Vector	Source*
d	m	y				Strike	Dip	Rake		
2	7	1957				256°	44°	259°	30°	M72
3	2	1976				298°	72°	184°	28°	JM84
25	5	1977				112°	60°	112°	22°	JM84
1	10	1979	35(F)	0.4	5.0	304°	20°	-63°	214°	HVD
9	12	1979	15(F)	2.8	5.6	350°	44°	121°	40°	HVD
22	7	1980	30	2.6	5.5	310°	70°	88°	40°	HVD
3	12	1980	16(F)	1.2	5.3	281°	57°	47°	11°	HVD
19	11	1981	33(F)	0.6	5.1	131°	73°	23°	41°	HVD
26	3	1983	10(F)	1.2	5.3	104°	61°	17°	14/96°	HVD
11	6	1986	50	0.8	5.2	291°	43°	-123°	201°	HVD
10	4	1987	15	0.5	5.1	292°	45°	30°	22°	HVD
19	12	1987	33(F)	0.3	4.9	322°	36°	110°	28°	HVD
23	8	1988	15(F)	0.6	5.1	348°	32°	-41°	204°	HVD
20	1	1990	33(F)	10.0	5.9	357°	66°	172°	0/87°	HVD
20	6	1990	14	880.0	7.2	292°	88°	-4°	112°	GW91

(F) denotes fixed depth for moment sensor solution

M72 first motion fault plane solution from McKenzie (1972)

M84 first motion fault plane solution from Jackson and McKenzie(1984)

HVD Harvard Centroid Moment Tensor Catalogue

GW91 Moment tensor solution from Gao and Wallace (1991)

## FIGURE CAPTIONS

Figure 5, Distribution of epicenters for earthquakes greater than magnitude 4 occurring in the region surrounding the Caspian Sea during the period 1962-1988. Epicenters are taken from the NEIS catalogue.

Figure 6. Map of the Caspian Sea region a) showing the 1,000, 2,000 and 3,000 m topographic contours, region of "oceanic-like" crust, contours of sediment thickness, and fold axes in sedimentary cover; b) showing region of "oceanic-like" crust, major fault systems, and seismicity ( $M \geq 4$ ) for the period 1962-1988. Geologic features and location of the "oceanic-like" crust are adapted from Shikalibeily & Grigoriantz (1981), Berberian (1983) and Jackson & McKenzie (1984).

Figure 7. Lower hemisphere equal area projections of P-wave first motion polarity data. Station positions have been plotted with a velocity of  $6.8 \text{ km s}^{-1}$  beneath the source, the same as used in the waveform inversions. Filled circles are compressional first motions; open circles are dilational; nodal onsets are marked with crosses. Large symbols are polarities read on long-period WWSSN instruments, small symbols are polarities based on clear short-period seismograms whose onset displays the short-period impulse response (see Jackson & McKenzie, 1984). P- and T- axes are denoted by the letters P and T. Nodal planes are those of the minimum misfit waveform inversion solutions. Above each focal sphere is the event's date (year, month, day). Comments on individual first motion polarity plots accompany the discussion of each event in the appendix, except for 1978.11.04 and 1986.03.06 which are discussed in the main body of the text.

Figure 8. The P and SH radiation patterns of the minimum misfit solution for the 4 November 1978 (1978.11.04) earthquake are shown in the center of the upper and lower portions of this figure, respectively, and the corresponding values of strike, dip, slip (in degrees), centroid depth (in km), and seismic moment (in units of  $10^{18} \text{ Nm}$ ) are listed beneath the event header. The focal spheres are shown with the P and SH nodal planes, in lower hemisphere projections. The P and T axes are marked by the solid and open circles, respectively. Surrounding the focal sphere, the observed P and SH waveforms (solid lines) are compared with synthetic waveforms (dashed lines) computed for the minimum misfit solution. For the waveform comparison, amplitudes have been normalized to that of an instrument with a gain of 3000 at an epicentral distance of  $40^\circ$ . The time windows for the waveform inversion are denoted by the solid, vertical lines on the waveform. The label to

the left of each waveform identifies the station code, an upper case letter corresponding to the location on the focal sphere, and a lower case letter denoting the instrument type (*w* = WWSSN LP, *d* = GDSN LP). The source time function is shown below the P-wave focal sphere. Below the source time function is the waveform time scale. The waveform amplitude scales are to the left of the focal spheres.

Figure 9. This shows the results of the source region velocity structure test for the 4 November 1978 event. To the left of the waveforms are the P and SH focal spheres and source time function corresponding to the minimum misfit solutions for the particular test. The strike, dip, rake, and centroid depth are listed above the focal spheres. The upper row (A) of the observed (solid line) - synthetic (dashed line) comparison is for the velocity structure used in determining the minimum misfit solution shown in Figure 8. Rows (B - D) shows waveforms for minimum misfit solutions obtained for velocity structures B - D below; all of which might represent reasonable crustal velocity models. These synthetic waveforms are indistinguishable from those in Row A and the source orientations have hardly changed. Rows E - F compare minimum misfit synthetics for more radical changes in the source velocity structure, neither of which is probably reasonable for the Caspian region. Row F is for a mantle source, but the centroid depth resulting from the inversion is at the base of the crust. We conclude from these tests that the focal parameters strike, dip, and rake are insensitive to reasonable variations in the velocity structure.

Velocity Structure	Depth To Interface (km)	$V_p$ ( $kms^{-1}$ )	$V_s$ ( $kms^{-1}$ )	density $kgm^{-3}$
A	0.0	5.6	3.2	2600
	12.0	6.8	3.9	2900
B	0.0	6.2	3.6	2700
	13.2	6.8	3.9	2900
C	0.0	6.2	3.6	2700
	18.0	6.8	3.9	2900
D	0.0	6.5	3.8	2800
E	0.0	5.6	3.2	2500
F	0.0	6.2	3.6	2700
	25.0	8.1	4.7	3300



Figure 10. This figure summarizes the tests we have made to assess the uncertainties for the strike, dip, rake, and centroid depth for the 4 November 1978 earthquake. The format for this figure is the same as for Figure 9. Row A compares selected waveforms for the minimum misfit solution shown in Figure 8. Row B shows the comparison for the minimum misfit solution obtained when the depth is held fixed at 13 km but all other parameters are free. Rows C, D, and E show the similar comparison except when the strike, dip, and rake, respectively, are held fixed at the values shown after the source time function. The rake for this event is poorly constrained.

Figure 11. The minimum misfit solution for the 6 March 1986 earthquake in the central Caspian Sea. The figure format is the same as that for Figure 8. a) single source solution; b) double source solution.

Figure 12. This figure compares observed waveforms and synthetic waveforms computed for various inversion solutions for the 1986.03.06 earthquake. The figure format is the same as for Figure 9. Row A compares waveforms for the single source inversion solution; row B compares waveforms for the double source inversion solution. Note the improvement in the fits for the four nodal P-wave seismograms (SHL, KOD, PTO, STU). Rows C and D show the contribution of the two individual sources of the double source solution.

Figure 13. Comparison of waveforms at same common seismograph stations for the three largest central Caspian Sea earthquakes (1986.03.06, 1989.09.16, 1989.09.17). Dotted lines denote the synthetic seismograms computed for these from the minimum misfit solutions shown in Figures 11b, A13, A14 and given in Table 3. The amplitude scale (d-GDSN, w-W WSSN) is to the left of each row and all seismograms have a common time scale. All stations are WWSSN except GDH which is a GDSN station.

Figure 14. Minimum misfit fault plane solutions of the earthquakes analyzed in this paper (Table 3) (a), and fault plane solutions for other earthquakes that we did not study (Table 4), from Jackson & McKenzie (1984), Gao & Wallace (1991), and the Harvard CMT catalogue (b). Focal spheres are lower hemisphere equal area projections, with compressional quadrants shaded. Next to each sphere is the date of the event (year, month, day). In (a) the centroid depth in km is noted near the epicenter. The focal mechanism of the 1990.06.20 event is denoted by the larger fault plane solution in 10b and its depth is noted near the epicenter.

Figure 15. Horizontal projection of the slip vectors for earthquakes whose focal mechanisms are shown in Figure 14. Heavy solid arrows are slip vectors from events whose P- and SH-waveforms we analyzed in this study (Fig. 14a) and from the 1990.06.20 earthquake (Gao & Wallace, 1991). Light open arrows are slip vectors from first motion solutions of Jackson & McKenzie (1984) or from Harvard CMT solutions (Fig. 14b). The sense of slip shown is of the south or east side of the fault relative to the north or west side. We have shown the slip vector implied by our minimum misfit solution for 1971.02.14 and labeled it  $62^\circ$  (?) to indicate that we do not have a great deal of confidence in this solution. The inset in the upper right-hand corner of the figure shows the orientation of the T axes of the normal faulting events in the central Caspian Sea

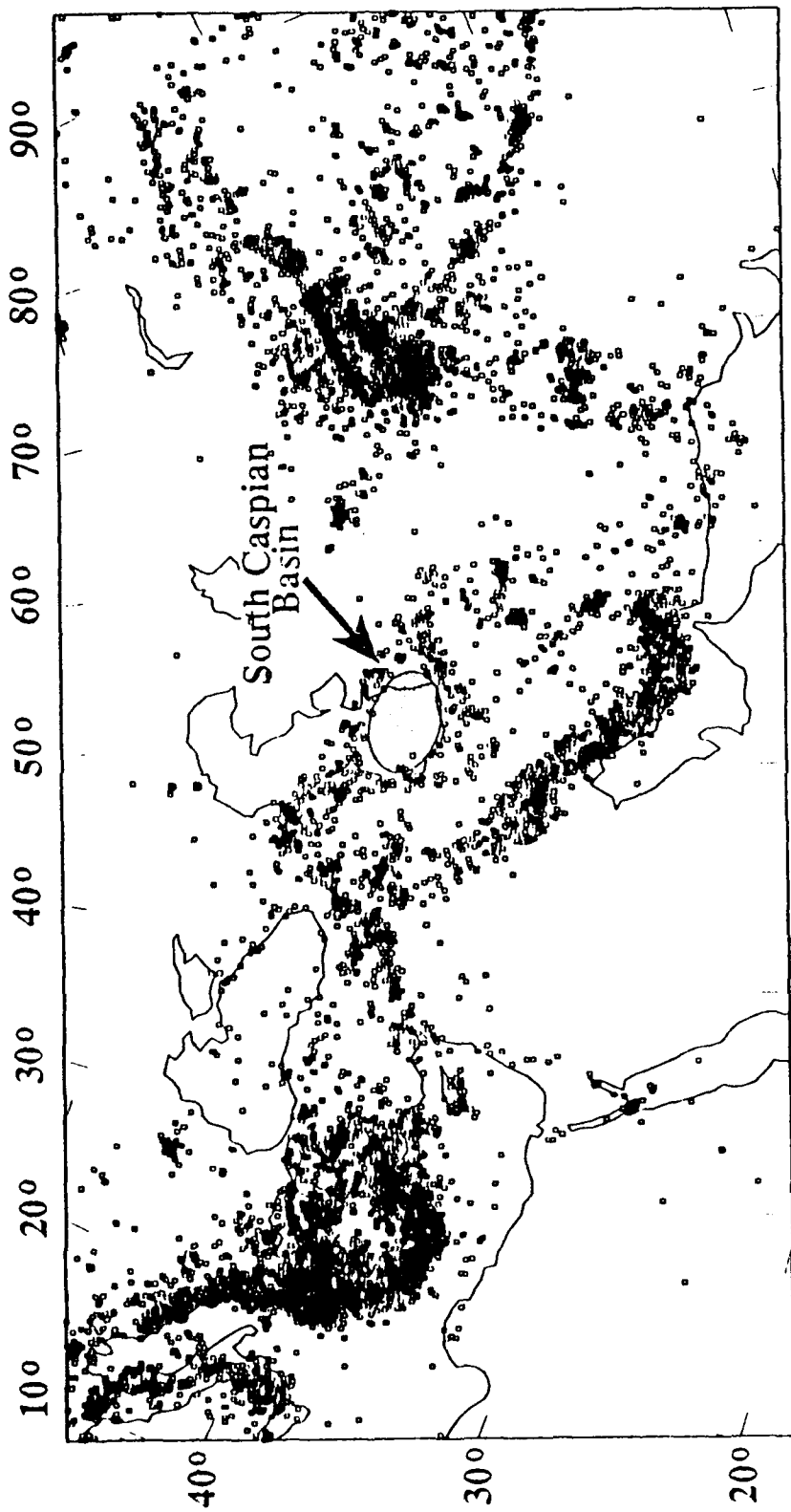


FIGURE 5

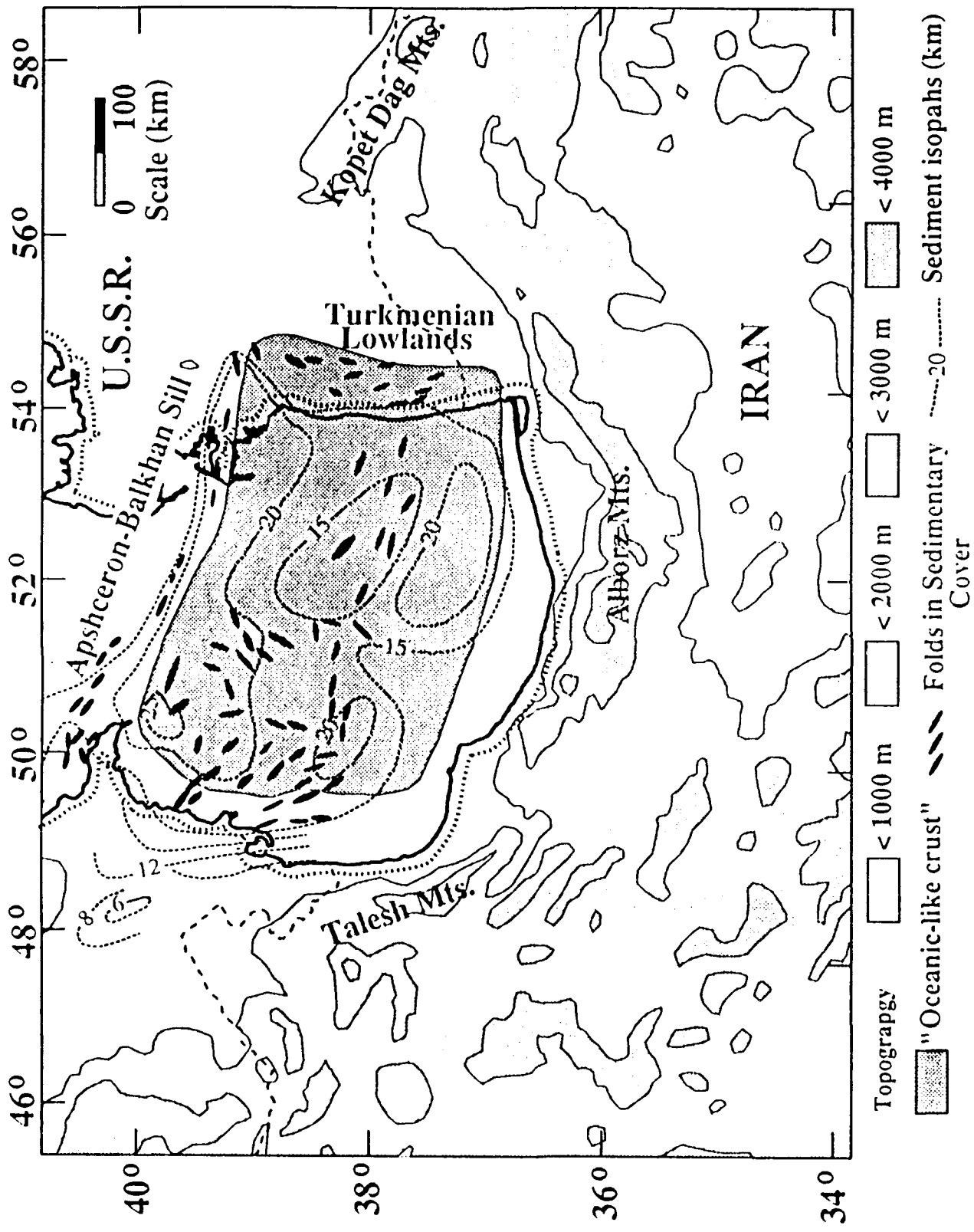


FIGURE 6a

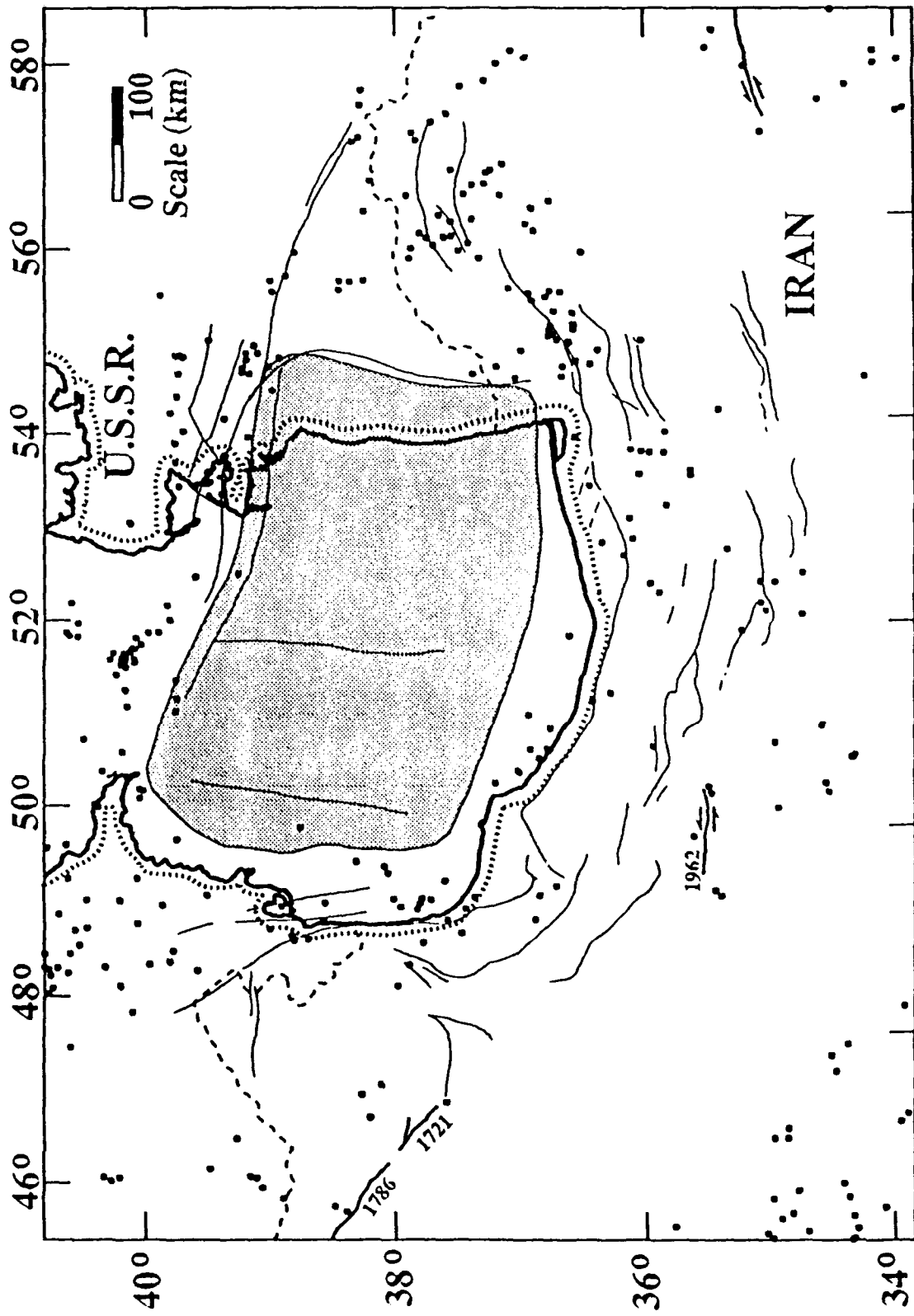
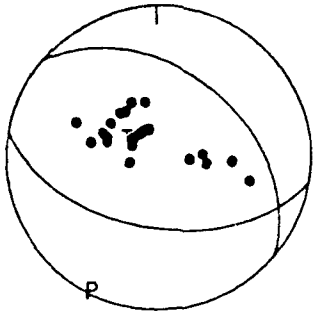
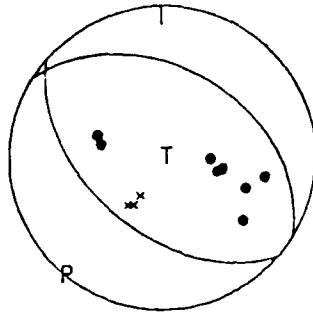


FIGURE 6b

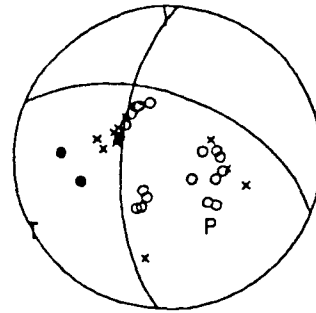
620901



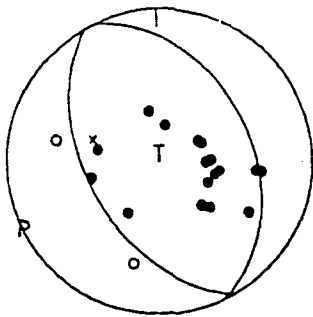
690103



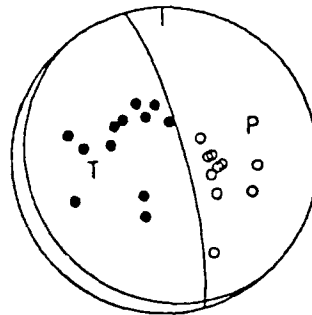
700730



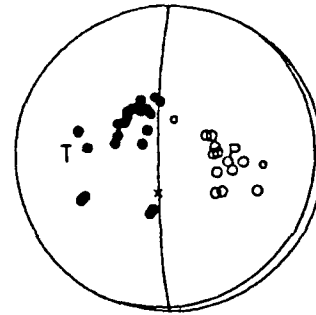
710214



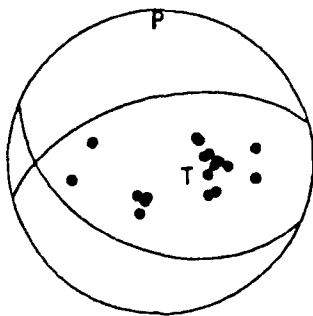
781104



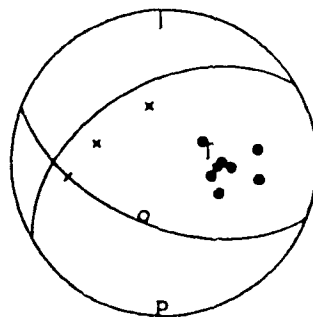
800504



801219



801222



810804

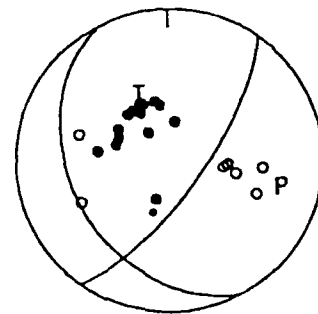
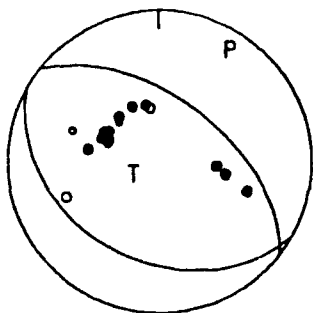
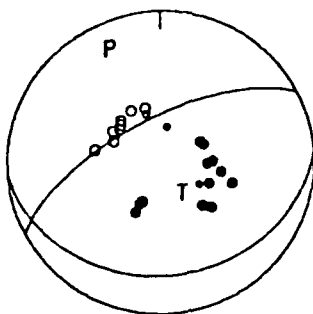


FIGURE 7

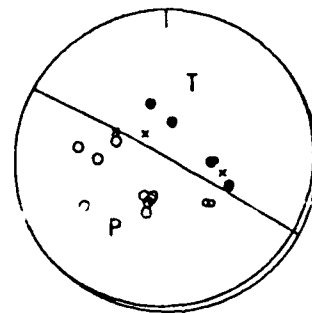
830722



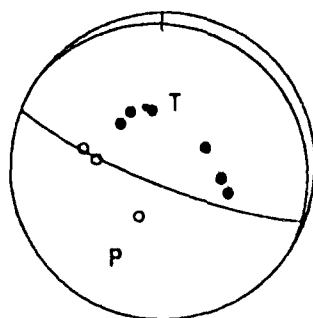
851029



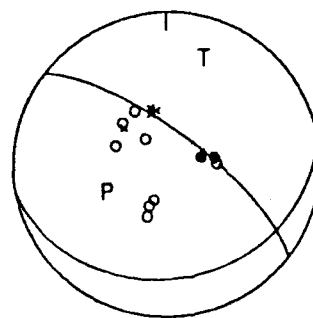
860306



870907



890916



890917

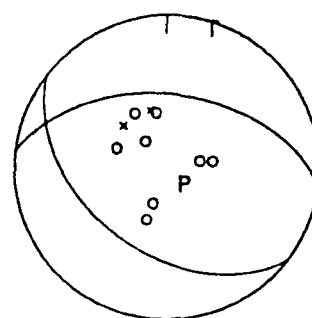


FIGURE 7 (Cont)

4 November, 1978  
 346/79/95/21/1.90 × 10<sup>18</sup>

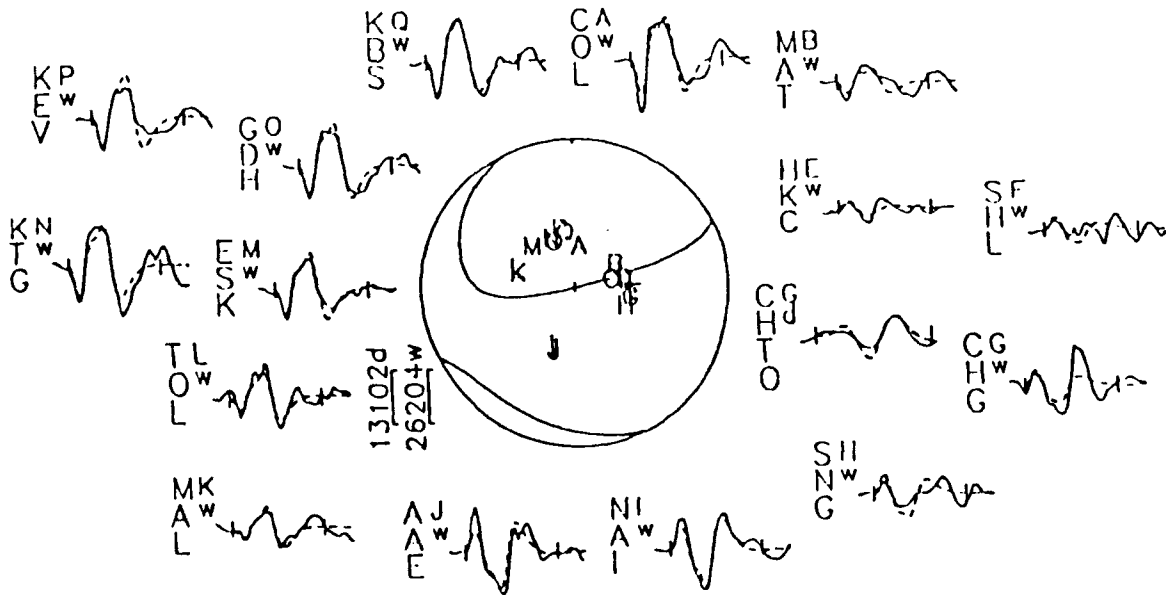
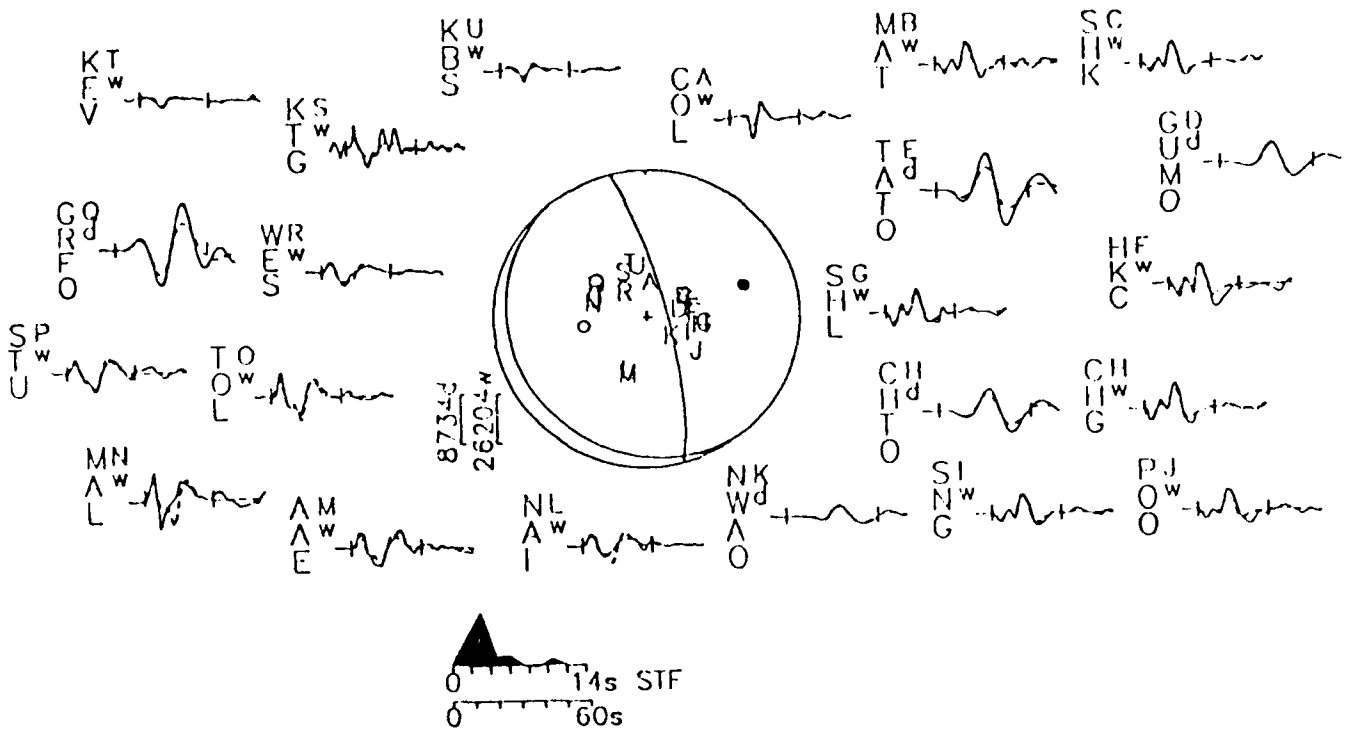


FIGURE 8



November 4, 1978 1521  
 346/79/95/21/1.902E18

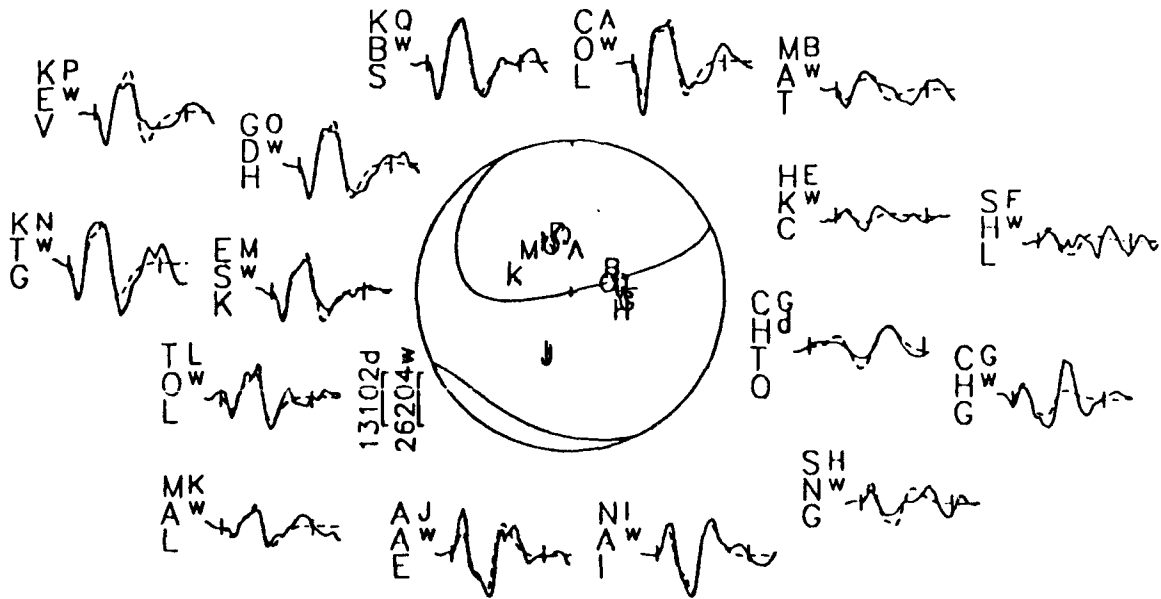
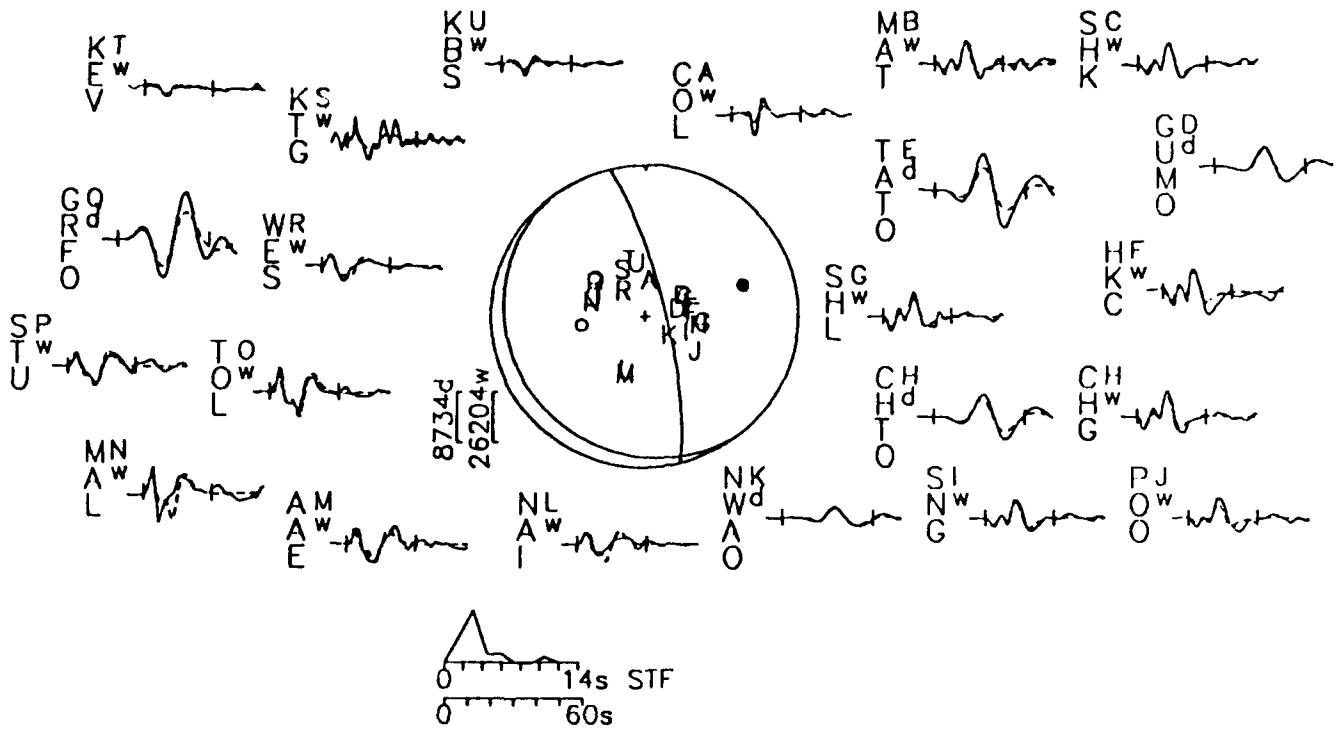
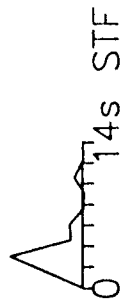
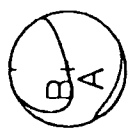
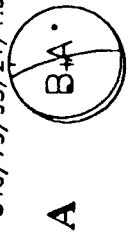


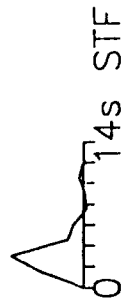
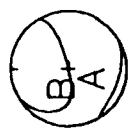
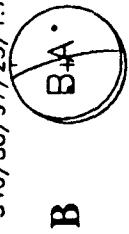
FIGURE 8 (Cont)

SHK-P TOL-P AAE-S TOL-S

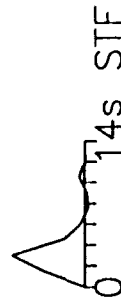
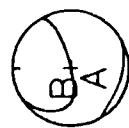
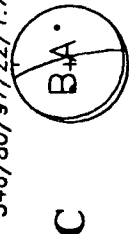
346/79/95/21/1.902E18



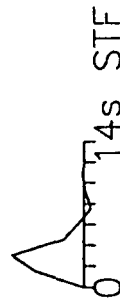
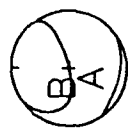
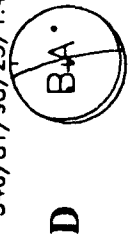
346/80/97/23/1.729E18



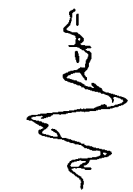
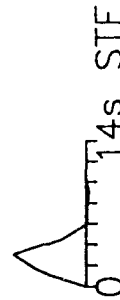
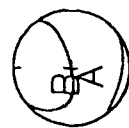
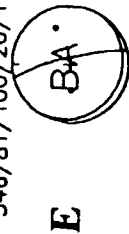
346/80/97/22/1.737E18



346/81/98/23/1.468E18



346/81/100/20/1.165E18



346/83/100/25/2.093E18

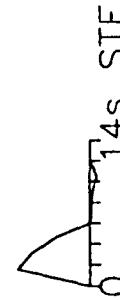
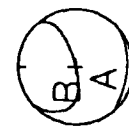
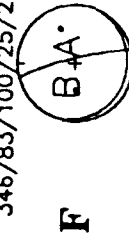


FIGURE 9

COL-P MAT-P POO-P KEV-P TOL-S MAL-S

Minimum Misfit Solution

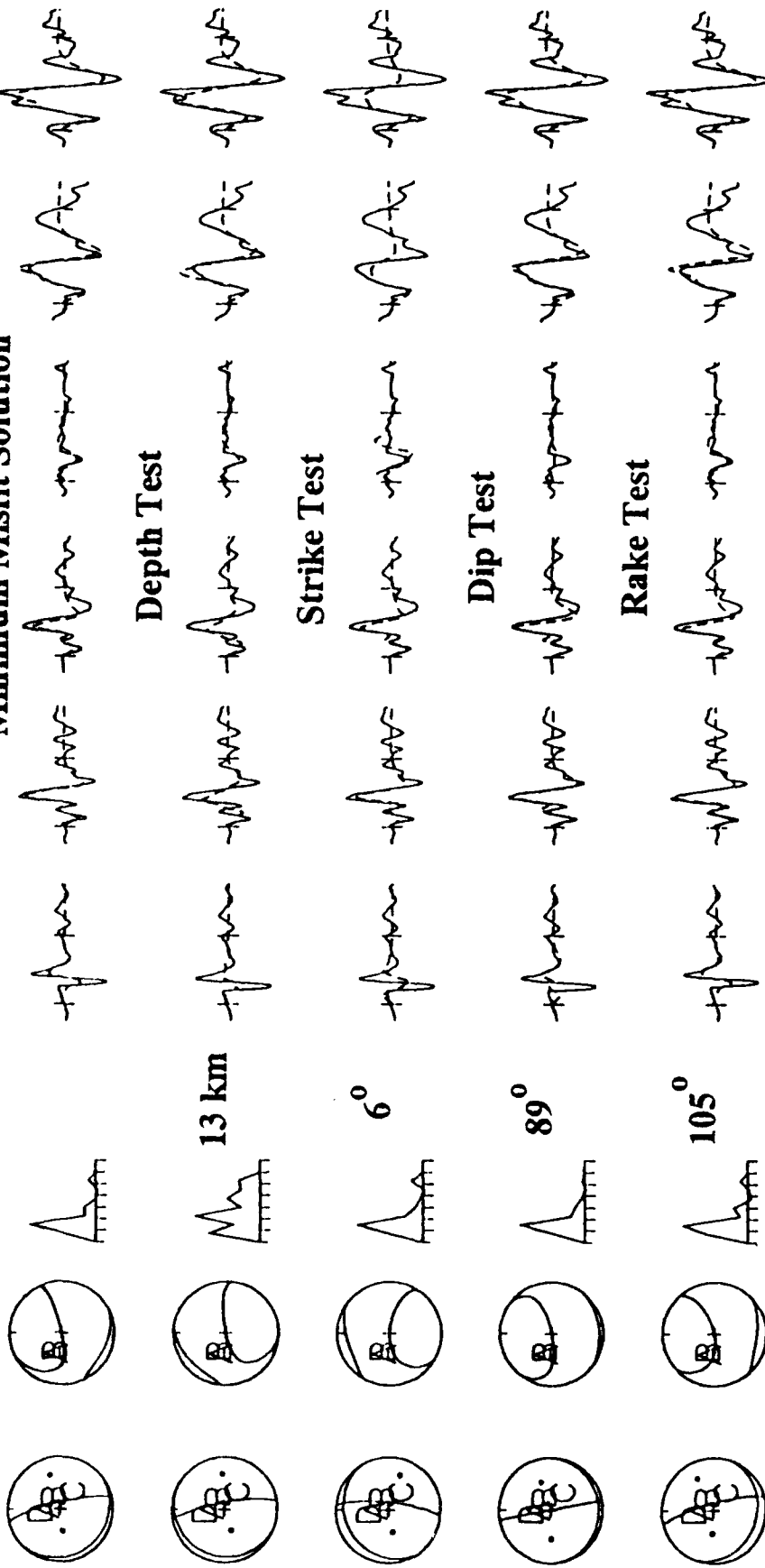


FIGURE 10

6 March, 1986  
 303/81/268/35/2.44 × 10<sup>18</sup>

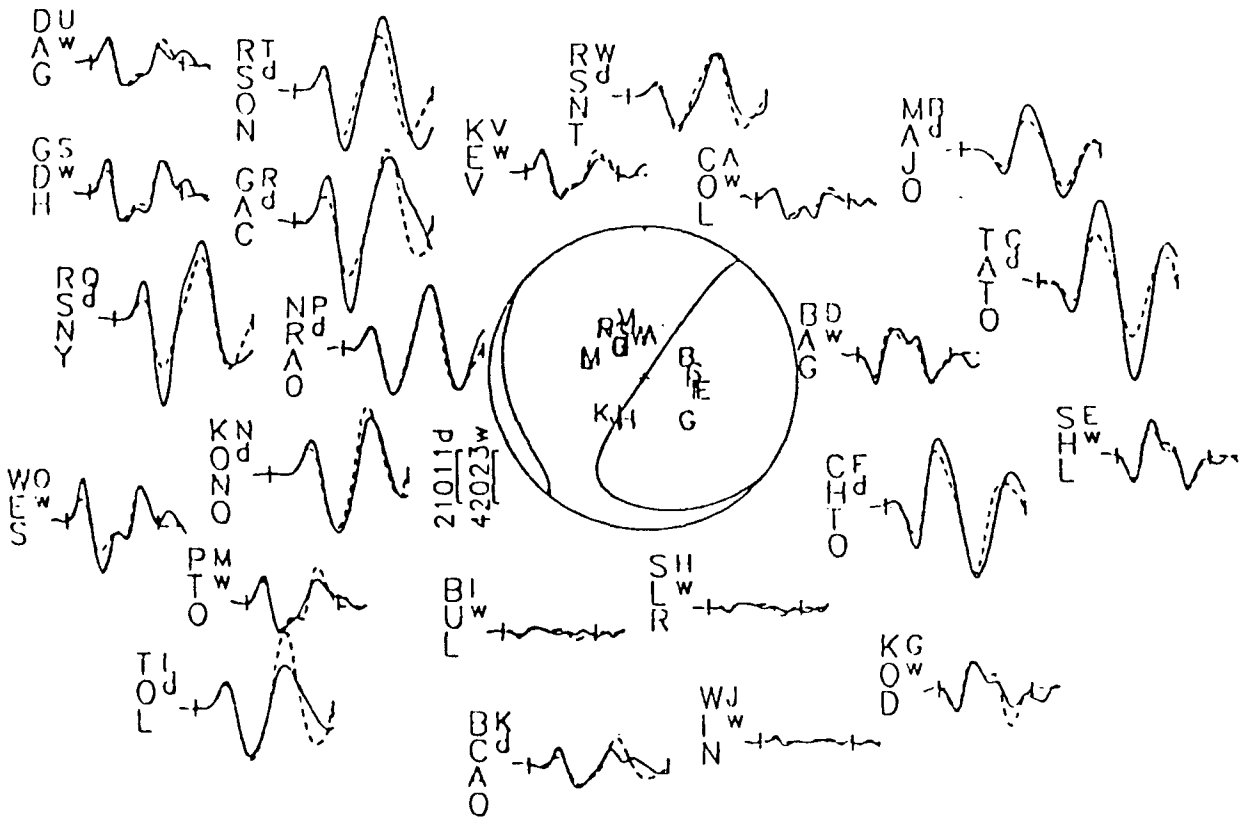
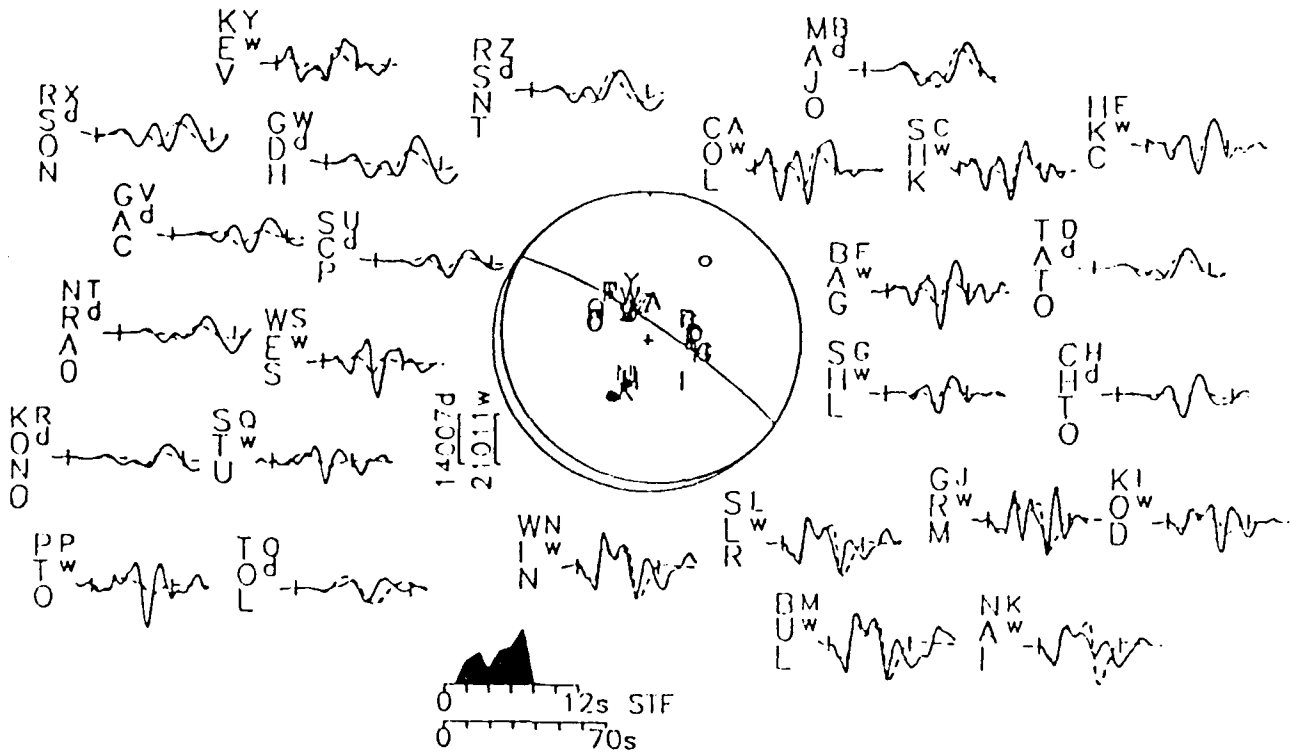


FIGURE 11a

March 6, 1986  
 303/81/268/35/2.435E18

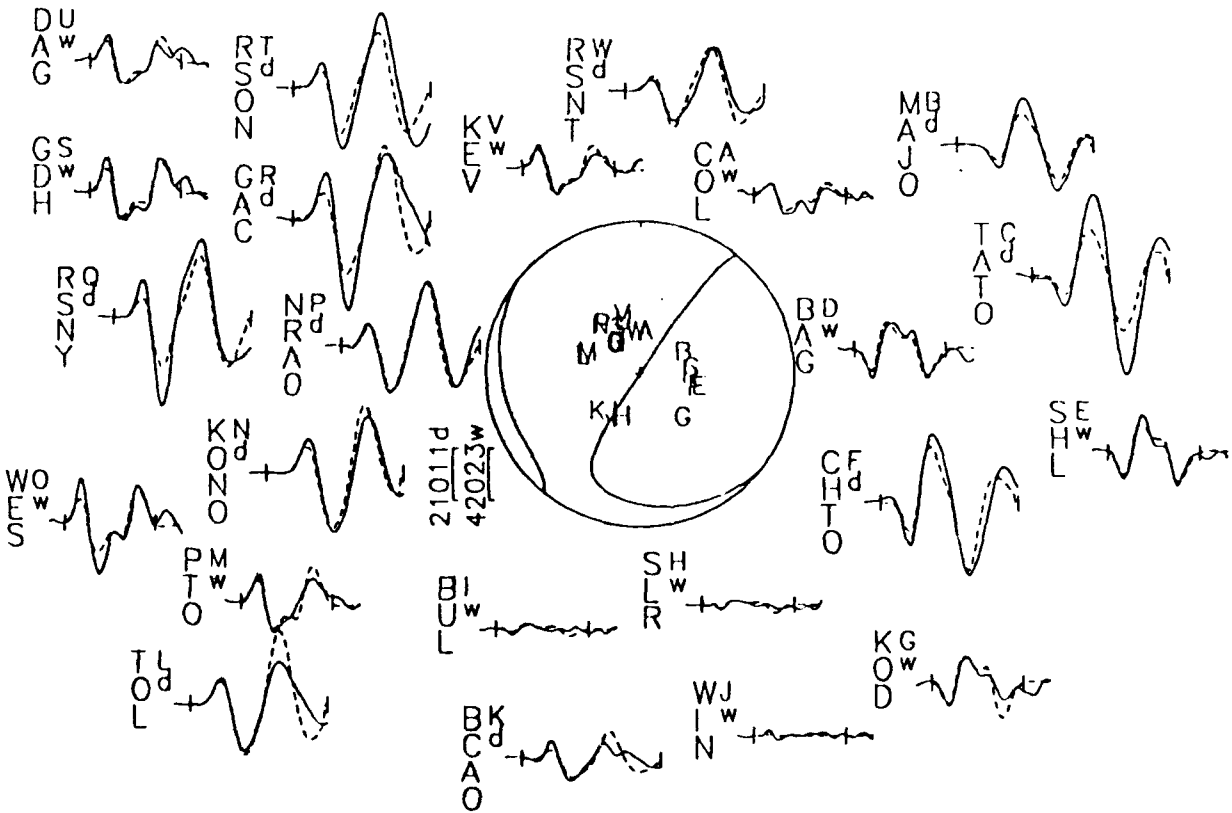
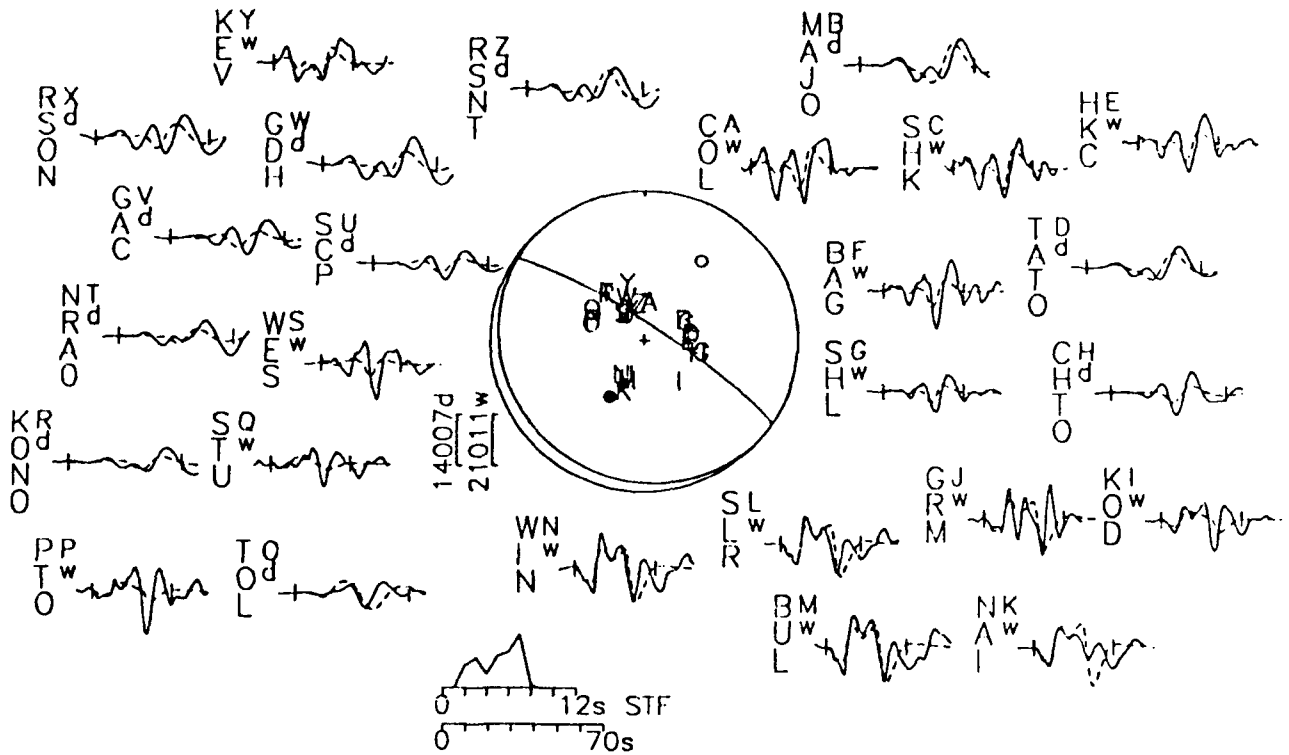


FIGURE 11a

6 March, 1986

Source 1 299/88/275/31/2.52 × 10<sup>18</sup>

Source 2 114/63/87/13/2.18 × 10<sup>18</sup>

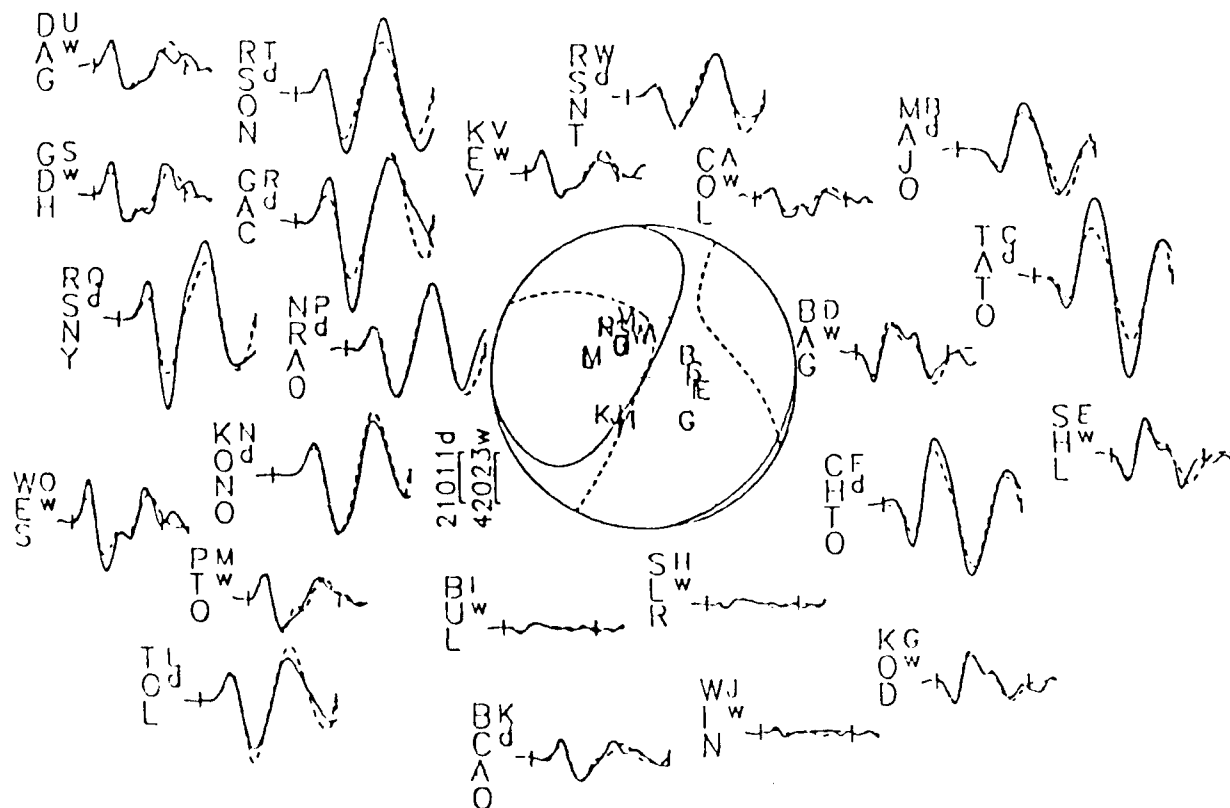
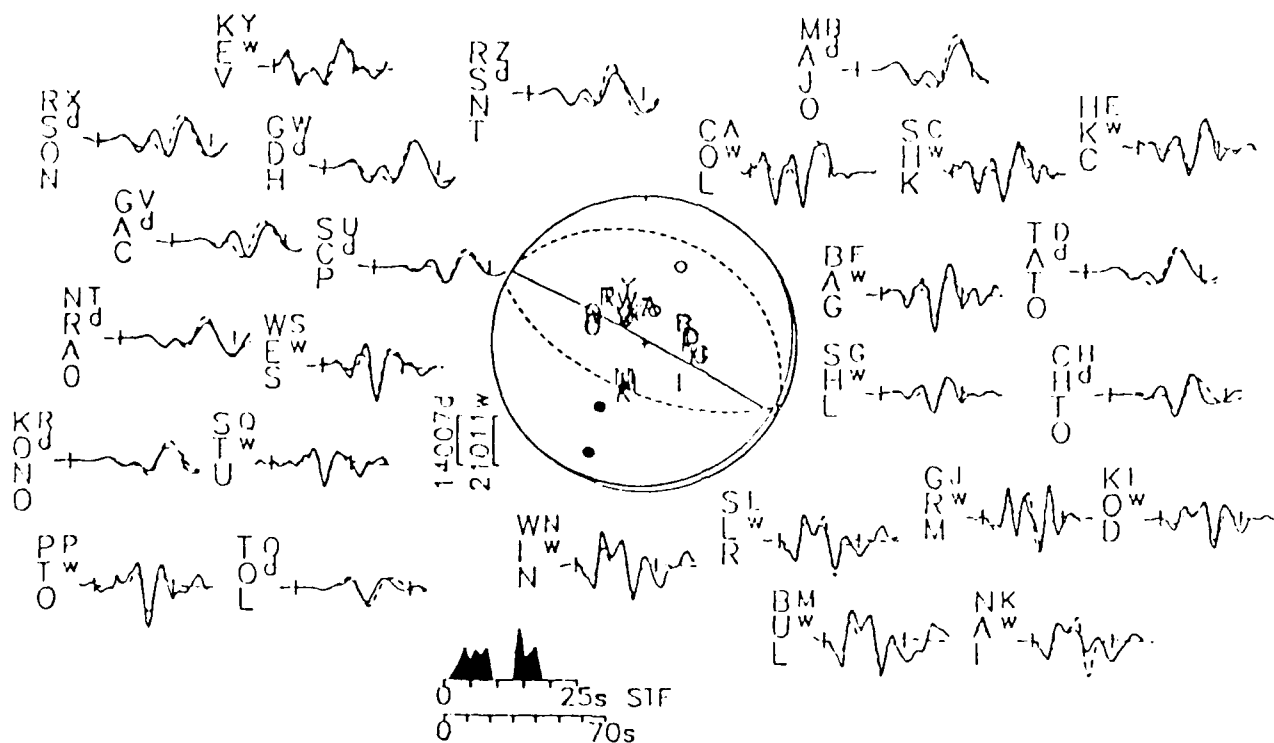


FIGURE 11b

March 6, 1986  
 1:299/88/275/31/2.523E18  
 2:114/63/87/13/2.177E18

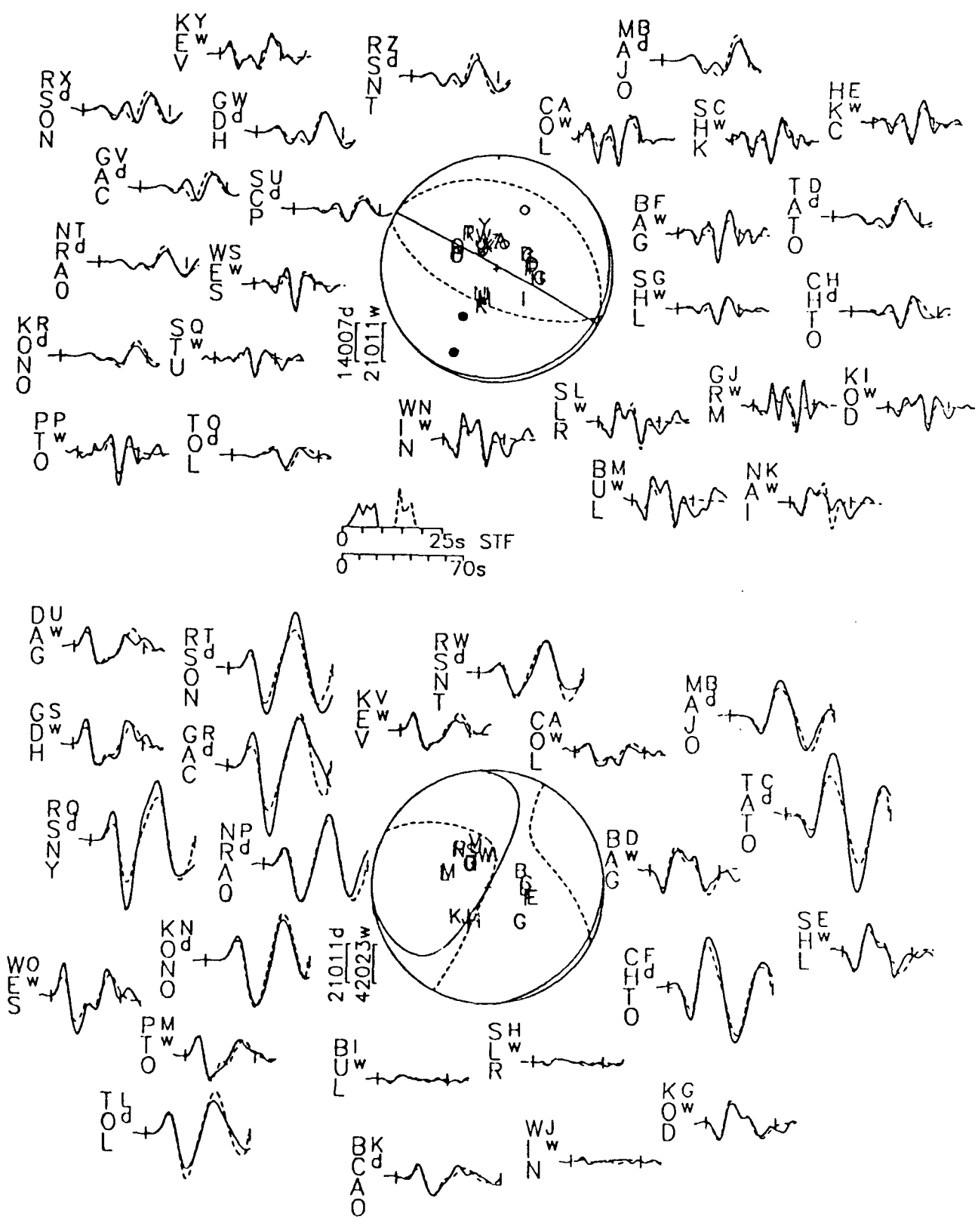


FIGURE 11b

SHL-P KOD-P SRL-P PTO-P STU-P KOD-S WIN-S

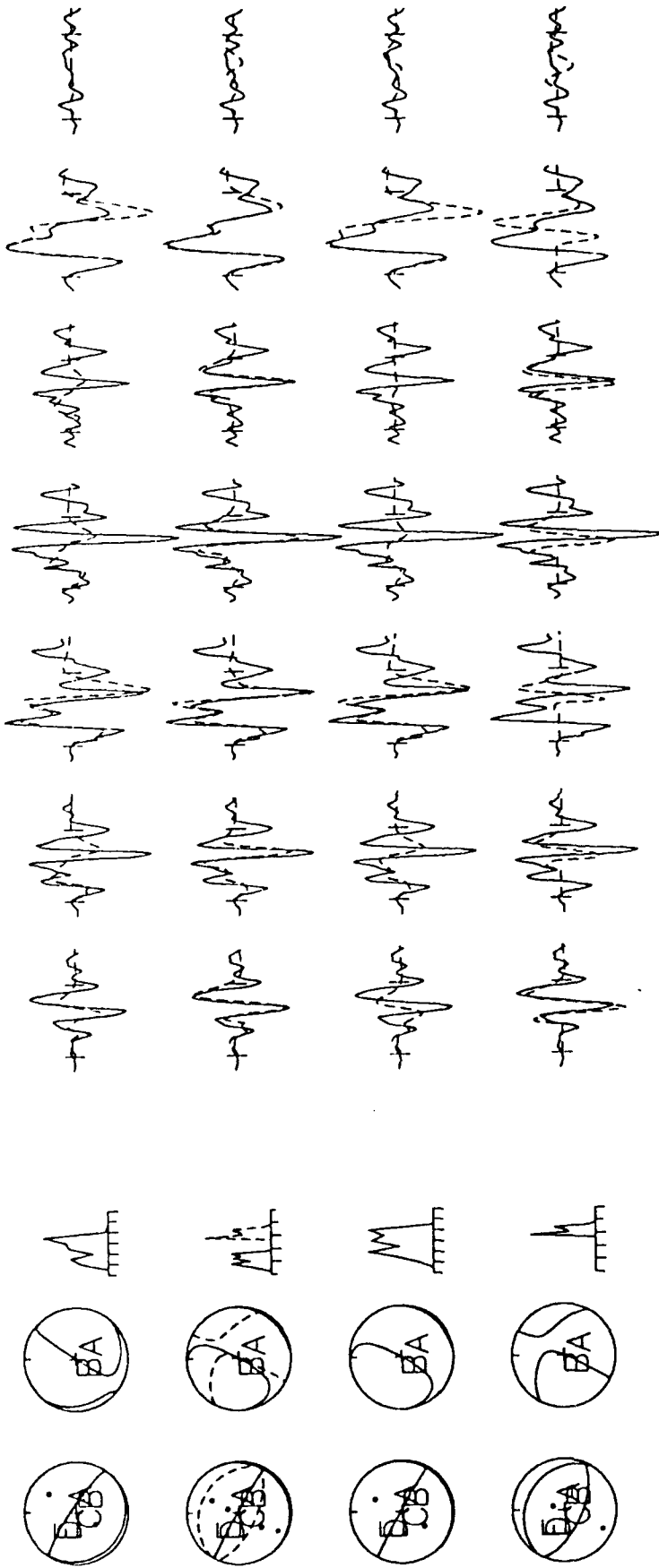


FIGURE 12



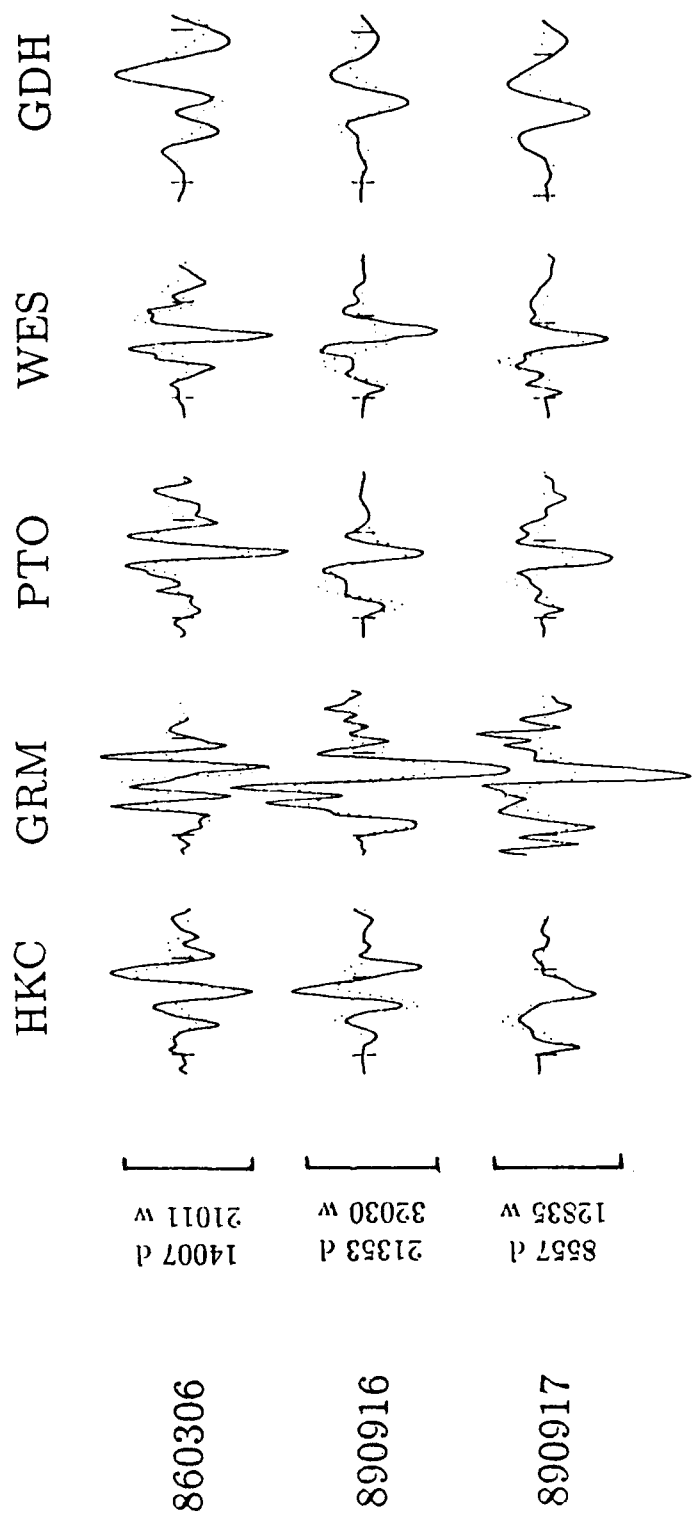


FIGURE 13

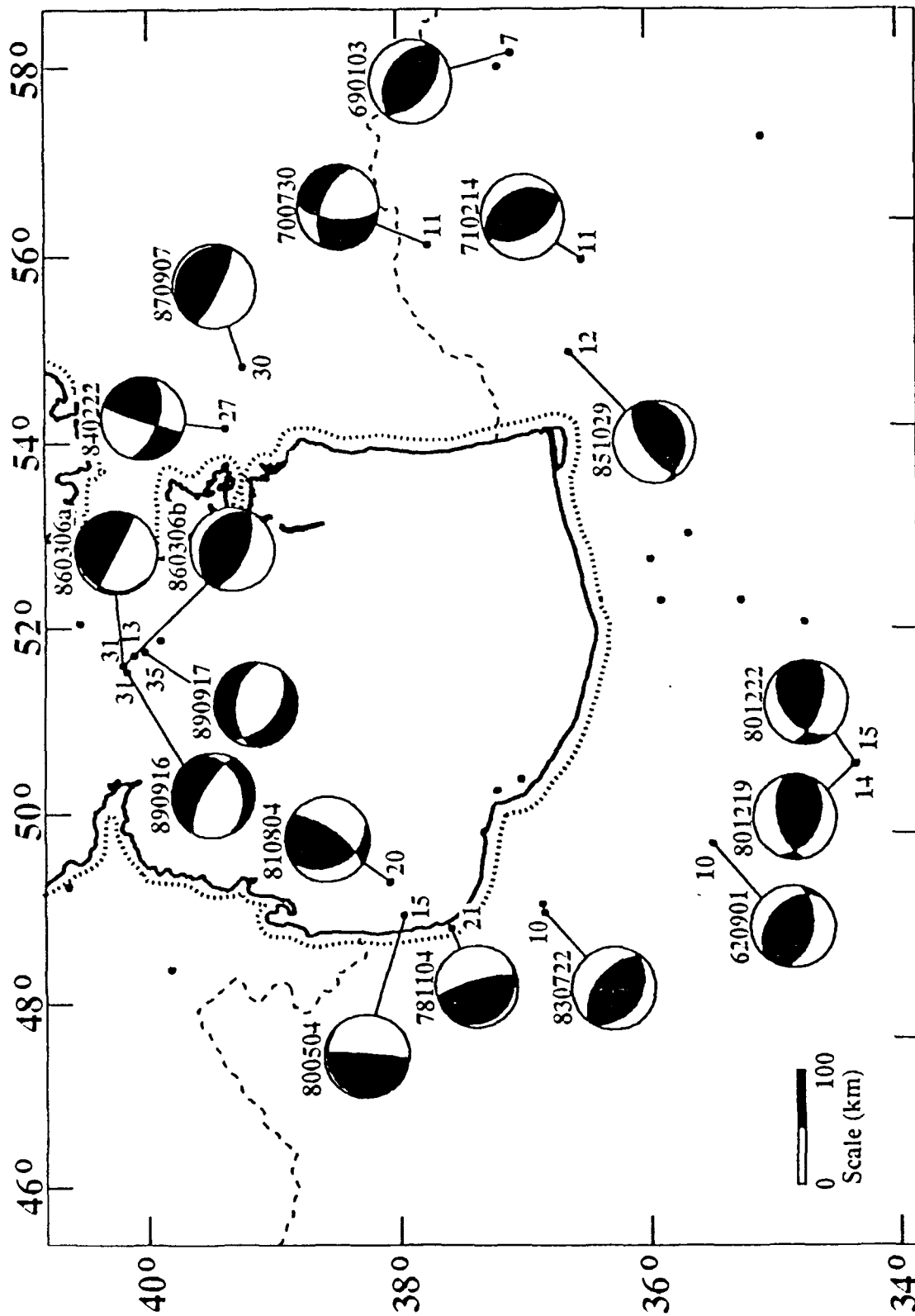


FIGURE 14a

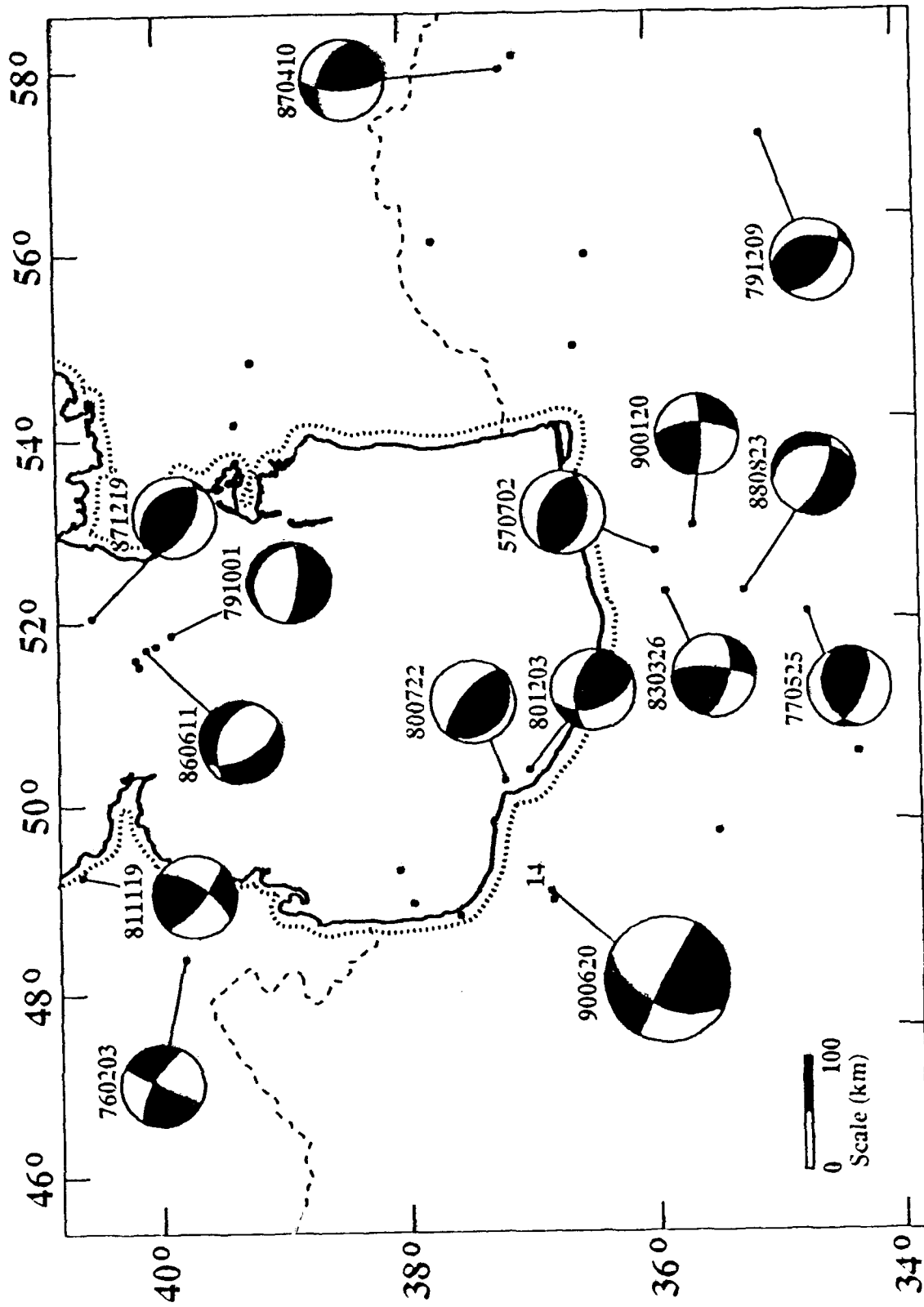


FIGURE 14b

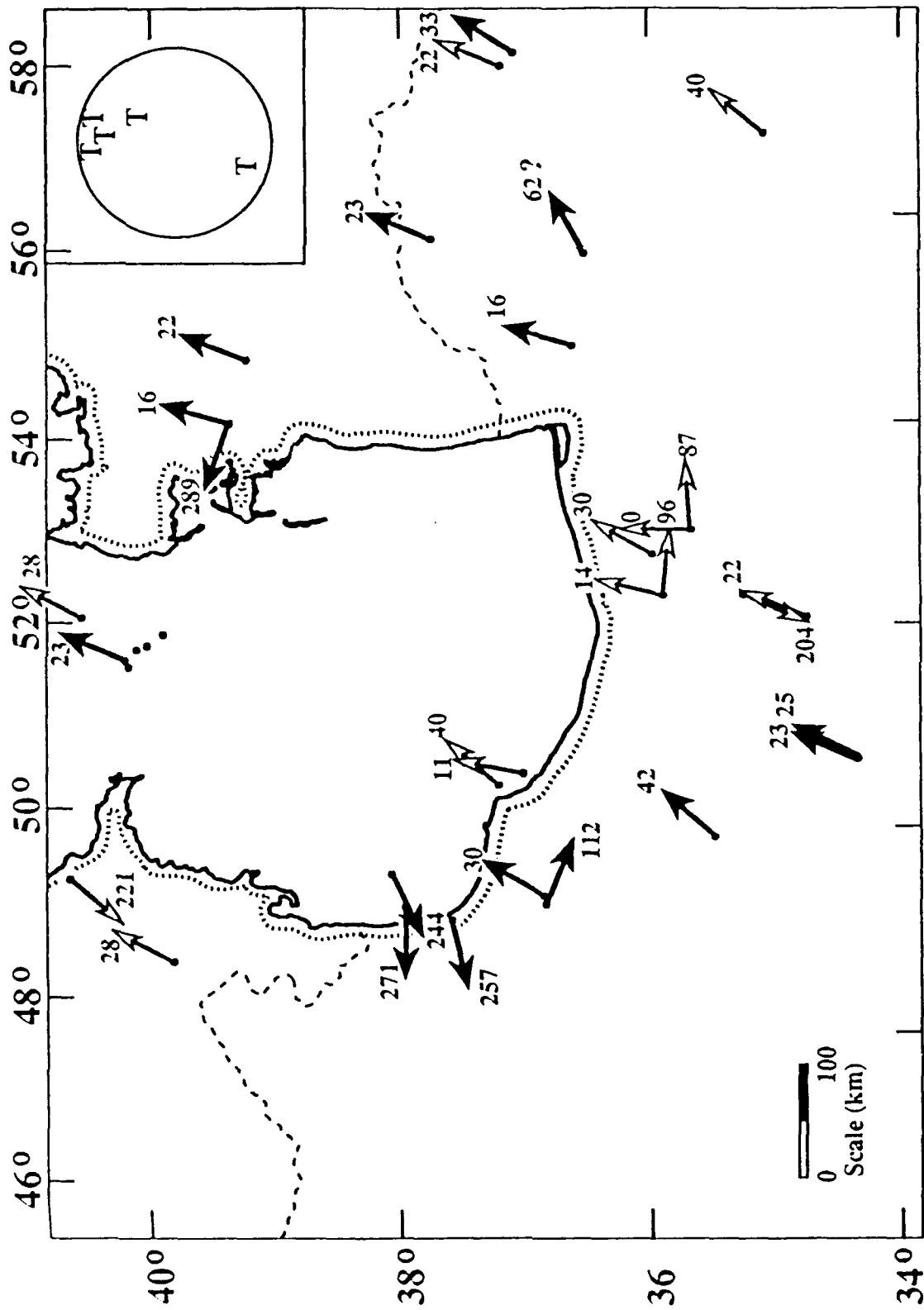


FIGURE 15

## APPENDIX

In this appendix we show the observed seismograms for the events not discussed in detail in the main text, and compare them with synthetic seismograms computed for the minimum misfit inversion solution. For each one of these events we have conducted a series of tests identical to those shown in Figure 10 to place bounds on the strike, dip, slip, and centroid depth. Focal parameters for the minimum misfit solution from the inversion and bounds on these parameters from the test are given in Table 3. The format of each figure is the same as in Figure 8.

Figure A1. 1962 September 1 - The Buyin Zara earthquake ( $M_S$  7.2,  $m_b$  6.9) devastated the area south of Qazvin in northern Iran, killing around 12,200 people. Faulting was discontinuous, but was observed in a zone striking  $103^\circ$  over a distance of about 80 km (Ambraseys 1962; Ambraseys & Melville 1982). Displacements generally involved both thrusting on planes dipping south and also left-lateral strike slip. Fault segments typically had a strike of around  $100^\circ$ . Average amplitudes were about 1.4 m vertical displacement and 0.6 m strike-slip.

Many of the seismograms of this earthquake were off-scale, and, because it occurred in the early days of the WWSSN, not many seismograms were available anyway. Those we were able to obtain are shown in Figure A1a. The coverage of the focal sphere is not very good, with most stations in the NW and only two in the SE. The first motions are better distributed (Fig. 7), and require a large reverse slip component. To obtain the minimum misfit solution, shown in Figure A1a, we used only three SH waveforms: at BAG, PMG, and STU. We gave the PMG SH waveform only half the weight it would normally have, because of its distance ( $101^\circ$ ), at which the ScS phase might be expected to interfere. We justified its retention because of its similarity to the SH waveform at BAG (distance  $65^\circ$ , at which ScS does not interfere with S). We did not use the MDS SH waveform in the inversion because of its distance ( $93^\circ$ ), and because we had no independent check on the ScS contamination; it is shown because the polarity of its onset suggests an SH nodal plane between its position and that of STU on the focal sphere. By comparing the amplitude of the seismograms at BAG with those of other stations, we deduced that its gain was erroneously given as 1500 on the WWSSN film chip, and that it should have been 3000: the inversion was not sensitive to this change, which we have corrected.

The fit to observed waveforms in Figure A1a is reasonable, and demonstrates a long time function of about 24 seconds. At a rupture velocity of  $3 \text{ kms}^{-1}$  this can account for 72 km of faulting, which is compatible with what was observed (Ambraseys & Melville

1982). The moment of  $3.68 \times 10^{19}$  Nm ( $M_w$  7.0) can account for 1.4 m of displacement on a fault 72 km long, extending to a depth of 10 km with a dip of  $52^\circ$ . This amount, its sense (which is predominantly reverse with a smaller left-lateral component), and its strike, are also compatible with surface observations.

We were particularly interested in the slip vector of this earthquake, and so carried out tests on the resolution of the rake, which controls the strike of the auxiliary (north-dipping) plane, and hence slip vector. These tests are shown in Figure A1b.

The minimum misfit solution (rake =  $70^\circ$ ) is shown in row 2. In rows 1,3 and 4 the rake was fixed at some other value, and the other parameters were allowed to change in the inversion. The rake cannot have a value below  $60^\circ$  without producing the wrong polarity for SH at STU, thus limiting the maximum left-lateral component. The minimum left-lateral component is less well resolved: the SH fit at STU improves if the rake exceeds  $70^\circ$ , and a value of  $100^\circ$  produces a better fit than the minimum misfit solution (row 4): but it requires a right-lateral component, which is incompatible with surface observations. The minimum misfit slip vector is  $42^\circ$ , but we conclude it could have a value between  $30^\circ$  and  $50^\circ$  (corresponding to a rake of  $70^\circ - 10^\circ / + 15^\circ$ ). Note that there is some trade-off between strike and rake in this case. The dip, depth, and moment change little when the strike and rake are perturbed. We estimate the mechanism of this event to be: strike  $101^\circ \pm 10^\circ$ ; dip  $52^\circ \pm 3^\circ$ ; rake  $70^\circ - 10^\circ / + 15^\circ$ ; depth  $10 \pm 4$  km.

Figure A2. 1969 January 3 - P-wave first motion polarities (Fig. 7) require high angle reverse faulting, but cannot constrain the strike and rake well. Waveform inversion and testing constrain the focal depth to  $7 \pm 4$  km. The SH waveforms at SHL, CHG, and NAI constrain the strike to  $132^\circ \pm 15^\circ$ , dip  $50^\circ \pm 5^\circ$ , and rake to  $95^\circ \pm 8^\circ$ .

Figure A3. 1970 July 30 - P-wave first motion polarities for this event were studied by Jackson and McKenzie (1984). They plotted first motions of this event with a mantle source velocity of  $V_p$   $8.1 \text{ km s}^{-1}$  because they could not fit orthogonal nodal planes otherwise. We suspect that some of the polarities at European stations, which they gave as dilatational, are in fact, nodal. With these changes, the nodal planes for the minimum misfit solution are consistent with the first motion polarities plotted with the focal velocity of  $6.8 \text{ km s}^{-1}$ . We estimate the centroid depth to be  $11 \pm 4$  km.

Figure A4. 1971 February 14 - P-wave first motions and P-wave waveform inversion require this event to result from high-angle reverse faulting. First motion data suggest a nodal

plane roughly as shown. P-waveforms constrain the centroid depth to  $11 \pm 5$  km but do not greatly aid in constraining other focal parameters, particularly strike and slip vector azimuth. No suitable SH waveforms were available for this event.

Figure A5. 1980 May 4 - First motion polarities require this event to have one almost vertical nodal plane and this is confirmed by the waveform inversion. Inversion and testing constrain the centroid depth to  $15 \pm 5$  km, the strike to  $28^\circ \pm 10^\circ$ , the dip to  $7^\circ \pm 10^\circ$ , and the rake to  $297^\circ \pm 15^\circ$ .

Figure A6. 1980 December 19 - First motion P-wave polarities require high angle reverse faulting, but do not constrain the strike and rake well. Waveform inversion and testing constrain the centroid depth to  $14 \pm 8$  km, the strike to  $115^\circ \pm 20^\circ$ , the dip to  $41^\circ \pm 8^\circ$ , and the rake to  $120^\circ \pm 15^\circ$ .

Figure A7. 1980 December 22 - First motion P-wave polarities require high angle reverse faulting, but do not constrain the strike and rake well. Waveform inversion and testing constrain the centroid depth to  $15 \pm 5$  km, the strike to  $113^\circ \pm 20^\circ$ , the dip to  $56^\circ \pm 8^\circ$ , and the rake to  $125^\circ \pm 15^\circ$ . The first motion at NAI is incompatible with the planes as shown (Fig. 7) but lies very close to a nodal plane and within the acceptable error in its dip.

Figure A8. 1981 August 4 - First motion data constrain the steeply dipping plane (Fig. 7). Two first motion polarities (JER, IST) are inconsistent with the minimum misfit solution (strike  $154^\circ \pm 15^\circ$ , dip  $35^\circ \pm 15^\circ$ , rake  $32^\circ \pm 20^\circ$ ). Both are near a nodal plane and are at regional distances, so that their precise position on the focal sphere is uncertain. For comparison with our results, the Harvard CMT solution gives strike  $159^\circ$ , dip  $26^\circ$ , rake  $40^\circ$ , and centroid depth of 25 km for this event, which is within the uncertainty bounds, identical to our solution.

Figure A9. 1983 July 22 - This event occurred one minute prior to the 1983 Coalinga earthquake ( $M_w$  5.75) in California, whose seismograms caused interference at some stations. We chose seismograms from stations where the Coalinga P- or SH- phases do not arrive within the inversion window. P-wave first motion polarities (Fig. 7) require high angle reverse faulting, but do not constrain the strike and rake well. Waveform inversion constrains the strike to  $120^\circ \pm 20^\circ$ , the dip to  $35^\circ \pm 8^\circ$ , and the rake to  $83^\circ \pm 15^\circ$ . The nodal planes shown in Figure 7 are for the minimum misfit solution and violate the first

motion data for JER and IST. Both of these stations are at regional distances and their precise position on the focal sphere is uncertain.

**Figure A10. 1984 February 22** - We could not read any reliable first motion polarities for this event. Only a limited number of P-waveforms are available and all but one of these are from the GDSN. The mechanism (strike  $106^\circ \pm 20^\circ$ , dip  $60^\circ \pm 10^\circ$ , rake  $174^\circ \pm 20^\circ$ ) is primarily constrained by the SH-waveforms. The depth is  $27 \pm 4$  km. The Harvard CMT solution is: strike  $109^\circ$ ; dip  $83^\circ$ ; rake  $175^\circ$ , and centroid depth 40 km. Except for the depth, this is indistinguishable from our waveform inversion solution.

**Figure A11. 1985 October 29** - First motion polarities (Fig. 7) require this event to have a relatively steep nodal plane dipping NW. The source orientation (strike  $106^\circ \pm 15^\circ$ , dip  $30^\circ \pm 10^\circ$ , rake  $126^\circ \pm 10^\circ$ ) is well constrained by the abundant P- and SH-waveforms. The depth is  $13 \pm 5$  km. The Harvard CMT solution for 1985.10.29 is strike  $97^\circ$ , dip  $31^\circ$ , rake  $72^\circ$ , and centroid depth 15 km. The strike and dip of the CMT solution is indistinguishable from our waveform inversion solution; however, the rake is significantly different. We are more confident in our waveform inversion results.

**Figure A12. 1987 September 7** - First motion polarities constrain a WNW striking, steeply dipping nodal plane. Waveform inversion and testing constrain the centroid depth to  $30 \pm 8$  km, the strike to  $305^\circ \pm 10^\circ$ , dip  $10^\circ \pm 10^\circ$ , and rake  $103^\circ \pm 20^\circ$ . The Harvard CMT solution for 1987.09.07 is strike  $312^\circ$ , dip  $14^\circ$ , rake  $106^\circ$ , and centroid depth 29 km, indistinguishable from our waveform inversion solution.

**Figure A13. 1989 September 16** - First motion polarities imply normal faulting for this event but poorly constrain the mechanism. Waveform inversion for a single source gives a mechanism involving either faulting on a WNW striking, steeply-dipping plane, or on a ENE striking, shallow-dipping plane. Because of the similarity of the waveforms of this event and 1986.03.06 (Fig. 13), we also inverted waveforms of this event for a second, delayed source. This cannot be as definitive as in the case of 1986.03.06 because the GDSN instrument response tends to blur source details and because of the lack of WWSSN stations which have a higher frequency response. The inversion with a second source produced marginally better fit to the waveforms than the single source solution, and gave a moment for the second source that was approximately 10% of the moment of the first event. Our preferred single source solution from the waveform inversion is strike  $80^\circ \pm 15^\circ$ ,



dip  $26^\circ \pm 5^\circ$ , rake  $225^\circ \pm 15^\circ$  and depth  $31 \pm 10$ km. For comparison, the Harvard CMT solution is strike  $104^\circ$ , dip  $36^\circ$ , rake  $228^\circ$ , and centroid depth 34 km. The strike and dip of the CMT solution is slightly different from our waveform inversion solution, which we have more confidence in.

Figure A14. 1989 17 September - Waveforms of this event are similar those of to the 1989.09.16 earthquake. First motion polarities imply normal faulting but poorly constrain the orientation. Waveform inversion for a single source yields a mechanism that corresponds either to faulting on a WNW striking, steeply dipping plane, or on a ENE striking, shallow dipping plane. Figure 13 compares P-waveforms of this event and the 1986.03.06 and 1989.09.16 earthquakes at common stations. Because of the scarcity of WWSSN seismograms, we have only inverted this event assuming a single source. The resulting orientation is strike  $128^\circ \pm 15^\circ$ , dip  $44^\circ \pm 5^\circ$ , and rake  $295^\circ \pm 15^\circ$  and depth  $35 \pm 10$ km. The Harvard CMT solution for 1989.09.17 is strike  $142^\circ$ , dip  $58^\circ$ , rake  $287^\circ$ , and centroid depth 34 km. The dip of the CMT solution is different from our waveform inversion solution, however, we are more confident in our result.

1 September, 1962  
 101/52/70/10/3.68 × 10<sup>19</sup>

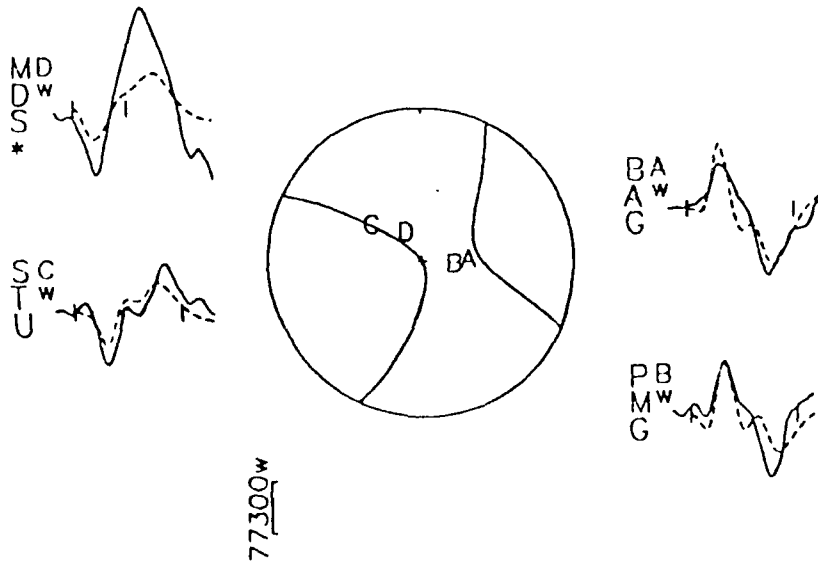
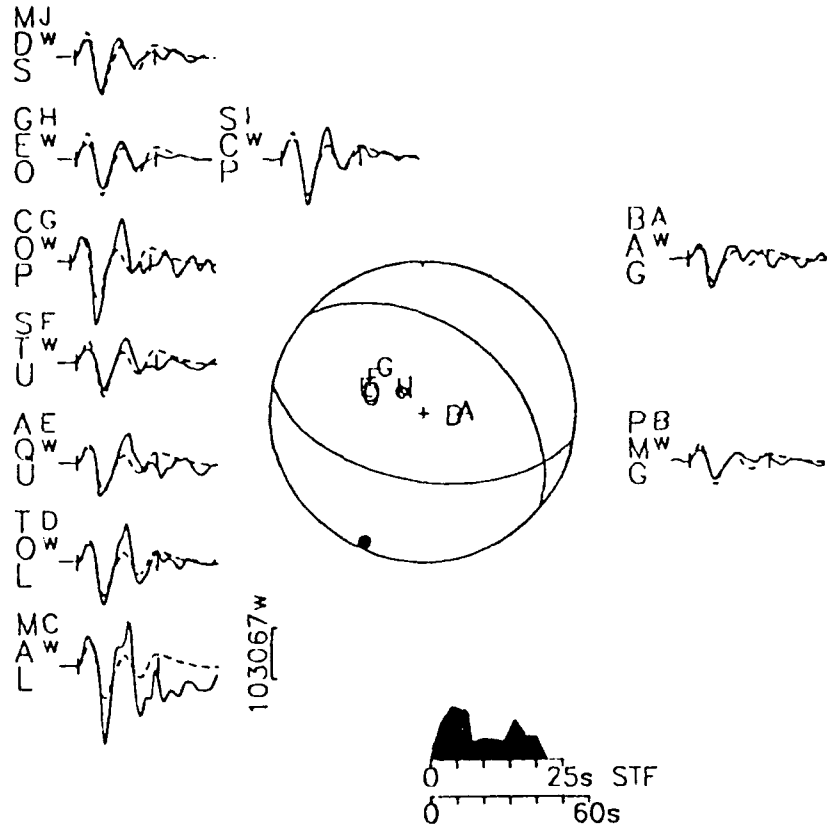


FIGURE 10a

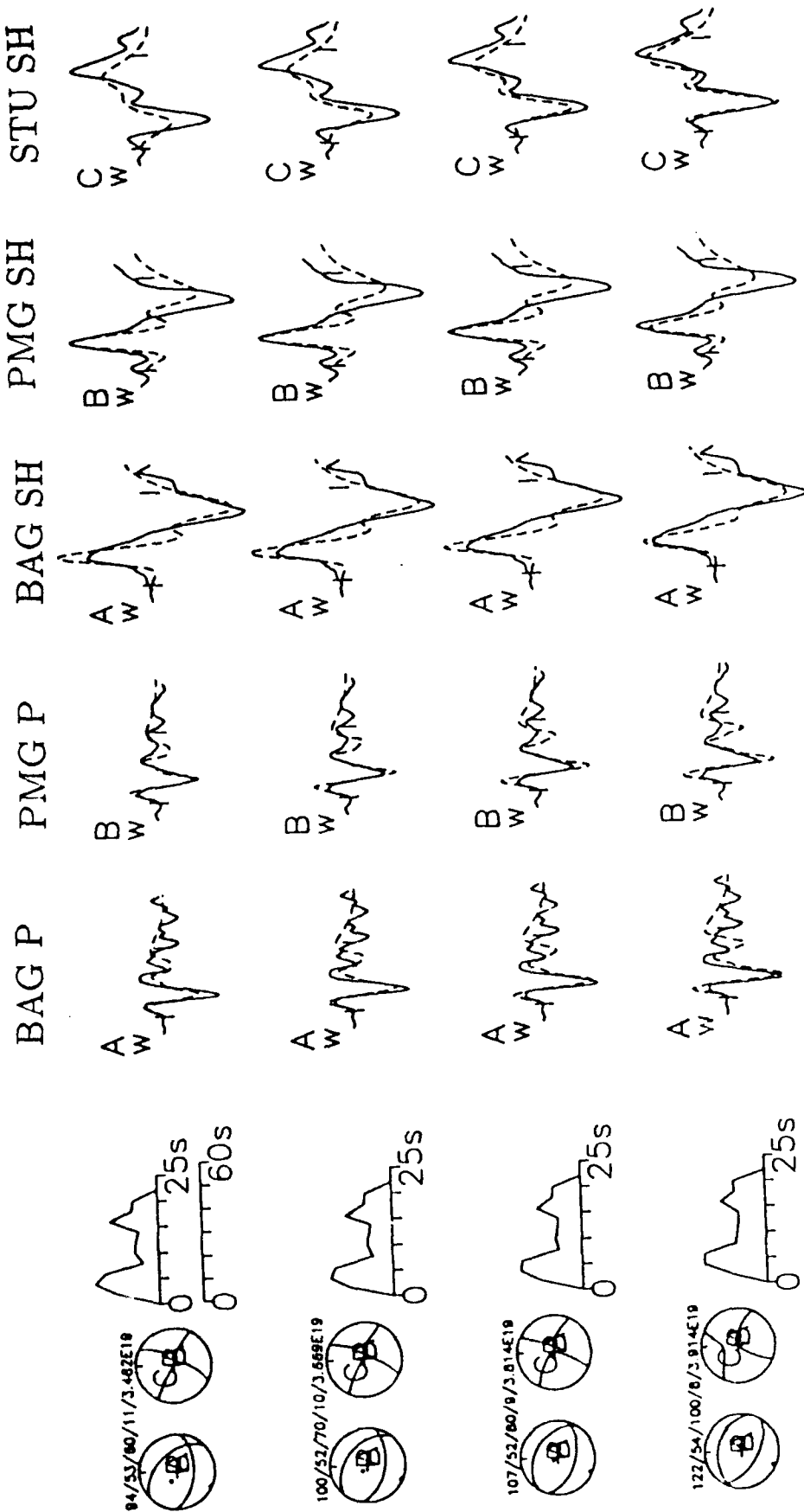


FIGURE A1b

3 January, 1969  
 132/50/95/7/1.89 × 10<sup>17</sup>

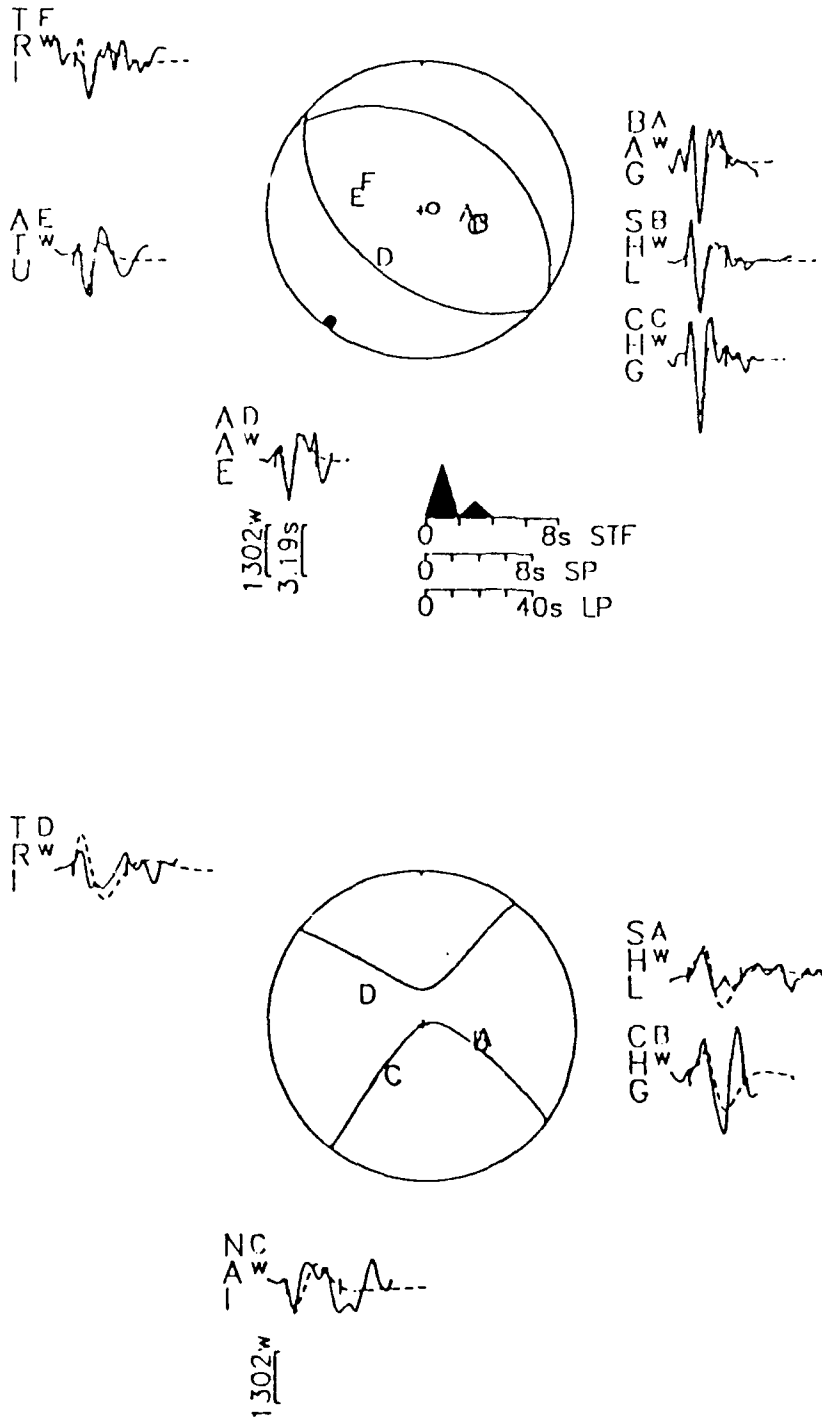


FIGURE A2

30 July, 1970  
 293/56/210/11/4.29 × 10<sup>18</sup>

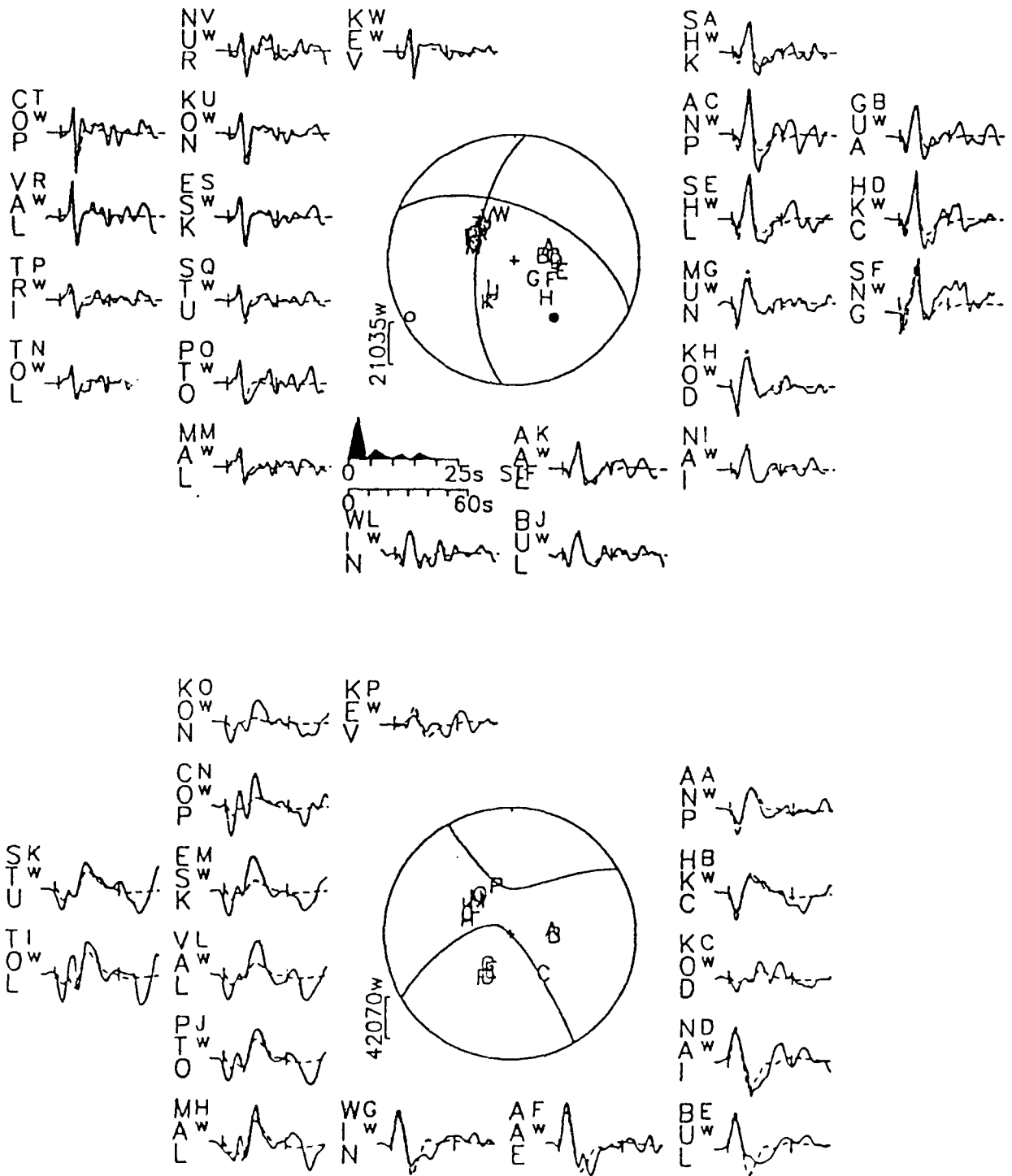


FIGURE A3

14 February, 1971  
336/39/93/11/4.05 × 10<sup>17</sup>

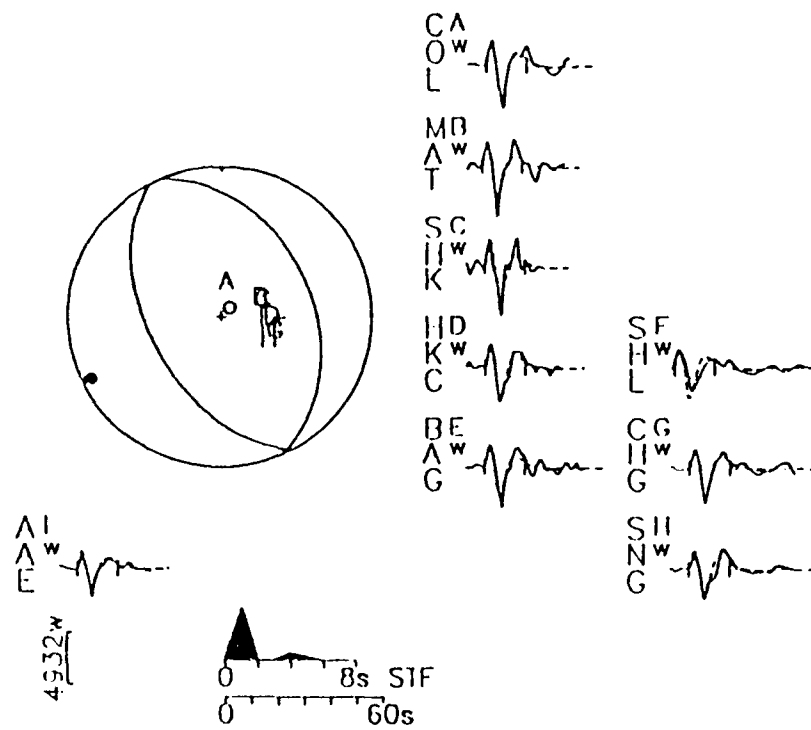


FIGURE A4

4 May, 1980  
 181/84/267/15/4.02 × 10<sup>18</sup>

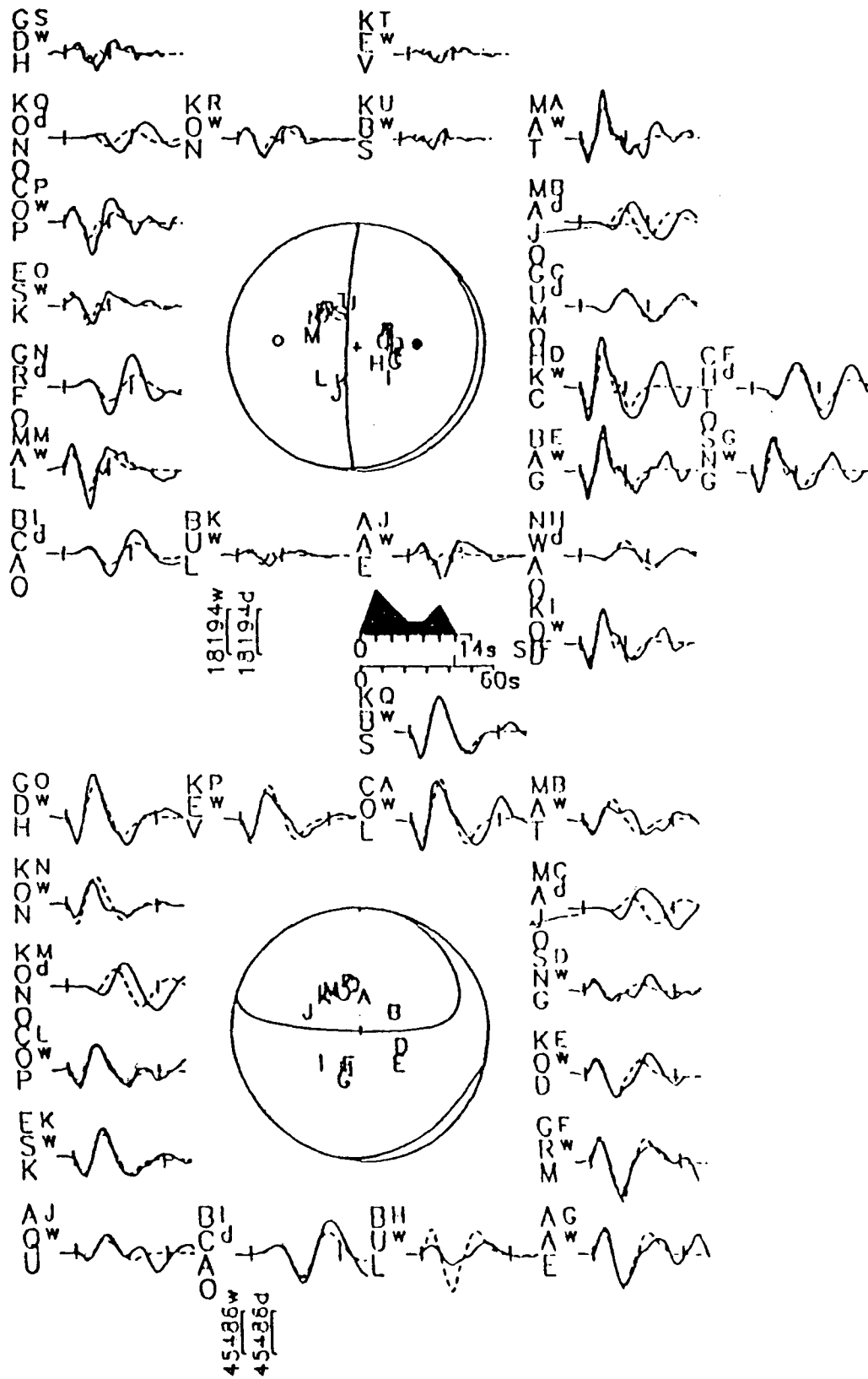


FIGURE A5

19 December, 1980  
 115/41/120/14/1.40 × 10<sup>18</sup>

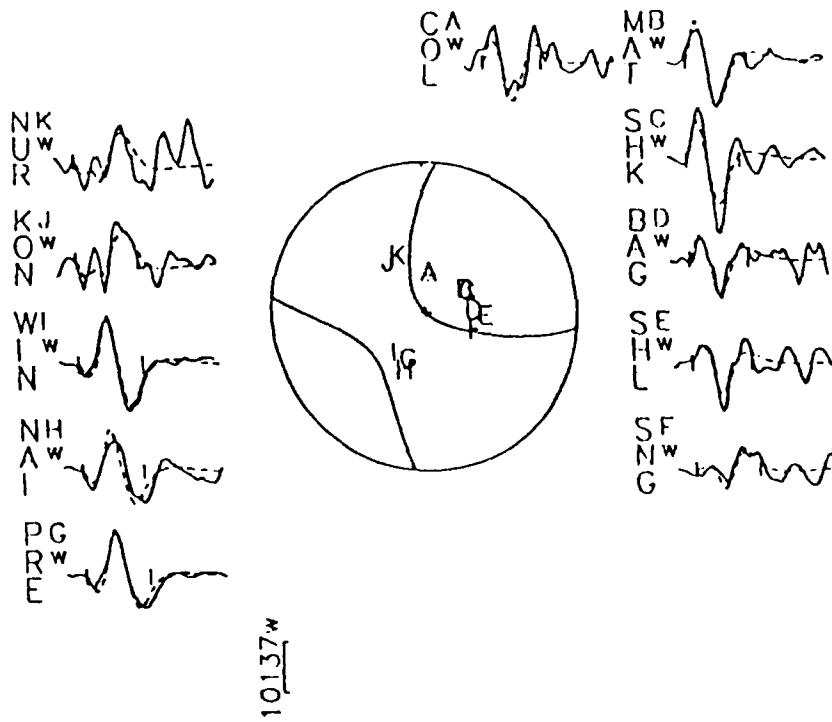
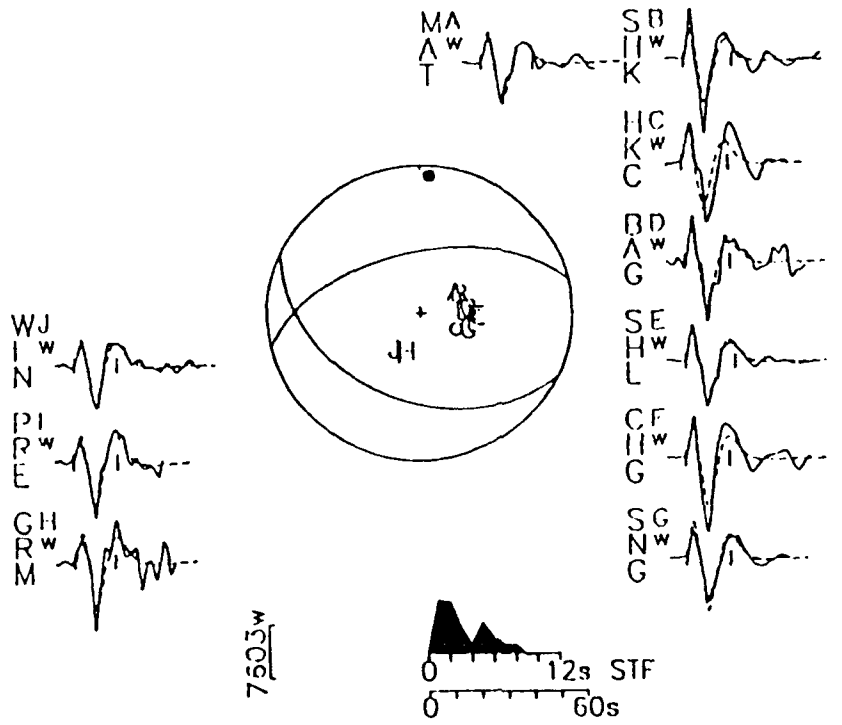


FIGURE A6



22 December, 1980  
 113/56/125/15/2.81 × 10<sup>17</sup>

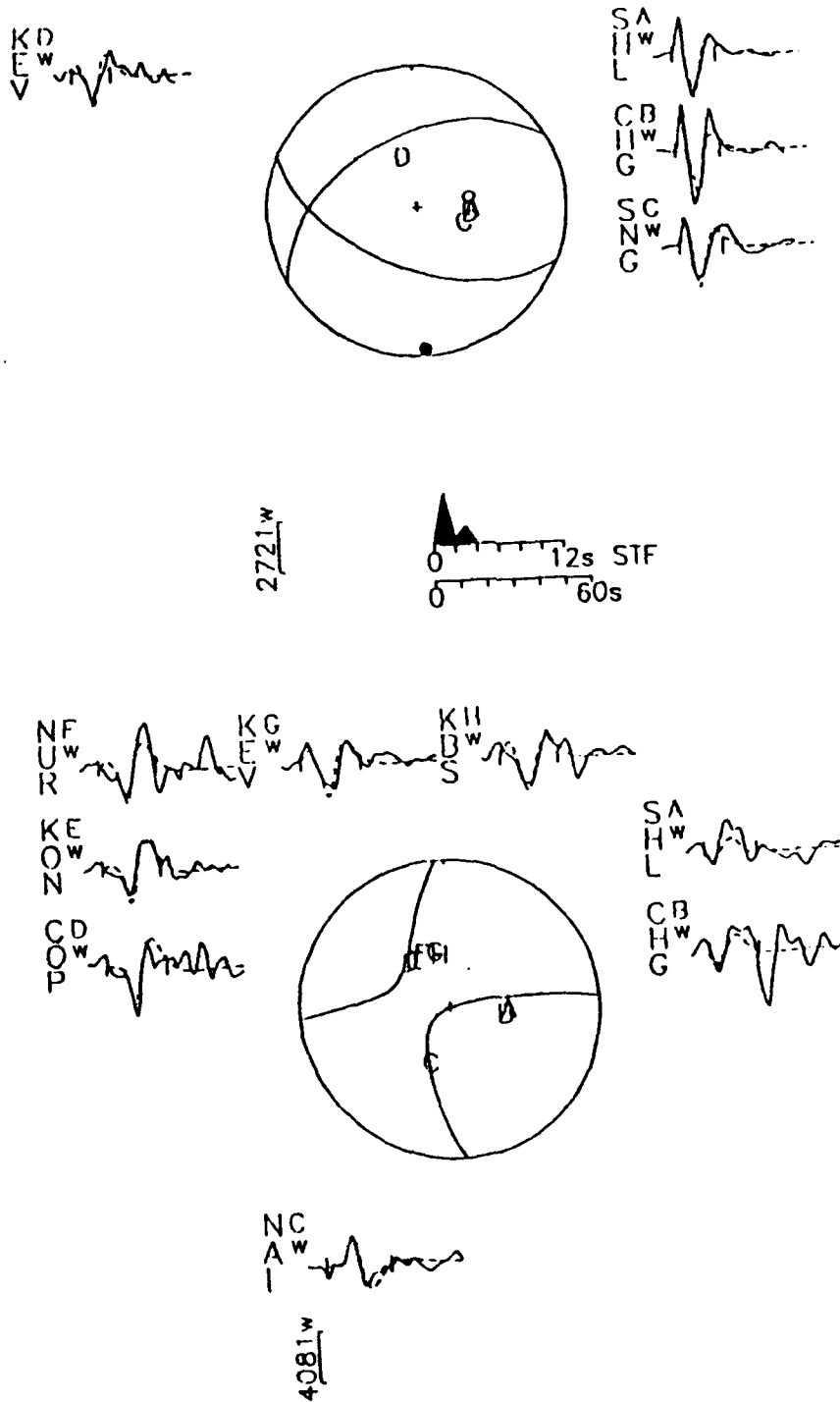


FIGURE A7

4 August, 1981  
 154/35/32/20/2.38 × 10<sup>17</sup>

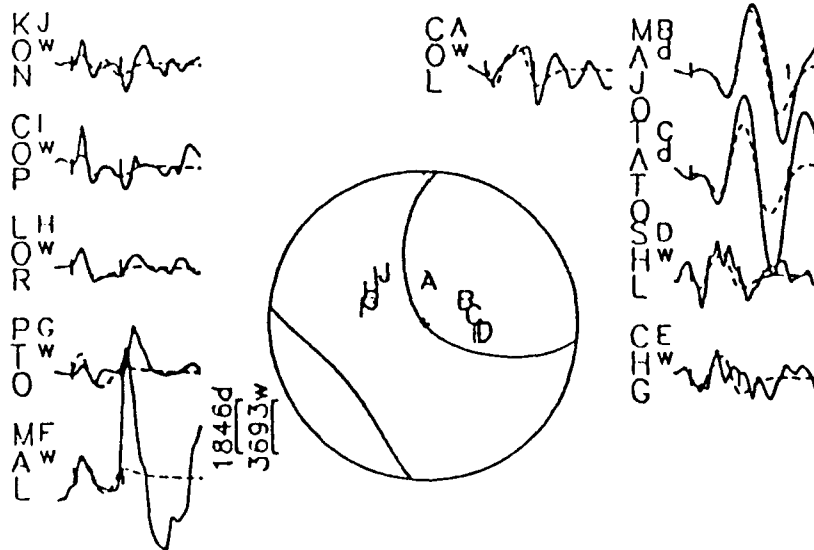
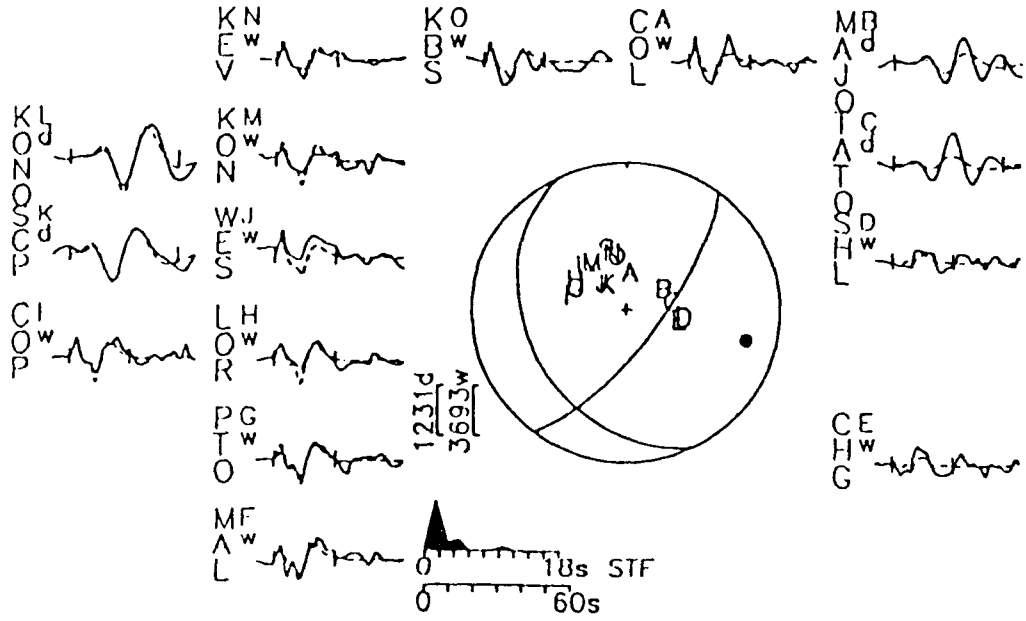


FIGURE A8

22 July, 1983  
120/35/83/10/1.88 × 10<sup>17</sup>

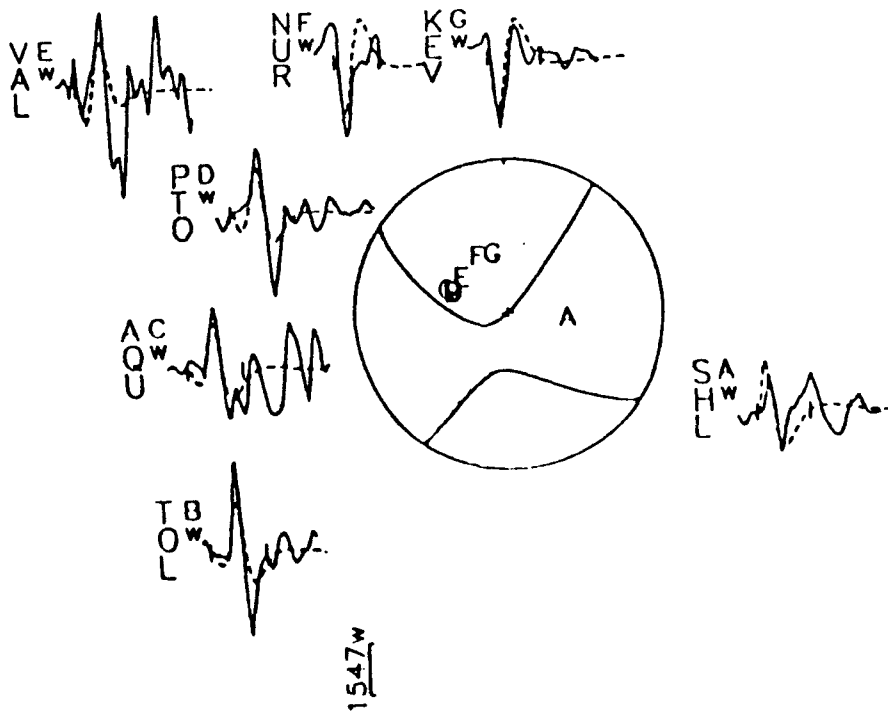
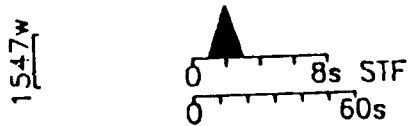
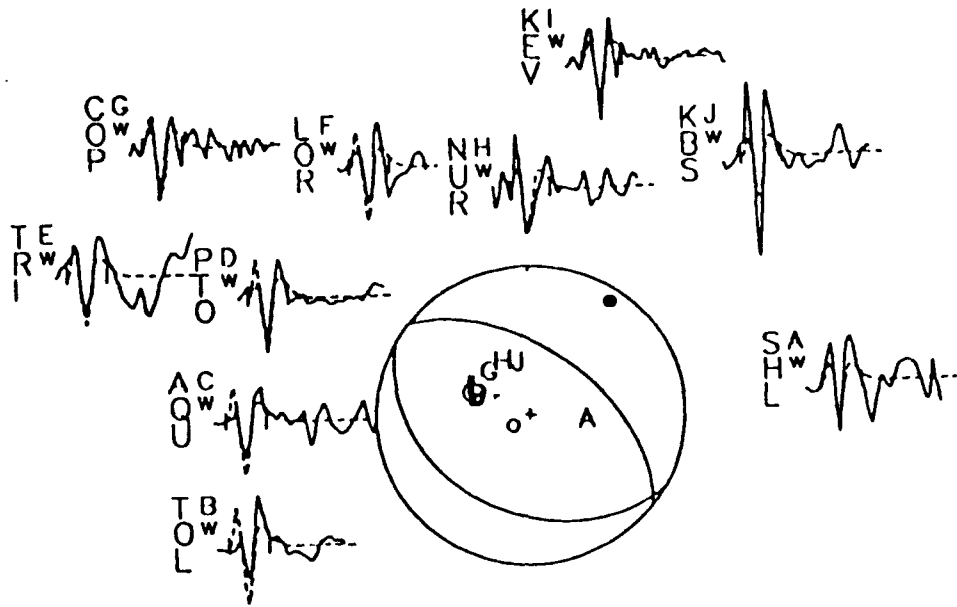


FIGURE A9

22 February, 1984  
 106/60/174/27/5.10 × 10<sup>17</sup>

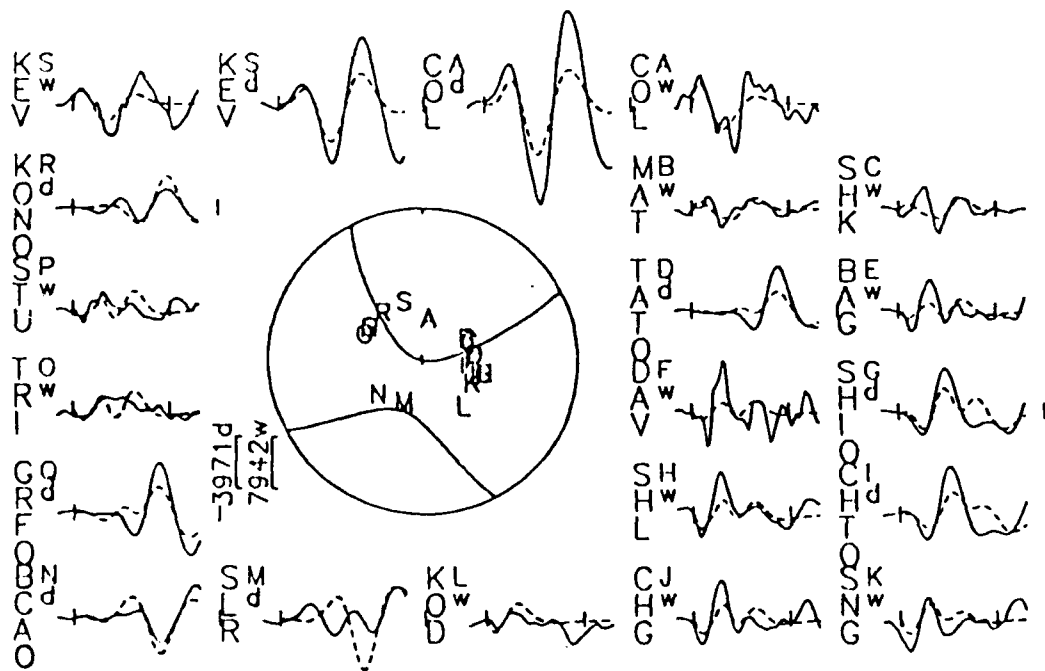
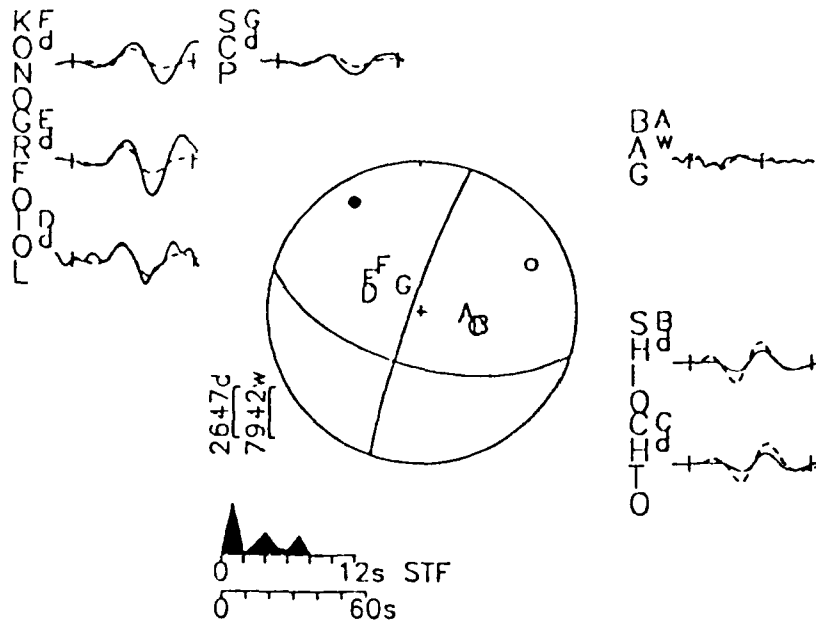


FIGURE A10

29 October, 1985  
 246/66/71/13/2.18 × 10<sup>18</sup>

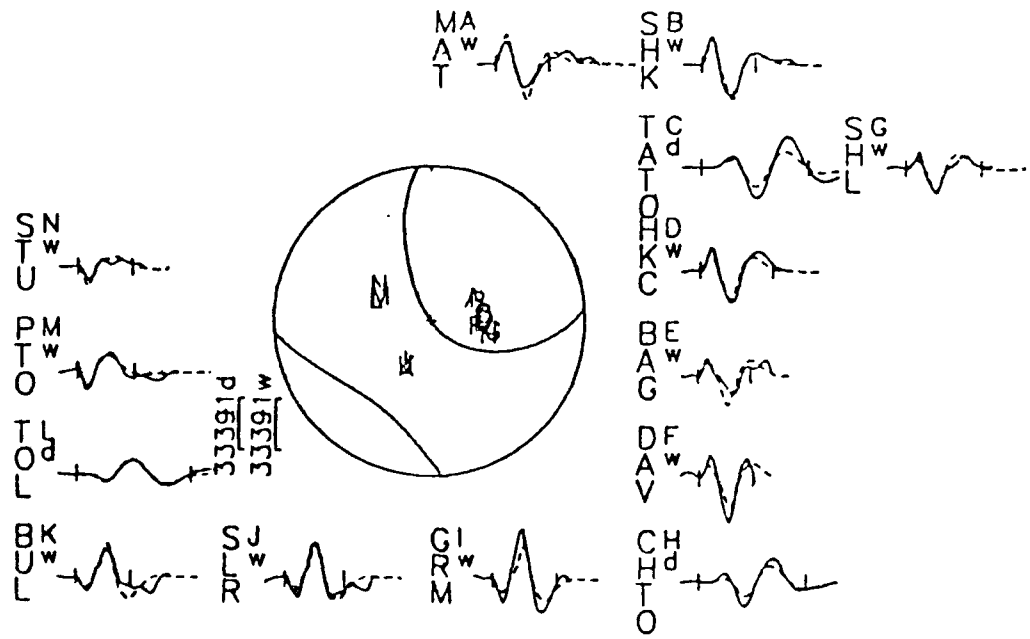
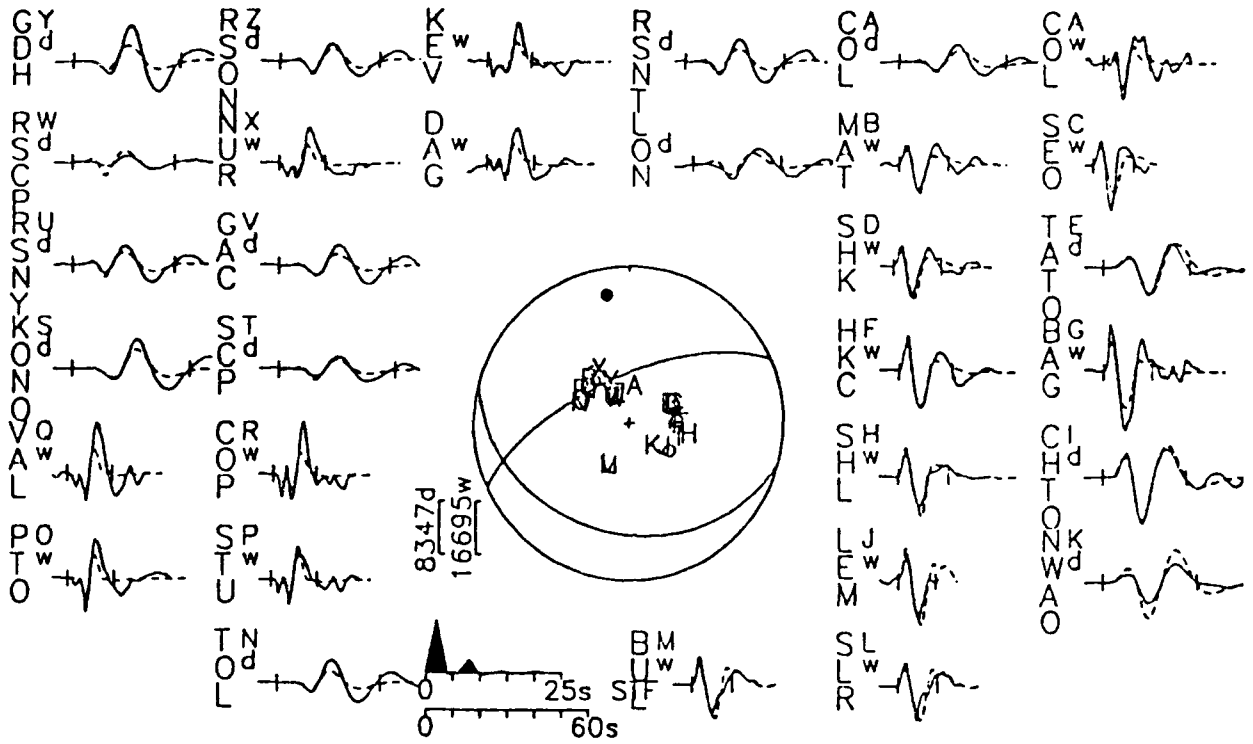


FIGURE A11

7 September 1987

305/10/103/30/2.33 × 10<sup>17</sup>

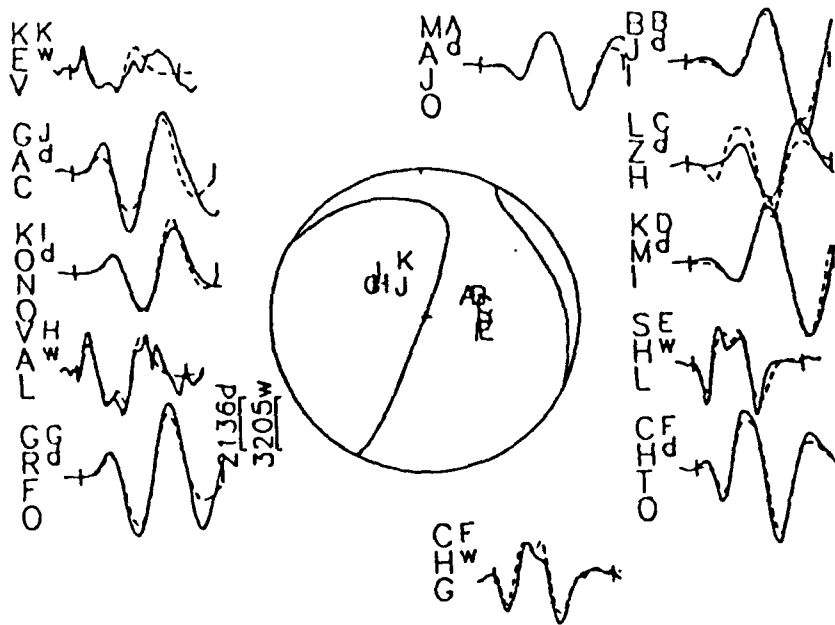
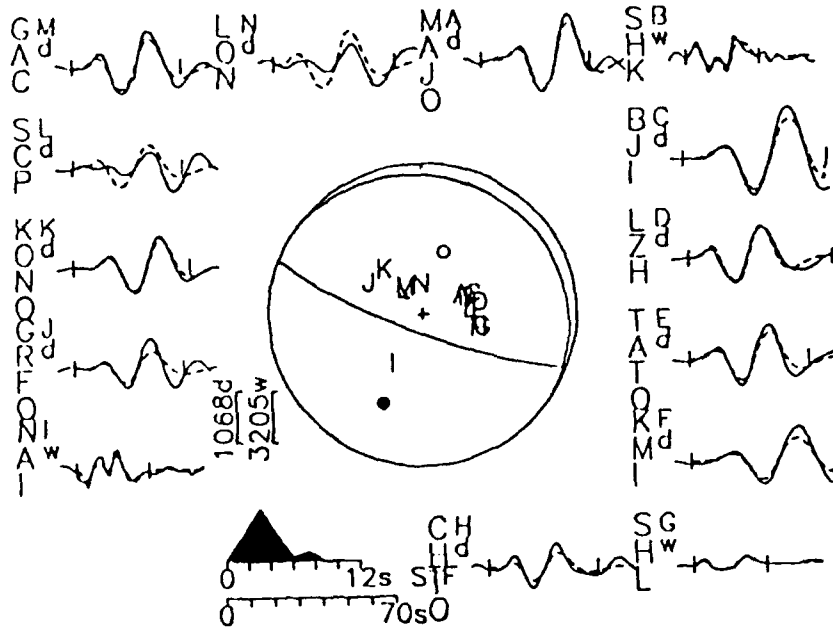


FIGURE A12

16 September, 1989  
 80/26/225/31/6.84 × 10<sup>18</sup>

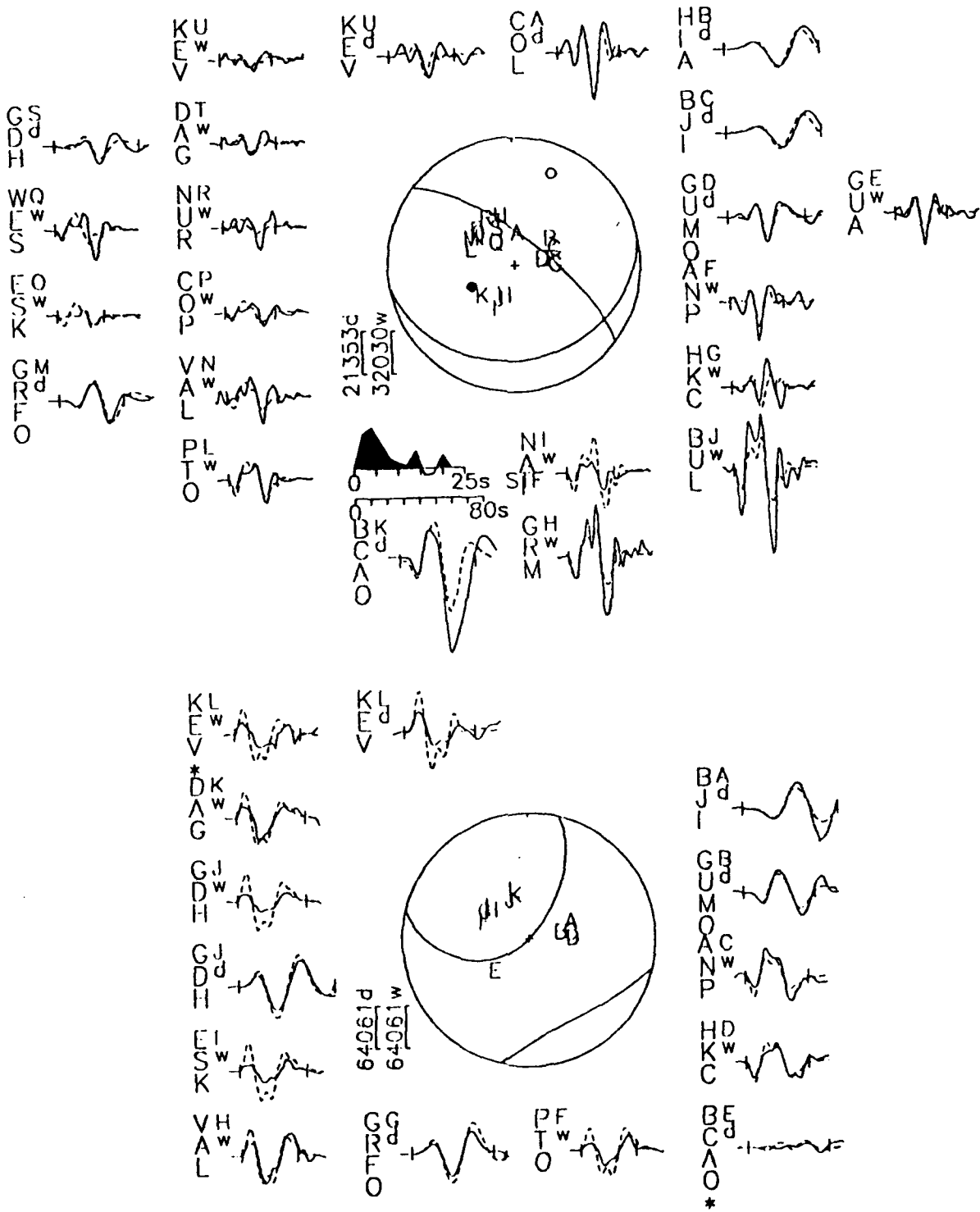


FIGURE A13

17 September, 1989  
277/50/249/35/2.17 × 10<sup>18</sup>

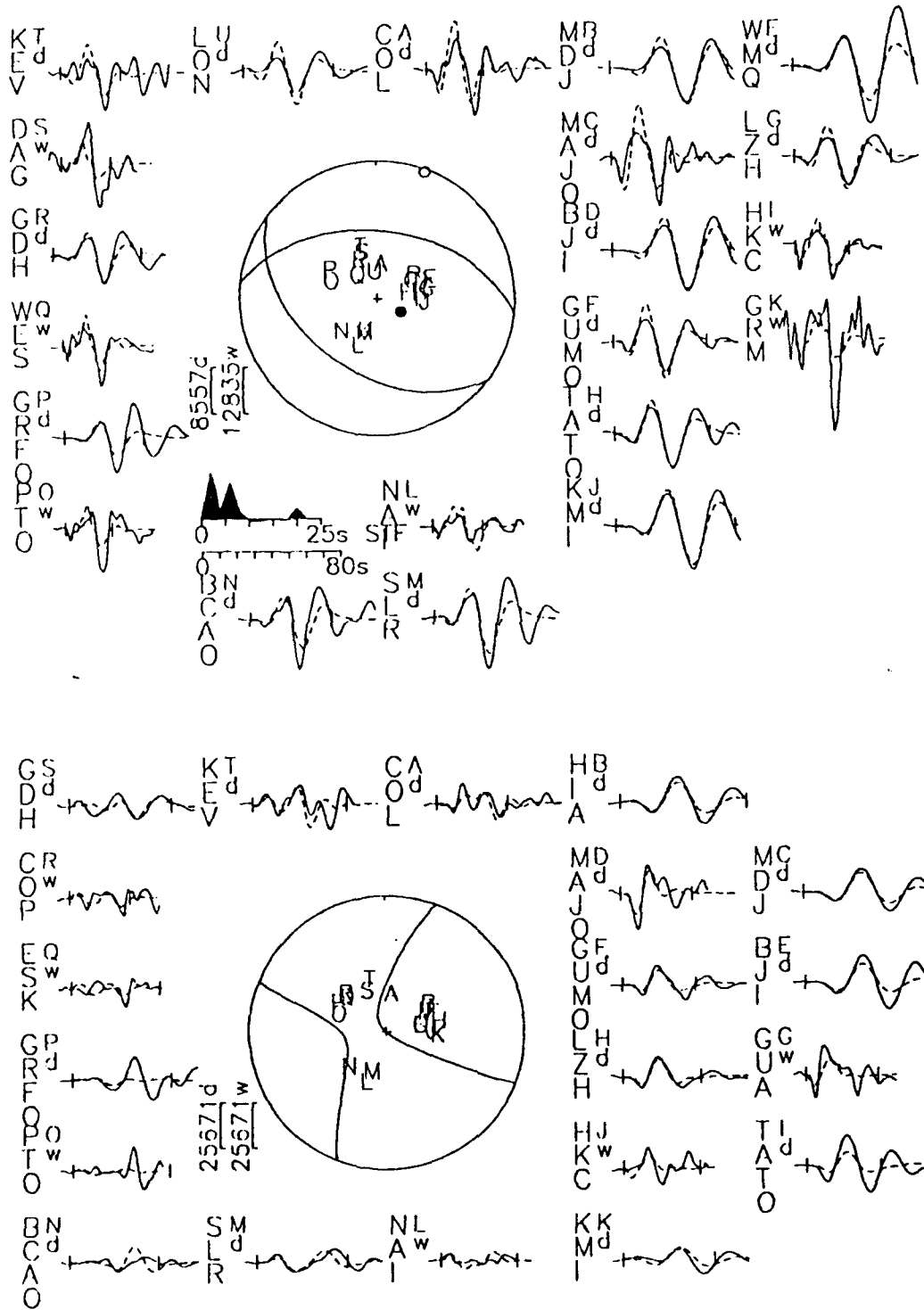


FIGURE A14



DISTRIBUTION LIST

Prof. Thomas Ahrens  
Seismological Lab, 252-21  
Division of Geological & Planetary Sciences  
California Institute of Technology  
Pasadena, CA 91125

Prof. Keiiti Aki  
Center for Earth Sciences  
University of Southern California  
University Park  
Los Angeles, CA 90089-0741

Prof. Shelton Alexander  
Geosciences Department  
403 Deike Building  
The Pennsylvania State University  
University Park, PA 16802

Dr. Ralph Alewine, III  
DARPA/NMRO  
3701 North Fairfax Drive  
Arlington, VA 22203-1714

Prof. Charles B. Archambeau  
CIRES  
University of Colorado  
Boulder, CO 80309

Dr. Thomas C. Bache, Jr.  
Science Applications Int'l Corp.  
10260 Campus Point Drive  
San Diego, CA 92121 (2 copies)

Prof. Muawia Barazangi  
Institute for the Study of the Continent  
Cornell University  
Ithaca, NY 14853

Dr. Jeff Barker  
Department of Geological Sciences  
State University of New York  
at Binghamton  
Vestal, NY 13901

Dr. Douglas R. Baumgardt  
ENSCO, Inc  
5400 Port Royal Road  
Springfield, VA 22151-2388

Dr. Susan Beck  
Department of Geosciences  
Building #77  
University of Arizona  
Tucson, AZ 85721

Dr. T.J. Bennett  
S-CUBED  
A Division of Maxwell Laboratories  
11800 Sunrise Valley Drive, Suite 1212  
Reston, VA 22091

Dr. Robert Blandford  
AFTAC/TT, Center for Seismic Studies  
1300 North 17th Street  
Suite 1450  
Arlington, VA 22209-2308

Dr. G.A. Bollinger  
Department of Geological Sciences  
Virginia Polytechnical Institute  
21044 Derring Hall  
Blacksburg, VA 24061

Dr. Stephen Bratt  
Center for Seismic Studies  
1300 North 17th Street  
Suite 1450  
Arlington, VA 22209-2308

Dr. Lawrence Burdick  
Woodward-Clyde Consultants  
566 El Dorado Street  
Pasadena, CA 91109-3245

Dr. Robert Burridge  
Schlumberger-Doll Research Center  
Old Quarry Road  
Ridgefield, CT 06877

Dr. Jerry Carter  
Center for Seismic Studies  
1300 North 17th Street  
Suite 1450  
Arlington, VA 22209-2308

Dr. Eric Chael  
Division 9241  
Sandia Laboratory  
Albuquerque, NM 87185

Prof. Vernon F. Cormier  
Department of Geology & Geophysics  
U-45, Room 207  
University of Connecticut  
Storrs, CT 06268

Prof. Steven Day  
Department of Geological Sciences  
San Diego State University  
San Diego, CA 92182

Marvin Denny  
U.S. Department of Energy  
Office of Armas Control  
Washington, DC 20585

Dr. Zoltan Der  
ENSCO, Inc.  
5400 Port Royal Road  
Springfield, VA 22151-2388

Prof. Adam Dziewonski  
Hoffman Laboratory, Harvard University  
Dept. of Earth Atmos. & Planetary Sciences  
20 Oxford Street  
Cambridge, MA 02138

Prof. John Ebel  
Department of Geology & Geophysics  
Boston College  
Chestnut Hill, MA 02167

Eric Fielding  
SNEE Hall  
INSTOC  
Cornell University  
Ithaca, NY 14853

Dr. Mark D. Fisk  
Mission Research Corporation  
735 State Street  
P.O. Drawer 719  
Santa Barbara, CA 93102

Prof Stanley Flatte  
Applied Sciences Building  
University of California, Santa Cruz  
Santa Cruz, CA 95064

Dr. John Foley  
NER-Geo Sciences  
1100 Crown Colony Drive  
Quincy, MA 02169

Prof. Donald Forsyth  
Department of Geological Sciences  
Brown University  
Providence, RI 02912

Dr. Art Frankel  
U.S. Geological Survey  
922 National Center  
Reston, VA 22092

Dr. Cliff Frolich  
Institute of Geophysics  
8701 North Mopac  
Austin, TX 78759

Dr. Holly Given  
IGPP, A-025  
Scripps Institute of Oceanography  
University of California, San Diego  
La Jolla, CA 92093

Dr. Jeffrey W. Given  
SAIC  
10260 Campus Point Drive  
San Diego, CA 92121

Dr. Dale Glover  
Defense Intelligence Agency  
ATTN: ODT-1B  
Washington, DC 20301

Dr. Indra Gupta  
Teledyne Geotech  
314 Montgomery Street  
Alexandria, VA 22314

Dan N. Hagedorn  
Pacific Northwest Laboratories  
Battelle Boulevard  
Richland, WA 99352

Dr. James Hannon  
Lawrence Livermore National Laboratory  
P.O. Box 808  
L-205  
Livermore, CA 94550

Dr. Roger Hansen  
HQ AFTAC/TIR  
Patrick AFB, FL 32925-6001

Prof. David G. Harkrider  
Seismological Laboratory  
Division of Geological & Planetary Sciences  
California Institute of Technology  
Pasadena, CA 91125

Prof. Danny Harvey  
CIRES  
University of Colorado  
Boulder, CO 80309

Prof. Donald V. Helmberger  
Seismological Laboratory  
Division of Geological & Planetary Sciences  
California Institute of Technology  
Pasadena, CA 91125

Prof. Eugene Herrin  
Institute for the Study of Earth and Man  
Geophysical Laboratory  
Southern Methodist University  
Dallas, TX 75275

Prof. Robert B. Herrmann  
Department of Earth & Atmospheric Sciences  
St. Louis University  
St. Louis, MO 63156

Prof. Lane R. Johnson  
Seismographic Station  
University of California  
Berkeley, CA 94720

Prof. Thomas H. Jordan  
Department of Earth, Atmospheric &  
Planetary Sciences  
Massachusetts Institute of Technology  
Cambridge, MA 02139

Prof. Alan Kafka  
Department of Geology & Geophysics  
Boston College  
Chestnut Hill, MA 02167

Robert C. Kemerait  
ENSCO, Inc.  
445 Pineda Court  
Melbourne, FL 32940

Dr. Max Koontz  
U.S. Dept. of Energy/DP 5  
Forrestal Building  
1000 Independence Avenue  
Washington, DC 20585

Dr. Richard LaCoss  
MIT Lincoln Laboratory, M-200B  
P.O. Box 73  
Lexington, MA 02173-0073

Dr. Fred K. Lamb  
University of Illinois at Urbana-Champaign  
Department of Physics  
1110 West Green Street  
Urbana, IL 61801

Prof. Charles A. Langston  
Geosciences Department  
403 Deike Building  
The Pennsylvania State University  
University Park, PA 16802

Jim Lawson, Chief Geophysicist  
Oklahoma Geological Survey  
Oklahoma Geophysical Observatory  
P.O. Box 8  
Leonard, OK 74043-0008

Prof. Thorne Lay  
Institute of Tectonics  
Earth Science Board  
University of California, Santa Cruz  
Santa Cruz, CA 95064

Dr. William Leith  
U.S. Geological Survey  
Mail Stop 928  
Reston, VA 22092

Mr. James F. Lewkowicz  
Phillips Laboratory/GPEH  
Hanscom AFB, MA 01731-5000( 2 copies)

Mr. Alfred Lieberman  
ACDA/VI-OA State Department Building  
Room 5726  
320-21st Street, NW  
Washington, DC 20451

Prof. L. Timothy Long  
School of Geophysical Sciences  
Georgia Institute of Technology  
Atlanta, GA 30332

Dr. Randolph Martin, III  
New England Research, Inc.  
76 Olcott Drive  
White River Junction, VT 05001

Dr. Robert Masse  
Denver Federal Building  
Box 25046, Mail Stop 967  
Denver, CO 80225

Dr. Gary McCartor  
Department of Physics  
Southern Methodist University  
Dallas, TX 75275

Prof. Thomas V. McEvelly  
Seismographic Station  
University of California  
Berkeley, CA 94720

Dr. Art McGarr  
U.S. Geological Survey  
Mail Stop 977  
U.S. Geological Survey  
Menlo Park, CA 94025

Dr. Keith L. McLaughlin  
S-CUBED  
A Division of Maxwell Laboratory  
P.O. Box 1620  
La Jolla, CA 92038-1620

Stephen Miller & Dr. Alexander Florence  
SRI International  
333 Ravenswood Avenue  
Box AF 116  
Menlo Park, CA 94025-3493

Prof. Bernard Minster  
IGPP, A-025  
Scripps Institute of Oceanography  
University of California, San Diego  
La Jolla, CA 92093

Prof. Brian J. Mitchell  
Department of Earth & Atmospheric Sciences  
St. Louis University  
St. Louis, MO 63156

Mr. Jack Murphy  
S-CUBED  
A Division of Maxwell Laboratory  
11800 Sunrise Valley Drive, Suite 1212  
Reston, VA 22091 (2 Copies)

Dr. Keith K. Nakanishi  
Lawrence Livermore National Laboratory  
L-025  
P.O. Box 808  
Livermore, CA 94550

Dr. Carl Newton  
Los Alamos National Laboratory  
P.O. Box 1663  
Mail Stop C335, Group ESS-3  
Los Alamos, NM 87545

Dr. Bac Nguyen  
HQ AFTAC/TTR  
Patrick AFB, FL 32925-6001

Prof. John A. Orcutt  
IGPP, A-025  
Scripps Institute of Oceanography  
University of California, San Diego  
La Jolla, CA 92093

Prof. Jeffrey Park  
Kline Geology Laboratory  
P.O. Box 6666  
New Haven, CT 06511-8130

Dr. Howard Patton  
Lawrence Livermore National Laboratory  
L-025  
P.O. Box 808  
Livermore, CA 94550

Dr. Frank Pilotte  
HQ AFTAC/TT  
Patrick AFB, FL 32925-6001

Dr. Jay J. Pulli  
Radix Systems, Inc.  
2 Taft Court, Suite 203  
Rockville, MD 20850

Dr. Robert Reinke  
ATTN: FCTVTD  
Field Command  
Defense Nuclear Agency  
Kirtland AFB, NM 87115

Prof. Paul G. Richards  
Lamont-Doherty Geological Observatory  
of Columbia University  
Palisades, NY 10964

Mr. Wilmer Rivers  
Teledyne Geotech  
314 Montgomery Street  
Alexandria, VA 22314

Dr. George Rothe  
HQ AFTAC/TTR  
Patrick AFB, FL 32925-6001

Dr. Alan S. Ryall, Jr.  
DARPA/NMRO  
3701 North Fairfax Drive  
Arlington, VA 22209-1714

Dr. Richard Sailor  
TASC, Inc.  
55 Walkers Brook Drive  
Reading, MA 01867

Prof. Charles G. Sammis  
Center for Earth Sciences  
University of Southern California  
University Park  
Los Angeles, CA 90089-0741

Prof. Christopher H. Scholz  
Lamont-Doherty Geological Observatory  
of Columbia University  
Palisades, CA 10964

Dr. Susan Schwartz  
Institute of Tectonics  
1156 High Street  
Santa Cruz, CA 95064

Secretary of the Air Force  
(SAFRD)  
Washington, DC 20330

Office of the Secretary of Defense  
DDR&E  
Washington, DC 20330

Thomas J. Sereno, Jr.  
Science Application Int'l Corp.  
10260 Campus Point Drive  
San Diego, CA 92121

Dr. Michael Shore  
Defense Nuclear Agency/SPSS  
6801 Telegraph Road  
Alexandria, VA 22310

Dr. Matthew Sibol  
Virginia Tech  
Seismological Observatory  
4044 Derring Hall  
Blacksburg, VA 24061-0420

Prof. David G. Simpson  
IRIS, Inc.  
1616 North Fort Myer Drive  
Suite 1440  
Arlington, VA 22209

Donald L. Springer  
Lawrence Livermore National Laboratory  
L-025  
P.O. Box 808  
Livermore, CA 94550

Dr. Jeffrey Stevens  
S-CUBED  
A Division of Maxwell Laboratory  
P.O. Box 1620  
La Jolla, CA 92038-1620

Lt. Col. Jim Stobie  
ATTN: AFOSR/NL  
Bolling AFB  
Washington, DC 20332-6448

Prof. Brian Stump  
Institute for the Study of Earth & Man  
Geophysical Laboratory  
Southern Methodist University  
Dallas, TX 75275

Prof. Jeremiah Sullivan  
University of Illinois at Urbana-Champaign  
Department of Physics  
1110 West Green Street  
Urbana, IL 61801

Prof. L. Sykes  
Lamont-Doherty Geological Observatory  
of Columbia University  
Palisades, NY 10964

Dr. David Taylor  
ENSCO, Inc.  
445 Pineda Court  
Melbourne, FL 32940

Dr. Steven R. Taylor  
Los Alamos National Laboratory  
P.O. Box 1663  
Mail Stop C335  
Los Alamos, NM 87545

Prof. Clifford Thurber  
University of Wisconsin-Madison  
Department of Geology & Geophysics  
1215 West Dayton Street  
Madison, WS 53706

Prof. M. Nafi Toksoz  
Earth Resources Lab  
Massachusetts Institute of Technology  
42 Carleton Street  
Cambridge, MA 02142

Dr. Larry Turnbull  
CIA-OSWR/NED  
Washington, DC 20505

DARPA/RMO/SECURITY OFFICE  
3701 North Fairfax Drive  
Arlington, VA 22203-1714

Dr. Gregory van der Vink  
IRIS, Inc.  
1616 North Fort Myer Drive  
Suite 1440  
Arlington, VA 22209

HQ DNA  
ATTN: Technical Library  
Washington, DC 20305

Dr. Karl Veith  
EG&G  
5211 Auth Road  
Suite 240  
Suitland, MD 20746

Defense Intelligence Agency  
Directorate for Scientific & Technical Intelligence  
ATTN: DTIB  
Washington, DC 20340-6158

Prof. Terry C. Wallace  
Department of Geosciences  
Building #77  
University of Arizona  
Tuscon, AZ 85721

Defense Technical Information Center  
Cameron Station  
Alexandria, VA 22314 (2 Copies)

Dr. Thomas Weaver  
Los Alamos National Laboratory  
P.O. Box 1663  
Mail Stop C335  
Los Alamos, NM 87545

TACTEC  
Battelle Memorial Institute  
505 King Avenue  
Columbus, OH 43201 (Final Report)

Dr. William Wortman  
Mission Research Corporation  
8560 Cinderbed Road  
Suite 700  
Newington, VA 22122

Phillips Laboratory  
ATTN: XPG  
Hanscom AFB, MA 01731-5000

Prof. Francis T. Wu  
Department of Geological Sciences  
State University of New York  
at Binghamton  
Vestal, NY 13901

Phillips Laboratory  
ATTN: GPE  
Hanscom AFB, MA 01731-5000

AFTAC/CA  
(STINFO)  
Patrick AFB, FL 32925-6001

Phillips Laboratory  
ATTN: TSML  
Hanscom AFB, MA 01731-5000

DARPA/PM  
3701 North Fairfax Drive  
Arlington, VA 22203-1714

Phillips Laboratory  
ATTN: SUL  
Kirtland, NM 87117 (2 copies)

DARPA/RMO/RETRIEVAL  
3701 North Fairfax Drive  
Arlington VA 22203-1714

Dr. Michel Bouchon  
I.R.I.G.M.-B.P. 68  
38402 St. Martin D'Herès  
Cedex, FRANCE

Dr. Michel Campillo  
Observatoire de Grenoble  
I.R.I.G.M.-B.P. 53  
38041 Grenoble, FRANCE

Dr. Jorg Schlittenhardt  
Federal Institute for Geosciences & Nat'l Res.  
Postfach 510153  
D-3000 Hannover 51, GERMANY

Dr. Kin Yip Chun  
Geophysics Division  
Physics Department  
University of Toronto  
Ontario, CANADA

Dr. Johannes Schweitzer  
Institute of Geophysics  
Ruhr University/Bochum  
P.O. Box 1102148  
4360 Bochum 1, GERMANY

Prof. Hans-Peter Harjes  
Institute for Geophysic  
Ruhr University/Bochum  
P.O. Box 102148  
4630 Bochum 1, GERMANY

Prof. Eystein Husebye  
NTNF/NORSAR  
P.O. Box 51  
N-2007 Kjeller, NORWAY

David Jepsen  
Acting Head, Nuclear Monitoring Section  
Bureau of Mineral Resources  
Geology and Geophysics  
G.P.O. Box 378, Canberra, AUSTRALIA

Ms. Eva Johannisson  
Senior Research Officer  
National Defense Research Inst.  
P.O. Box 27322  
S-102 54 Stockholm, SWEDEN

Dr. Peter Marshall  
Procurement Executive  
Ministry of Defense  
Blacknest, Brimpton  
Reading FG7-FRS, UNITED KINGDOM

Dr. Bernard Massinon, Dr. Pierre Mechler  
Societe Radiomana  
27 rue Claude Bernard  
75005 Paris, FRANCE (2 Copies)

Dr. Svein Mykkeltveit  
NTNT/NORSAR  
P.O. Box 51  
N-2007 Kjeller, NORWAY (3 Copies)

Prof. Keith Priestley  
University of Cambridge  
Bullard Labs, Dept. of Earth Sciences  
Madingley Rise, Madingley Road  
Cambridge CB3 0EZ, ENGLAND